

# Journal of Astronomical Telescopes, Instruments, and Systems

AstronomicalTelescopes.SPIEDigitalLibrary.org

## Review: far-infrared instrumentation and technological development for the next decade

Duncan Farrah  
Kimberly Ennico Smith  
David Ardila  
Charles M. Bradford  
Michael Dipirro  
Carl Ferkinhoff  
Jason Glenn  
Paul Goldsmith  
David Leisawitz  
Thomas Nikola  
Naseem Rangwala  
Stephen A. Rinehart  
Johannes Staguhn  
Michael Zemcov  
Jonas Zmuidzinas  
James Bartlett  
Sean Carey  
William J. Fischer

Julia Kamenetzky  
Jeyhan Kartaltepe  
Mark Lacy  
Dariusz C. Lis  
Lisa Locke  
Enrique Lopez-Rodriguez  
Meredith MacGregor  
Elisabeth Mills  
Samuel H. Moseley  
Eric J. Murphy  
Alan Rhodes  
Matt Richter  
Dimitra Rigopoulou  
David Sanders  
Ravi Sankrit  
Giorgio Savini  
John-David Smith  
Sabrina Stierwalt

Duncan Farrah, Kimberly Ennico Smith, David Ardila, Charles M. Bradford, Michael Dipirro, Carl Ferkinhoff, Jason Glenn, Paul Goldsmith, David Leisawitz, Thomas Nikola, Naseem Rangwala, Stephen A. Rinehart, Johannes Staguhn, Michael Zemcov, Jonas Zmuidzinas, James Bartlett, Sean Carey, William J. Fischer, Julia Kamenetzky, Jeyhan Kartaltepe, Mark Lacy, Dariusz C. Lis, Lisa Locke, Enrique Lopez-Rodriguez, Meredith MacGregor, Elisabeth Mills, Samuel H. Moseley, Eric J. Murphy, Alan Rhodes, Matt Richter, Dimitra Rigopoulou, David Sanders, Ravi Sankrit, Giorgio Savini, John-David Smith, Sabrina Stierwalt, "Review: far-infrared instrumentation and technological development for the next decade," *J. Astron. Telesc. Instrum. Syst.* **5**(2), 020901 (2019), doi: 10.1117/1.JATIS.5.2.020901.

**SPIE.**

# Review: far-infrared instrumentation and technological development for the next decade

Duncan Farrah,<sup>a,b,\*</sup> Kimberly Ennico Smith,<sup>c</sup> David Ardila,<sup>d</sup> Charles M. Bradford,<sup>d,e</sup> Michael Dipirro,<sup>f</sup> Carl Ferkinhoff,<sup>g</sup> Jason Glenn,<sup>h</sup> Paul Goldsmith,<sup>d</sup> David Leisawitz,<sup>f</sup> Thomas Nikola,<sup>i</sup> Naseem Rangwala,<sup>c,j</sup> Stephen A. Rinehart,<sup>l</sup> Johannes Staguhn,<sup>k,f</sup> Michael Zemcov,<sup>l,d</sup> Jonas Zmuidzinas,<sup>e</sup> James Bartlett,<sup>d</sup> Sean Carey,<sup>m</sup> William J. Fischer,<sup>n</sup> Julia Kamenetzky,<sup>o</sup> Jeyhan Kartaltepe,<sup>l</sup> Mark Lacy,<sup>p</sup> Dariusz C. Lis,<sup>q,e</sup> Lisa Locke,<sup>p,f</sup> Enrique Lopez-Rodriguez,<sup>c</sup> Meredith MacGregor,<sup>s</sup> Elisabeth Mills,<sup>t</sup> Samuel H. Moseley,<sup>f</sup> Eric J. Murphy,<sup>o</sup> Alan Rhodes,<sup>c</sup> Matt Richter,<sup>u</sup> Dimitra Rigopoulou,<sup>v,w</sup> David Sanders,<sup>b</sup> Ravi Sankrit,<sup>n,c</sup> Giorgio Savini,<sup>x</sup> John-David Smith,<sup>y</sup> and Sabrina Stierwalt<sup>m</sup>

<sup>a</sup>University of Hawaii, Department of Physics and Astronomy, Honolulu, Hawaii, United States

<sup>b</sup>University of Hawaii, Institute for Astronomy, Honolulu, Hawaii, United States

<sup>c</sup>NASA Ames Research Center, Moffet Field, California, United States

<sup>d</sup>Jet Propulsion Laboratory, California Institute of Technology, Pasadena, California, United States

<sup>e</sup>California Institute of Technology, Division of Physics, Mathematics, and Astronomy, Pasadena, California, United States

<sup>f</sup>NASA Goddard Space Flight Center, Greenbelt, Maryland, United States

<sup>g</sup>Winona State University, Department of Physics, Winona, Minnesota, United States

<sup>h</sup>University of Colorado, Department of Astrophysical and Planetary Sciences, Boulder, Colorado, United States

<sup>i</sup>Cornell University, Cornell Center for Astrophysics and Planetary Sciences, Ithaca, New York, United States

<sup>j</sup>Bay Area Environmental Research Institute, NASA Research Park, Moffet Field, California, United States

<sup>k</sup>Johns Hopkins University, The Henry A. Rowland Department of Physics and Astronomy, Baltimore, Maryland, United States

<sup>l</sup>Rochester Institute of Technology, School of Physics and Astronomy, Rochester, New York, United States

<sup>m</sup>California Institute of Technology, Infrared Processing Analysis Center, Pasadena, California, United States

<sup>n</sup>Space Telescope Science Institute, Baltimore, Maryland, United States

<sup>o</sup>Westminster College, Salt Lake City, Utah, United States

<sup>p</sup>National Radio Astronomy Observatory, Charlottesville, Virginia, United States

<sup>q</sup>Sorbonne Université, Observatoire de Paris, Université PSL, CNRS, LERMA, Paris, France

<sup>r</sup>National Research Council Canada, Herzberg Astronomy and Astrophysics, Victoria, British Columbia, Canada

<sup>s</sup>Carnegie Institution of Washington, Department of Terrestrial Magnetism, Washington, DC, United States

<sup>t</sup>Boston University, Department of Astronomy, Boston, Massachusetts, United States

<sup>u</sup>University of California at Davis, Department of Physics, Davis, California, United States

<sup>v</sup>University of Oxford, Department of Physics, Oxford, United Kingdom

<sup>w</sup>RAL Space, Science, and Technology Facilities Council, Rutherford Appleton Laboratory, Didcot, United Kingdom

<sup>x</sup>University College London, Physics and Astronomy Department, Gower Street, London, United Kingdom

<sup>y</sup>University of Toledo, Department of Physics and Astronomy, Toledo, Ohio, United States

**Abstract.** Far-infrared astronomy has advanced rapidly since its inception in the late 1950s, driven by a maturing technology base and an expanding community of researchers. This advancement has shown that observations at far-infrared wavelengths are important in nearly all areas of astrophysics, from the search for habitable planets and the origin of life to the earliest stages of galaxy assembly in the first few hundred million years of cosmic history. The combination of a still-developing portfolio of technologies, particularly in the field of detectors, and a widening ensemble of platforms within which these technologies can be deployed, means that far-infrared astronomy holds the potential for paradigm-shifting advances over the next decade. We examine the current and future far-infrared observing platforms, including ground-based, suborbital, and space-based facilities, and discuss the technology development pathways that will enable and enhance these platforms to best address the challenges facing far-infrared astronomy in the 21st century. © The Authors. Published by SPIE under a Creative Commons Attribution 4.0 Unported License. Distribution or reproduction of this work in whole or in part requires full attribution of the original publication, including its DOI. [DOI: [10.1117/1.JATIS.5.2.020901](https://doi.org/10.1117/1.JATIS.5.2.020901)]

Keywords: instrumentation; detectors; interferometers; miscellaneous; photometers; spectrographs; space vehicles; instruments; balloons; telescopes.

Paper 17072V received Sep. 5, 2017; accepted for publication Mar. 7, 2019; published online Apr. 5, 2019.

## 1 Introduction

Far-infrared astronomy, defined broadly as encompassing science at wavelengths of 30 to 1000  $\mu\text{m}$ , is an invaluable tool in understanding all aspects of our cosmic origins. Tracing its roots to the late 1950s, with the advent of infrared detectors sensitive enough for astronomical applications, far-infrared astronomy

has developed from a niche science, pursued by only a few teams of investigators, to a concerted worldwide effort pursued by hundreds of astronomers, targeting areas ranging from the origins of our Solar System to the ultimate origin of the Universe.

By their nature, far-infrared observations study processes that are mostly invisible at other wavelengths, such as young stars still embedded in their natal dust clouds or the obscured, rapid assembly episodes of supermassive black holes. Moreover, the 30 to 1000  $\mu\text{m}$  wavelength range includes a rich and diverse

\*Address all correspondence to Duncan Farrah, E-mail: [dfarrah@hawaii.edu](mailto:dfarrah@hawaii.edu)

assembly of diagnostic features. The most prominent of these are as follows:

- Continuum of absorption and emission from dust grains with equilibrium temperatures approximately in the range from 15 to 100 K. The dust is heated by any source of radiation at shorter wavelengths and cools via thermal emission.
- Line emission and absorption from atomic gas, the most prominent lines, including [O I], [N II], [C I], [C II], and several hydrogen recombination lines.
- A plethora of molecular gas features, including but not limited to CO, H<sub>2</sub>O, H<sub>2</sub>CO, HCN, HCO<sup>+</sup>, CS, NH<sub>3</sub>, CH<sub>3</sub>CH<sub>2</sub>OH, CH<sub>3</sub>OH, HNC, HNC, N<sub>2</sub>H<sup>+</sup>, H<sub>3</sub>O<sup>+</sup>, their isotopologs (e.g., <sup>13</sup>CO and H<sub>2</sub><sup>18</sup>O), and deuterated species (e.g., HD, HDO, and DCN).
- Amorphous absorption and emission features arising from pristine and processed ice and crystalline silicates.

These profusion and diversity of diagnostics allow for advances across a wide range of disciplines. We briefly describe four examples in the following paragraphs:

**Planetary systems and the search for life:** Far-infrared continuum observations in multiple bands over 50 to 200  $\mu\text{m}$  measure the size distributions, distances, and orbits of both trans-Neptunian objects<sup>1-4</sup> and zodiacal dust,<sup>5</sup> which give powerful constraints on the early formation stages of our Solar System and of others. Molecular and water features determine the composition of these small bodies, provide the first view of how water pervaded the early Solar System via deuterated species ratios, and constrain how water first arrived on Earth.<sup>6-8</sup> Far-infrared observations are also important for characterizing the atmospheric structure and composition of the gas giant planets and their satellites, especially Titan.

Far-infrared continuum observations also give a direct view of the dynamics and evolution of protoplanetary disks, thus constraining the early formation stages of other solar systems.<sup>9-12</sup> Deuterated species can be used to measure disk masses and ice features, and water lines give a census of water content and thus the earliest seeds for life,<sup>13</sup> whereas the water lines and other molecular features act as biomarkers, providing the primary tool in the search for life beyond Earth.<sup>14,15</sup>

**The early lives of stars:** The cold, obscured early stages of star formation make them especially amenable to study at far-infrared wavelengths. Far-infrared continuum observations are sensitive to the cold dust in star-forming regions, from the filamentary structures in molecular clouds<sup>16</sup> to the envelopes and disks that surround individual pre-main-sequence stars.<sup>17</sup> They, thus, trace the luminosities of young stellar objects and can constrain the masses of circumstellar structures. Conversely, line observations such as [O I], CO, and H<sub>2</sub>O probe the gas phase, including accretion flows, outflows, jets, and associated shocks.<sup>18-24</sup>

For protostars, as their spectral energy distributions (SEDs) peak in the far-infrared, photometry in this regime is required to refine estimates of their luminosities and evolutionary states<sup>25-27</sup> and can break the degeneracy between inclination angle and evolutionary state (at midinfrared and shorter wavelengths, a more evolved protostar seen through its edge-on disk has an SED similar to a deeply embedded protostar viewed from an intermediate angle<sup>28</sup>). With Herschel, it has become possible to measure temperatures deep within starless cores,<sup>29</sup> and young protostars have

been discovered that were only visible at far-infrared and longer wavelengths.<sup>30</sup> These protostars have ages of  $\sim 25,000$  years, only 5% of the estimated protostellar lifetime.

In the T Tauri phase, where the circumstellar envelope disperses, far-infrared observations probe the circumstellar disk.<sup>31</sup> At later phases, the far-infrared traces extrasolar analogs of the Kuiper belt in stars, such as Fomalhaut.<sup>32</sup>

Future far-infrared observations hold the promise of understanding the photometric variability of protostars. Herschel has shown that the far-infrared emission from embedded protostars in Orion could vary by as much as 20% over a timescale of weeks,<sup>33</sup> but such studies are limited by the <4-year lifetime of Herschel. Future observatories will allow for sensitive mapping of entire star-forming regions several times over the durations of their missions. This will enable a resolution to the long-running question of whether protostellar mass accretion happens gradually over a few hundred thousand years or more stochastically as a series of short, episodic bursts.<sup>34</sup>

**The physics and assembly history of galaxies:** The shape of the mid/far-infrared dust continuum is a sensitive diagnostic of the dust grain size distribution in the interstellar medium (ISM) of our Milky Way, and nearby galaxies, which in turn diagnoses energy balance in the ISM.<sup>35-38</sup> Emission and absorption features measure star formation, metallicity gradients, gas-phase abundances and ionization conditions, and gas masses, all independently of extinction, providing a valuable perspective on how our Milky Way, and other nearby galaxies, formed and evolved.<sup>39-43</sup> Continuum and line surveys at far-infrared wavelengths measure both obscured star formation rates and black hole accretion rates over the whole epoch of galaxy assembly, up to  $z \gtrsim 7$ , and are essential to understand why the comoving rates of both star formation and supermassive black hole accretion peaked at redshifts of  $z = 2 - 3$ , when the Universe was only 2 or 3 billion years old and have declined strongly since then.<sup>44,45</sup>

Of particular relevance in this context are the infrared-luminous galaxies in which star formation occurs embedded in molecular clouds, hindering the escape of optical and ultraviolet radiation; however, the radiation heats dust, which reradiates infrared light, enabling star-forming galaxies to be identified and their star formation rates to be inferred. These infrared-luminous galaxies may dominate the comoving star formation rate density at  $z > 1$  and are most optimally studied via infrared observations.<sup>46-50</sup> Furthermore, far-infrared telescopes can study key processes in understanding stellar and black hole mass assemblies, whether or not they depend directly on each other and how they depend on environment, redshift, and stellar mass.<sup>51-53</sup>

**The origins of the Universe:** Millimeter-wavelength investigations of primordial B- and E-modes in the cosmic microwave background (CMB) provide the most powerful observational constraints on the very early Universe, at least until the advent of space-based gravitational-wave observatories.<sup>54,55</sup> However, polarized dusty foregrounds are a pernicious barrier to such observations, as they limit the ability to measure B-modes produced by primordial gravitational waves, and thus to probe epochs up to  $10^{-30}$  s after the Big Bang. Observations at far-infrared wavelengths are the only way to isolate and remove these foregrounds. CMB instruments that also include far-infrared channels thus allow for internally consistent component separation and foreground subtraction.

The maturation of far-infrared astronomy as a discipline has been relatively recent, in large part catalyzed by the advent of

truly sensitive infrared detectors in the early 1990s. Moreover, the trajectory of this development over the past two decades has been steep, going from one dedicated satellite and a small number of other observatories by the mid-1980s to at least eight launched infrared-capable satellites, three airborne facilities, and several balloon/sub-orbital and dedicated ground-based observatories by 2018. New detector technologies are under development, and advances in areas such as mechanical coolers enable those detectors to be deployed within an expanding range of observing platforms. Even greater returns are possible in the future, as far-infrared instrumentation capabilities remain far from the fundamental sensitivity limits of a given aperture.

This recent, rapid development of the far-infrared is reminiscent of the advances in optical and near-infrared astronomy from the 1940s to the 1990s. Optical astronomy has benefited greatly from developments in sensor, computer, and related technologies that had been driven in large part by commercial and other applications, and which by now are fairly mature. Far-infrared astronomers have only recently started to benefit from comparable advances in capability. The succession of rapid technological breakthroughs, coupled with a wider range of observing platforms, means that far-infrared astronomy holds the potential for paradigm-shifting advances in several areas of astrophysics over the next decade.

We here review the technologies and observing platforms for far-infrared astronomy and discuss potential technological developments for those platforms, including in detectors and readout systems; optics; telescope and detector cooling; platform infrastructure on the ground, sub-orbital, and in space; software development; and community cohesion. We aim to identify the technologies needed to address the most important science goals accessible in the far-infrared. We do not review the history of infrared astronomy, as informative historical reviews can be found elsewhere.<sup>56–65</sup> We focus on the 30- to 1000  $\mu\text{m}$  wavelength range, though we do consider science down to  $\sim 10 \mu\text{m}$ , and into the millimeter range, as well. We primarily address the U.S. mid/far-infrared astronomy community; there also exist roadmaps for both European<sup>66</sup> and Canadian<sup>67</sup> far-infrared astronomy, and for THz technology covering a range of applications.<sup>68–70</sup>

## 2 Observatories: Atmosphere-Based

### 2.1 Ground-Based

Far-infrared astronomy from the ground faces the fundamental limitation of absorption in Earth's atmosphere, primarily by water vapor. The atmosphere is mostly opaque in the mid-infrared through far-infrared, with only a few narrow wavelength ranges with modest transmission. This behavior is shown in Fig. 1, which compares atmospheric transmission for ground-based observing, observing from Stratospheric Observatory for Infrared Astronomy (SOFIA) (Sec. 2.2), with two higher altitudes that are accessible by balloon-based platforms. The difficulties of observing from the ground at infrared wavelengths are evident. Moreover, the transmissivity and widths of these windows are heavily weather-dependent. Nevertheless, there do exist spectral windows at 34, 350, 450, 650, and 850  $\mu\text{m}$  with good, albeit weather-dependent transmission at dry, high-altitude sites, with a general improvement toward longer wavelengths. At wavelengths longward of about 1 mm, there are large bands with good transmission. These windows have enabled an

extensive program of ground-based far-infrared astronomy, using both single-dish and interferometer facilities.

#### 2.1.1 Single-dish facilities

Single-dish telescopes dedicated to far-infrared through millimeter astronomy have been operated for over 30 years. Examples include the 15-m James Clerk Maxwell Telescope (JCMT), the 12-m Caltech Submillimeter Observatory (CSO, closed September 2015), the 30-m telescope operated by the Institut de Radioastronomie Millimétrique (IRAM), the 12-m Atacama Pathfinder Experiment (APEX), the 50-m Large Millimeter Telescope (LMT) in Mexico, the 10-m Submillimeter Telescope (formerly the Heinrich Hertz SMT) in Arizona, and the 10-m South Pole Telescope. These facilities have made major scientific discoveries in almost every field of astronomy, from planet formation to high-redshift galaxies. They have also provided stable development platforms, resulting in key advances in detector technology, and pioneering techniques that subsequently found applications in balloon-borne and space missions.

There is an active program of ground-based single-dish far-infrared astronomy, with current and near-future single-dish telescopes undertaking a range of observation types, from wide-field mapping to multiobject wideband spectroscopy. This, in turn, drives a complementary program of technology development. In general, many applications for single-dish facilities motivate development of detector technologies capable of very large pixel counts (Sec. 5.1). Similarly, large pixel counts are envisioned for planned space-based far-infrared observatories, including the Origins Space Telescope (OST; see Sec. 3.3). As far-infrared detector arrays have few commercial applications, they must be built and deployed by the science community itself. Thus, ground-based instruments represent a vital first step toward achieving NASA's long-term far-infrared goals.

We here briefly describe two new ground-based facilities: CCAT-prime (CCAT-p), and the LMT:

**CCAT-p:** It is a 6-m telescope at 5600-m altitude, near the summit of Cerro Chajnantor in Chile.<sup>72</sup> CCAT-p is being built by Cornell University and a German consortium that includes the universities of Cologne and Bonn, and in joint venture with the Canadian Atacama Telescope Corporation. In addition, CCAT-p collaborates with CONICYT and several Chilean universities. The project is funded by a private donor and by the collaborating institutions and is expected to achieve first light in 2021.

The design of CCAT-p is an optimized crossed-Dragone<sup>73</sup> system that delivers an 8-deg field of view (FoV) with a nearly flat image plane. At 350  $\mu\text{m}$ , the FoV with adequate Strehl ratio reduces to about 4 deg. The wavelength coverage of the anticipated instruments will span wavelengths of 350  $\mu\text{m}$  to 1.3 mm. With the large FoV and a telescope surface root mean square of below 10.7  $\mu\text{m}$ , CCAT-p is an exceptional observatory for survey observations. As the 200  $\mu\text{m}$  zenith transmission is  $\geq 10\%$  in the first quartile at the CCAT-p site,<sup>74</sup> a 200  $\mu\text{m}$  observing capability will be added in a second-generation upgrade.

The primary science drivers for CCAT-p are (1) tracing the epoch or reionization via [CII] intensity mapping; (2) studying the evolution of galaxies at high redshifts; (3) investigating dark energy, gravity, and neutrino masses via measurements of the Sunyaev–Zel'dovich effect; and (4) studying the dynamics of the ISM in the Milky Way and nearby galaxies via high spectral resolution mapping of fine structure and molecular lines.

CCAT-p will host two facility instruments: the CCAT Heterodyne Array Instrument (CHAI), and the direct detection

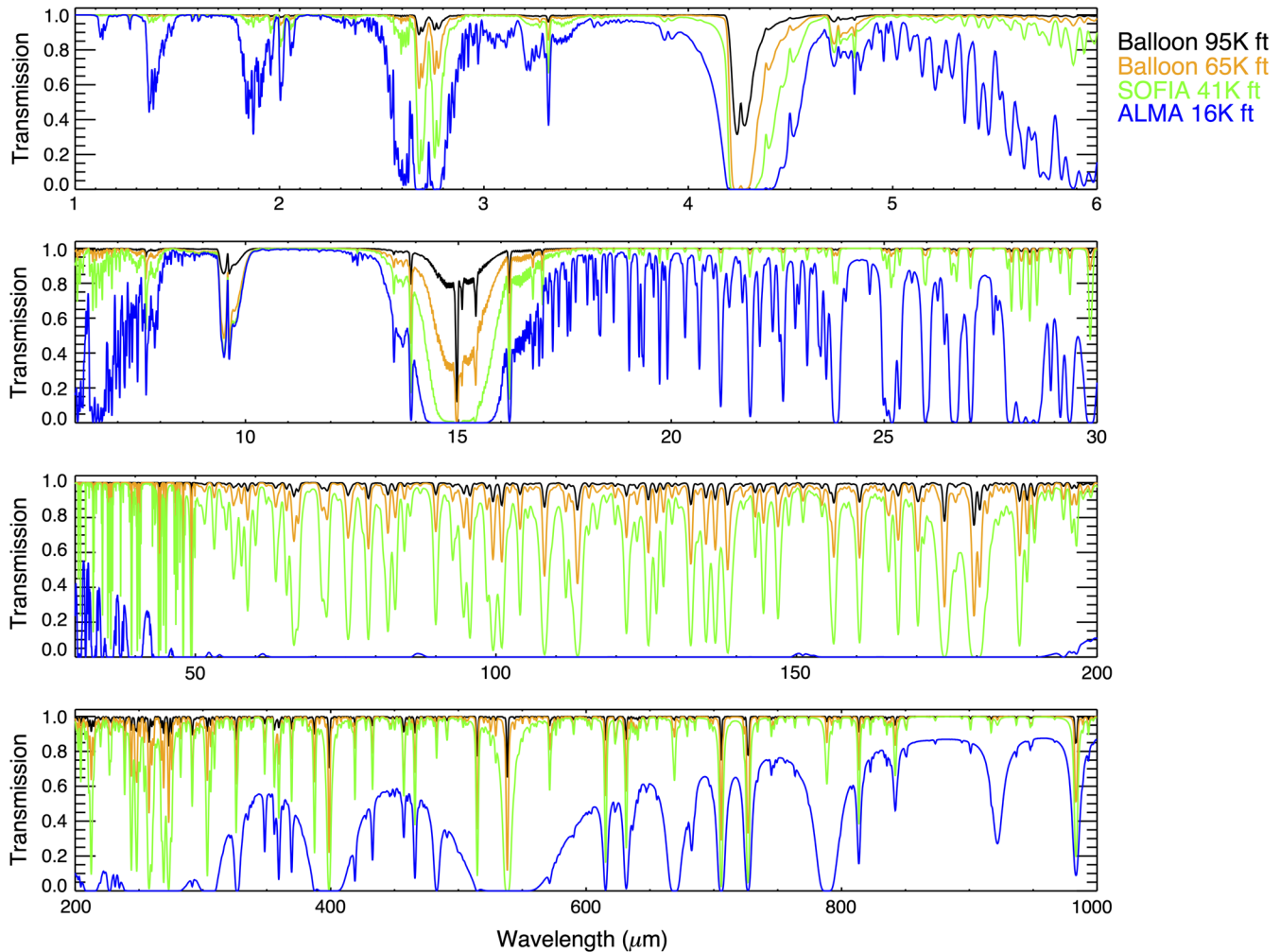


**Fig. 1** Atmospheric transmission over 1 to 1000  $\mu\text{m}$ .<sup>71</sup> The curves for ALMA and SOFIA are computed with a 35-deg telescope zenith angle. The two balloon profiles are computed with a 10-deg telescope zenith angle. The PWV for ALMA (5060 m), SOFIA (12,500 m), and the 19,800- and 29,000-m altitudes are 500, 7.3, 1.1, and 0.2  $\mu\text{m}$ , respectively. The data are smoothed to a resolution of  $R = 2000$ .

instrument Prime-Cam (P-Cam). CHAI is being built by the University of Cologne and will have two focal plane arrays that simultaneously cover the 370- and 610- $\mu\text{m}$  bands. The arrays will initially have  $8 \times 8$  elements, with a planned expansion to 128 elements each. The direct detection instrument P-Cam, which will be built at Cornell University, will encompass seven individual optic tubes. Each tube has a FoV of about 1.3 deg. For first light, three tubes will be available: (1) a four-color, polarization-sensitive camera with 9000 pixels that simultaneously covers the 1400-, 1100-, 850-, and 730- $\mu\text{m}$  bands; (2) a 6000-pixel Fabry-Pérot spectrometer; and (3) a 18,000-pixel camera for the 350- $\mu\text{m}$  band.

**LMT:** The LMT is a 50-m diameter telescope sited at 4600 m on Sierra Negra in Mexico. The LMT has a FoV of  $4'$  and is optimized for maximum sensitivity and small beam size at far-infrared and millimeter wavelengths. It too will benefit from large-format new instrumentation in the coming years. A notable example is TolTEC, a wide-field imager operating at 1.1, 1.4, and 2.1 mm, and with an anticipated mapping speed at 1.1 mm of  $12 \text{ deg}^2 \text{ mJy}^{-2} \text{ hour}^{-1}$  (Table 1). At 1.1 mm, the TolTEC beam size is anticipated to be  $\sim 5''$ , which is smaller than the  $6''$  beam size of the 24  $\mu\text{m}$  Spitzer extragalactic survey

maps. As a result, the LMT confusion limit at 1.1 mm is predicted to be  $\sim 0.1 \text{ mJy}$ , thus making LMT capable of detecting sources with star formation rates below  $100 M_{\odot} \text{ year}^{-1}$  at  $z \sim 6$ . This makes TolTEC an excellent “discovery machine” for high-redshift obscured galaxy populations. As a more general example of the power of new instruments mounted on single-aperture ground-based telescopes, a  $\sim 100$ -object steered-beam multi-object spectrometer mounted on the LMT would exceed the abilities of any current ground-based facility, including Atacama large millimeter/submillimeter array (ALMA), for survey spectroscopy of galaxies, and would require an array of  $\sim 10^{5.5}$  pixels.

### 2.1.2 Interferometry

Interferometry at far-infrared wavelengths is now routinely possible from the ground and has provided order of magnitude improvements in spatial resolution and sensitivity over single-dish facilities. Three major ground-based far-infrared/millimeter interferometers are currently operational. The NOEMA array (the successor to the IRAM Plateau de Bure interferometer) consists of nine 15-m dishes at 2550-m elevation in the French

**Table 1** Selected examples of sensitivities achieved by far-infrared to millimeter-wave detector arrays, along with some required for future missions.

Observatory and instrument	Waveband $\mu\text{m}$	Aperture meters	$T_{\text{aper}}$ K	$T_{\text{det}}$ K	NEP $\text{W}/\sqrt{\text{Hz}}$	Detector technology	Detector count	Notes
JCMT–SCUBA	450/850	15	275	0.1	$2 \times 10^{-16}$	Bolometers	91/36	
JCMT–SCUBA2	450/850	15	275	0.1	$2 \times 10^{-16}$	TES	5000/5000	
APEX–ArTeMis	200 to 450	12	275	0.3	$4.5 \times 10^{-16}$	Bolometers	5760	
APEX–A-MKID	350/850	12	275	0.3	$1 \times 10^{-15}$	KIDs	25,000	
APEX–ZEUS-2	200 to 600	12	275	0.1	$4 \times 10^{-17}$	TES	555	$R \sim 1000$
CSO–MAKO	350	10.4	275	0.2	$7 \times 10^{-16}$	KIDs	500	Low-\$/pix
CSO–Z-Spec	960 to 1500	10.4	275	0.06	$3 \times 10^{-18}$	Bolometers	160	
IRAM–NIKA2	1250/2000	30	275	0.1	$1.7 \times 10^{-17}$	KIDs	4000/1000	
LMT–ToITEC	1100	50	275	0.1	$7.4 \times 10^{-17}$	KIDs	3600	Also at 1.4, 2.1 mm
SOFIA–HAWC+	40 to 250	2.5	240	0.1	$6.6 \times 10^{-17}$	TES	2560	
SOFIA–HIRMES	25 to 122	2.5	240	0.1	$2.2 \times 10^{-17}$	TES	1024	Low-res channel
BLAST–TNG	200 to 600	2.5	240	0.3	$3 \times 10^{-17}$	KIDs	2344	
Herschel–SPIRE	200 to 600	3.5	80	0.3	$4 \times 10^{-17}$	Bolometers	326	
Herschel–PACS bol.	60 to 210	3.5	80	0.3	$2 \times 10^{-16}$	Bolometers	2560	
Herschel–PACS phot.	50 to 220	3.5	80	1.7	$5 \times 10^{-18}$	Photoconductors	800	$R \sim 2000$
Planck–HFI	300 to 3600	1.5	40	0.1	$1.8 \times 10^{-17}$	Bolometers	54	
SuperSpec	850 to 1600	—	N/A	0.1	$1.0 \times 10^{-18}$	KIDs	$\sim 10^2$	$R \lesssim 700$
SPACEKIDS	—	—	N/A	0.1	$3 \times 10^{-19}$	KIDs	1000	
SPICA–SAFARI	34 to 210	3.2	<6	0.05	$2 \times 10^{-19}$		4000	
SPIRIT	25 to 400	1.4	4	0.05	$1 \times 10^{-19}$		$\sim 10^2$	
OST–imaging	100 to 300	5.9 to 9.1	4	0.05	$2 \times 10^{-19}$		$\sim 10^5$	
OST–spectroscopy	100 to 300	5.9 to 9.1	4	0.05	$2 \times 10^{-20}$		$\sim 10^5$	$R \sim 500$

Note: Requirements for the SPICA/SAFARI instrument are taken from Ref. 75. Requirements for the SPIRIT interferometer (whose aperture is the effective aperture diameter for an interferometer with two 1-m diameter telescopes) are taken from Ref. 76.

Alps. The submillimeter array (SMA) consists of eight 6-m dishes on the summit of Mauna Kea in Hawaii (4200-m elevation). Both NOEMA and the SMA are equipped with heterodyne receivers. NOEMA has up to 16-GHz instantaneous bandwidth, whereas the SMA has up to 32 GHz of instantaneous bandwidth (or 16 GHz with dual polarization) with 140-KHz uniform spectral resolution.

Finally, the ALMA is sited on the Chajnantor Plateau in Chile at an elevation of 5000 m. It operates from 310 to 3600  $\mu\text{m}$  in eight bands covering the primary atmospheric windows. ALMA uses heterodyne receivers based on superconductor–insulator–superconductor (SIS) mixers in all bands, with 16-GHz maximum instantaneous bandwidth split across two polarizations and four basebands. ALMA consists of two arrays: the main array of fifty 12-m dishes (of which typically 43 are in use at any one time), and the Morita array (also known as the

Atacama Compact Array), which consists of up to twelve 7-m dishes and up to four 12-m dishes equipped as single-dish telescopes.

At the ALMA site (which is the best of the three ground-based interferometer sites), the precipitable water vapor (PWV) is below 0.5 mm for 25% of the time during the five best observing months (May to September). This corresponds to a transmission of about 50% in the best part of the 900-GHz window (ALMA band 10). In more typical weather (PWV = 1 mm), the transmission at 900 GHz is 25%.

There are plans to enhance the abilities of ALMA over the next decade by (1) increasing the bandwidth, (2) achieving finer angular resolutions, (3) improving wide-area mapping speeds, and (4) improving the data archive. The primary improvement in bandwidth is expected to come from an upgrade to the ALMA correlator, which will effectively double the instantaneous

bandwidth and increase the number of spectral points by a factor of 8. This will improve ALMA's continuum sensitivity by a factor  $\sqrt{2}$  and will make ALMA more efficient at line surveys. Further bandwidth improvements include the addition of a receiver covering 35 to 50 GHz (ALMA band 1, expected in 2022) and 67 to 90 GHz (ALMA band 2). To improve angular resolution, studies are underway to explore the optimal number and placement of antennas for baseline lengths of up to tens of kilometers. Other possible improvements include increasing the number of antennas in the main array to 64, the incorporation of focal-plane arrays to enable wider field imaging, and improvements in the incorporation of ALMA into the global very long baseline interferometry network.

## 2.2 Stratospheric Observatory for Infrared Astronomy

The SOFIA<sup>77</sup> is an effective 2.5-m diameter telescope mounted within a Boeing 747SP aircraft that flies at altitudes of 13,700 m to get above over 99.9% of the Earth's atmospheric water vapor. The successor to the Learjet observatory and NASA's Kuiper Airborne Observatory (KAO), SOFIA saw first light in May 2010, began prime operations in May 2014, and offers ~600 h per year for community science observations.<sup>78</sup> SOFIA is the only existing public observatory with access to far-infrared wavelengths inaccessible from the ground, though CMB polarization studies at millimeter wavelengths have also been proposed from platforms at similar altitudes to SOFIA.<sup>79</sup>

SOFIA's instrument suite can be changed after each flight and is evolvable with new or upgraded instruments as capabilities improve. SOFIA is also a versatile platform, allowing for (1) continuous observations of single targets for up to 5 h, (2) repeated observations over multiple flights in a year, and (3) in principle, observations in the visible though millimeter-wavelength range. Example flight paths for SOFIA are shown in Fig. 2. Each flight path optimizes observing conditions (e.g., elevation, percentage of water vapor, and maximal on-target integration time). SOFIA can be positioned to where the science needs, enabling all-sky access. Annually, SOFIA flies from Christchurch, New Zealand, to enable Southern Hemisphere observations.

SOFIA's instruments include the 5- to 40- $\mu\text{m}$  camera and grism spectrometer FORCAST,<sup>80,81</sup> the high-resolution (up to  $R = \lambda/\Delta\lambda = 100,000$ ) 4.5- to 28.3- $\mu\text{m}$  spectrometer EXES,<sup>82</sup> the 51- to 203- $\mu\text{m}$  integral field spectrometer FIFI-LS,<sup>83</sup> the

50- to 203- $\mu\text{m}$  camera and polarimeter HAWC,<sup>84</sup> and the  $R \sim 10^8$  heterodyne spectrometer GREAT.<sup>85,86</sup> The first-generation HIPO<sup>87</sup> and FLITECAM<sup>88</sup> instruments retired in early 2018. The sensitivities of these instruments as a function of wavelength are presented in Fig. 3. Upgrades to instruments over the past few years have led to new science capabilities, such as adding a polarimetry channel to HAWC (HAWC+<sup>89</sup>), and including larger arrays and simultaneous channels on GREAT (upGREAT<sup>90</sup> & 4GREAT, commissioned in 2017), making it into an efficient mapping instrument. Figure 4 shows early polarimetry measurements from HAWC+.

Given the versatility and long-term nature of SOFIA, there is a continuous need for more capable instruments throughout SOFIA's wavelength range. However, the unique niche of SOFIA, given its warm telescope and atmosphere, the imminent era of the James Webb Space Telescope (JWST), and ever more capable ground-based platforms, is high-resolution spectroscopy. This is presently realized with two instruments (GREAT and EXES). An instrument under development, the

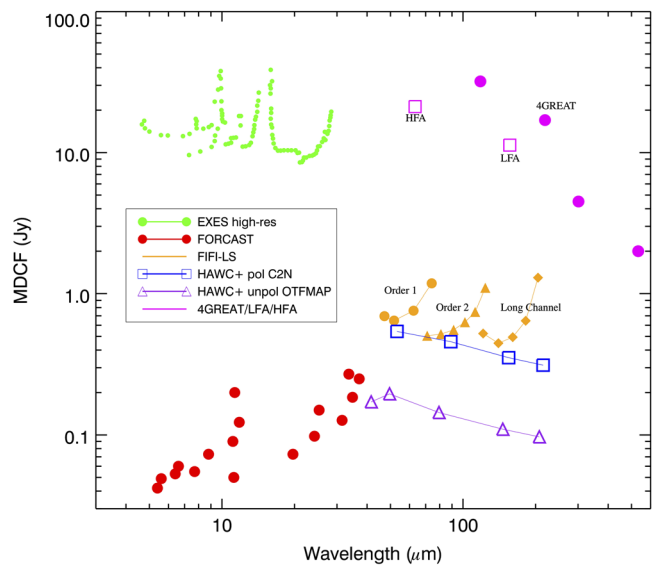


**Fig. 3** The continuum sensitivities, as a function of wavelength, of SOFIA's mid- to far-infrared instrument suite. Shown are the  $4\sigma$  minimum detectable continuum flux densities for point sources in janskys for 900 s of integration time.

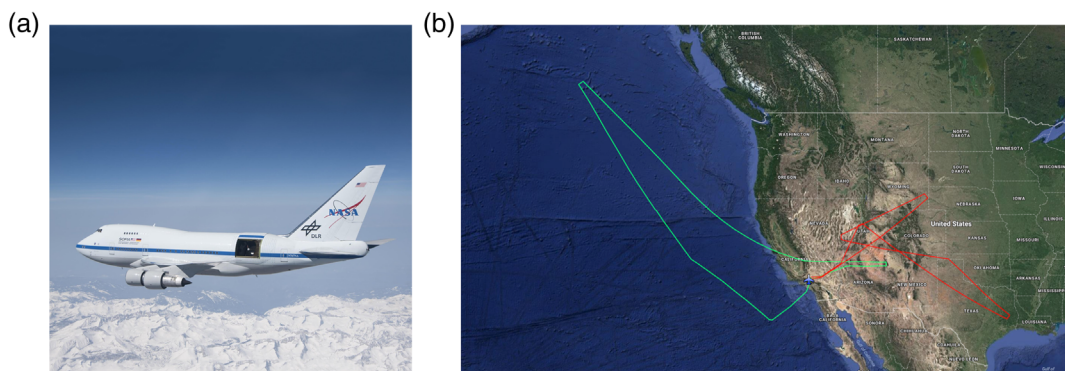


**Fig. 2** (a) The world's largest flying infrared astronomical observatory, SOFIA (Sec. 2.2). (b) Two flight plans, originating from SOFIA's prime base in Palmdale, California. In a typical 8- to 10-h flight, SOFIA can observe one to five targets.

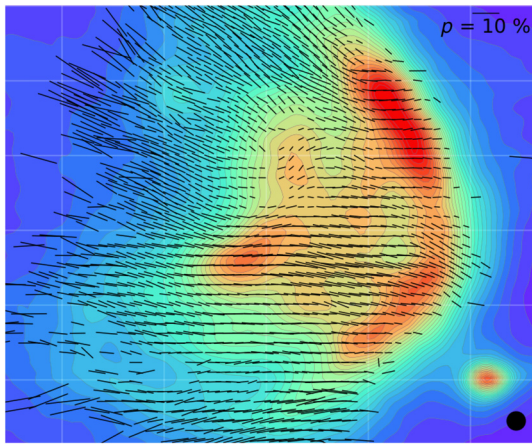


**Fig. 4** The  $89\ \mu\text{m}$  image (intensity represented by color) with polarization measurements at the same wavelength (black lines), taken using HAWC+ on SOFIA, of  $\rho$ -Ophiucus (courtesy of Fabio Santos, Northwestern University, Illinois). The length of the line is the degree of polarization. The SOFIA beam size is  $7.8''$ , which is indicated by the black circle in the lower right.

high-resolution midinfrared spectrometer (HIRMES), scheduled for commissioning in 2019, will enhance SOFIA's high-resolution spectroscopy capabilities. HIRMES covers 25 to  $122\ \mu\text{m}$ , with three spectroscopic modes ( $R = 600$ ,  $R = 10,000$ , and  $R = 100,000$ ), and an imaging spectroscopy mode ( $R = 2000$ ).

As SOFIA can renew itself with new instruments, it provides both new scientific opportunities and maturation of technology to enable future far-infrared space missions. SOFIA offers a 20-kVA cryocooler with two compressors capable of servicing two cold heads. The heads can be configured to operate two cryostats or in parallel within one cryostat to increase heat-pumping capacity, with second-stage cooling capacity of  $Q2 \geq 800\ \text{mW}$  at 4.2 K and first-stage cooling capacity of  $Q1 \geq 15\ \text{W}$  at 70 K. Instruments aboard SOFIA can weigh up to 600 kg, excluding the instrument electronics in the counterweight rack and PI Rack (s), and can draw power up to 6.5 kW. Their volume is limited by the aircraft's door access and must fit within the telescope assembly constraints.

Capabilities that would be invaluable in a next-generation SOFIA instrument include, but are not limited to, the following:

- Instruments with  $\geq 100$  beams that enable low- to high-resolution spectroscopy (up to sub- $\text{km s}^{-1}$  velocity resolution) from 30 to  $600\ \mu\text{m}$ . This would enable large-area, velocity-resolved spectral line maps of key fine-structure transitions in giant molecular clouds and complement the wavelengths accessible by JWST and ground-based telescopes. The current state of the art in SOFIA is upGREAT LFA: 14 beams, 44 kHz channel spacing.
- Medium- to wide-band imaging and imaging polarimetry from 30 to  $600\ \mu\text{m}$ , with  $10^{4-5}$  pixels and FoVs of tens of arcminutes. The current state of the art in SOFIA is HAWC+, with a  $64 \times 40$  pixel array and a largest possible FoV of  $8.0' \times 6.1'$ .
- High spectral resolution ( $R = 4000$  to 100,000) 5 to  $30\ \mu\text{m}$  mapping spectroscopy with factor  $\geq 3$  and greater observation efficiency and sensitivity than EXES. This would complement JWST, which observes in the same

wavelength range but at  $R < 3300$  with the midinfrared instrument (MIRI). Such an instrument on SOFIA could then identify the molecular lines that JWST may detect but not spectrally resolve. The current state of the art in SOFIA is EXES, with  $R \sim 100,000$  and sensitivities ( $10\sigma$ , 100s) of  $10\ \text{Jy}$  at  $10\ \mu\text{m}$ ;  $20\ \text{Jy}$  at  $20\ \mu\text{m}$  (NELB,  $10\sigma$ , 100 s:  $1.4 \times 10^{-6}\ \text{W m}^{-2}\ \text{sr}^{-1}$  at  $10\ \mu\text{m}$ ;  $7.0 \times 10^{-7}\ \text{W m}^{-2}\ \text{sr}^{-1}$  at  $20\ \mu\text{m}$ ).

- High-resolution ( $R \sim 100,000$ ) spectroscopy at 2.5 to  $8\ \mu\text{m}$ , to identify several gas-phase molecules. These molecules are not readily accessible from the ground (Fig. 1) and cannot be reliably identified by JWST as its near-infrared spectrometer NIRSpec only goes up to  $R = 2700$ . Currently, SOFIA does not have such an instrument.
- A wide-field, high-resolution integral-field spectrometer covering 30 to  $600\ \mu\text{m}$ . This would allow rapid, large-area, spectrally-resolved mapping of fine structure lines in the Milky Way, and integral field-spectroscopy of nearby galaxies. The current state of the art in SOFIA is FIFI-LS, with FoV  $12''$  over 115 to  $203\ \mu\text{m}$  and with FoV  $6''$  over 51 to  $120\ \mu\text{m}$ .
- A broadband, wide-field, multiobject spectrograph, with resolution  $R = 10^3 - 10^4$  and up to 1000 beams, over 30 to  $300\ \mu\text{m}$ . Such an instrument could map the velocity fields in galaxies or star-forming regions with enough beams to allow mapping of complex regions. SOFIA currently does not have any multiobject spectroscopic capability.
- An instrument to characterize exoplanet atmospheres: an ultraprecise spectroimager optimized for bands not available from the ground and with sufficient FoV to capture simultaneous reference stars to decorrelate time-variable effects. JWST's and European Space Agency (ESA)'s ARIEL mission will also contribute to this science. SOFIA currently does not have this capability. However, during early science with first-generation instruments, SOFIA demonstrated that it could measure atmospheres with transiting exoplanets with performance similar to existing ground assets.
- A mid/far-infrared spectropolarimeter. Spectropolarimetric observations of the relatively unexplored  $20\ \mu\text{m}$  silicate feature with SOFIA would be a unique capability and allow for, e.g., new diagnostics of the chemistry and composition of protoplanetary disks. SOFIA currently does not have a polarimetry shortward of  $50\ \mu\text{m}$ .

Other possible improvements to the SOFIA instrument suite include: (1) upgrading existing instruments (e.g., replacing the FIFI-LS germanium photoconductors to achieve finer spatial sampling through higher multiplexing factors), and (2) instruments that observe in current gaps in SOFIA wavelength coverage (e.g., 1 to  $5\ \mu\text{m}$ , 90 to  $150\ \mu\text{m}$ , and 210 to  $310\ \mu\text{m}$ ).

More general improvements include the ability to swap instruments faster than a 2-day timescale, or the ability to mount multiple instruments. Mounting multiple instruments improves observing efficiency if both instruments can be used on the same source, covering different wavelengths or capabilities. This would also allow for flexibility to respond to targets of opportunity, time domain, or transient phenomena, and increase flexibility as a development platform to raise technology readiness levels (TRLs<sup>91,92</sup>) of key technologies.

### 2.3 Scientific Ballooning

Balloon-based observatories allow for observations at altitudes of up to  $\sim 40,000$  m (130,000 ft). At these altitudes,  $<1\%$  of the atmosphere remains above the instrument, with negligible water vapor. Scientific balloons, thus, give access, relatively cheaply, to infrared discovery space that is inaccessible to any ground-based platform, and in some cases even to SOFIA. For example, several key infrared features are inaccessible even at aircraft altitudes (Fig. 1), including low-energy water lines and the [N II]  $122\text{-}\mu\text{m}$  line. Scientific ballooning is, thus, a valuable resource for infrared astronomy. Both standard balloons, with flight times of  $\sim 24$  h, and long duration balloons (LDBs) with typical flight times of 7 to 15 days (though flights have lasted as long as 55 days) have been used. Balloon projects include the Balloon-borne Large Aperture Submillimeter Telescopes (BLAST<sup>93–95</sup>), PILOT,<sup>96</sup> the Stratospheric Terahertz Observatory<sup>97</sup> (Fig. 5), and Far-Infrared Interferometric Telescope Experiment (FITE)<sup>99</sup> and Balloon Experimental Twin Telescope for Infrared Interferometry (BETTII),<sup>100</sup> both described in Sec. 4.1. Approved future missions include GUSTO, scheduled for launch in 2021. With the development of ultra-LDBs (ULDBs), with potential flight times of over 100 days, new possibilities for far-infrared observations have become available.

A further advantage of ballooning, in a conceptually similar manner to SOFIA, is that the payloads are typically recovered and available to reflly on  $\sim 1$ -year timescales, meaning that balloons are a vital platform for technology development and TRL raising. For example, far-infrared direct-detector technology shares many common elements (detection approaches, materials, and readouts) with CMB experiments, which are conducted on the ground,<sup>101–103</sup> from balloons,<sup>104–106</sup> and in space. These platforms have been useful for developing bolometer and read-out technology applicable to the far-infrared.

All balloon projects face challenges, as the payload must include the instrument and all of the ancillary equipment needed to obtain scientific data. For ULDBs, however, there are two additional challenges:

**Payload mass:** Whereas zero-pressure balloons (including LDBs) can lift up to about 2700 kg, ULDBs have a mass limit of about 1800 kg. Designing a payload to this mass limit is non-trivial, as science payloads can have masses in excess of

2500 kg. For example, the total mass of the GUSTO gondola is estimated to be 2700 kg.

**Cooling:** All far-infrared instruments must operate at cryogenic temperatures. Liquid cryogenics have been used for instruments on both standard and LDBs, with additional refrigerators (e.g.,  $^3\text{He}$ , adiabatic demagnetization) to bring detector arrays down to the required operating temperatures, which can be as low as 100 mK. These cooling solutions typically operate on timescales commensurate with LDB flights. For the ULDB flights, however, it is not currently possible to achieve the necessary cryogenic hold times. Use of mechanical coolers to provide first-stage cooling would solve this problem, but current technology does not satisfy the needs of balloon missions. Low-cost cryocoolers for use on the ground are available, but have power requirements that are hard to meet on balloons, which currently offer total power of up to about 2.5 kW. Low-power cryocoolers exist for space use, but their cost (typically  $\gtrsim 1\text{M}$ ) does not fit within typical balloon budgets. Cryocoolers are discussed in detail in Sec. 5.5.

In addition to addressing the challenges described above, there exist several avenues of development that would enhance many balloon experiments. Three examples are as follows:

- Large aperture, lightweight mirrors for 50 to 1000  $\mu\text{m}$  observing (see also Sec. 5.7).
- Common design templates for certain subsystems, such as star cameras, though attempting to standardize on gondola designs would be prohibitively expensive as most systems are still best implemented uniquely for each payload.
- Frameworks to enhance the sharing of information, techniques, and approaches. Although balloon experiments are in general more “PI-driven” than facility-class observatories (as much of the hardware is custom-built for each flight), there does exist a thriving user community in ballooning, within which information and ideas are shared. Nurturing the sharing of information would help in developing this community further. The PI-driven balloon missions also serve as pathfinders for larger facilities, as was the case for BLAST and Herschel, and thus may lay the groundwork for a future “general observatory”-class balloon mission.

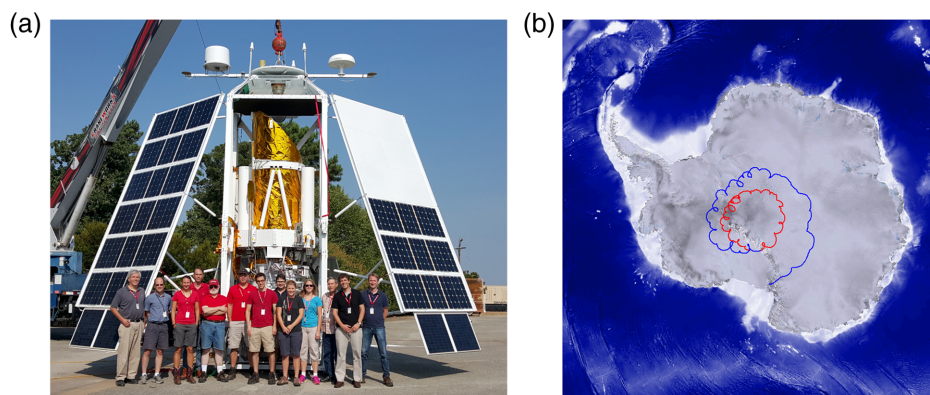


**Fig. 5** (a) The STO balloon observatory and science team, after the successful hang test in the Columbia Scientific Balloon Facility in Palestine, Texas, in August 2015. This image originally appeared on the Netherlands Institute for Space Research (SRON) STO website. (b) The second science flight of the STO took place from McMurdo in Antarctica on December 8, 2016, with a flight time of just under 22 days. This image was taken from Ref. 98.

## 2.4 Short Duration Rocket Flights

Sounding rockets inhabit a niche between high-altitude balloons and fully orbital platforms, providing 5 to 10 min of observation time above the Earth's atmosphere, at altitudes of 50 to ~1500 km. They have been used for a wide range of astrophysical studies, with a heritage in infrared astronomy stretching back to the 1960s.<sup>107–110</sup>

Though an attractive way to access space for short periods, the mechanical constraints of sounding rockets are limiting in terms of size and capability of instruments. However, sounding rockets observing in the infrared are flown regularly,<sup>111</sup> and rockets are a viable platform for both technology maturation and certain observations in the far-infrared. In particular, measurements of the absolute brightness of the far-infrared sky, intensity mapping, and development of ultra-low-noise far-infrared detector arrays are attractive applications of this platform.

Regular access to sounding rockets is now a reality, with the advent of larger, more capable Black Brant XI vehicles to be launched from southern Australia via the planned Australian NASA deployment in 2019–2020. Similarly, there are plans for recovered flights from Kwajalein Atoll using the recently tested NFORCE water recovery system. Long-duration sounding rockets capable of providing limited access to orbital trajectories and >30-min observation times have been studied,<sup>112</sup> and NASA is continuing to investigate this possibility. However, no missions using this platform are currently planned, and as a result the associated technology development is moving slowly.

## 3 Observatories: Space-Based

All atmospheric-based observing platforms, including SOFIA and balloons, suffer from photon noise from atmospheric emission. Even at balloon altitudes, of order 1% emissivity on average through the far-infrared remains from residual water vapor, which can contaminate astrophysical water lines, unless they are shifted by velocities of at least a few tens of  $\text{km s}^{-1}$ . The telescope optics is another source of loading, with an unavoidable 2% to 4% emissivity. Though the total emissivity can be <5%, these ambient-temperature (~250 K) background sources dominate that of the zodiacal and galactic dusts. Space-based platforms are, thus, for several paths of inquiry, the only way to perform competitive infrared observations.

There exists a rich history of space-based mid/far-infrared observatories (Fig. 6), including Infrared Atmospheric Sounder (IRAS),<sup>113</sup> Midcourse Space Experiment,<sup>114</sup> the Infrared Telescope in Space,<sup>115</sup> Infrared Space Observatory (ISO)<sup>116</sup> Submillimeter Wave Astronomy Satellite (SWAS)<sup>117</sup> Odin,<sup>118</sup> Akari,<sup>119</sup> Herschel,<sup>120</sup> Wide-Field Infrared Survey Explorer,<sup>121</sup> and Spitzer.<sup>122</sup> Far-infrared detector arrays are also used on space-based CMB missions, with past examples, including Planck,<sup>123</sup> Wilkinson microwave anisotropy probe,<sup>124</sup> and Cosmic Background Explorer,<sup>125,126</sup> as well as concepts, such as primordial inflation explorer,<sup>127</sup> LiteBIRD,<sup>128</sup> and Cosmic Origins Explorer.<sup>129</sup>

It is notable, however, that the performance of many past and present facilities is limited by thermal emission from telescope optics (Fig. 7). The comparison between infrared telescopes operating at 270 K and temperatures of a few kelvins is



**Fig. 6** Four examples of satellites that observe at mid/or far-infrared wavelengths (Sec. 3). (a) Spitzer and Herschel and (b) Planck and JWST, which also use V-groove radiators (thermal shields) to achieve passive cooling up to <40 K.

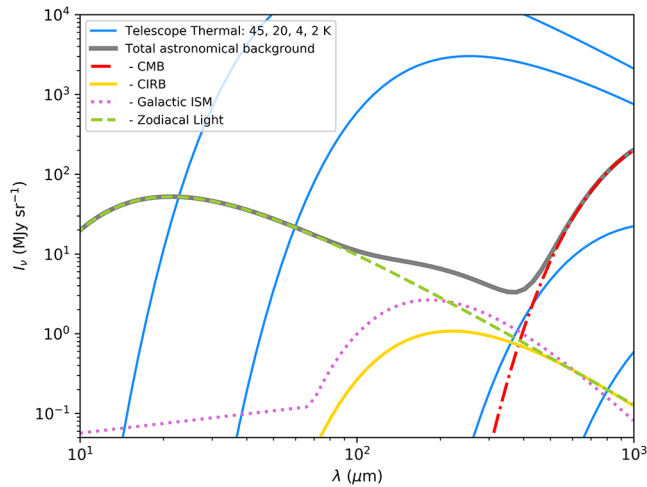


**Fig. 7** A comparison between the primary astrophysical continuum backgrounds at infrared wavelengths (the Cosmic Microwave Background,<sup>130</sup> the Cosmic Infrared Background,<sup>126</sup> Galactic ISM emission,<sup>131</sup> and Zodiacal emission from interplanetary dust<sup>132</sup>) and representative thermal emission from telescope optics at three temperatures, assuming uniform thermal emissivity of 4%. The astrophysical backgrounds assume observations outside the atmosphere toward high ecliptic and galactic latitudes, and at a distance of 1 AU from the Sun. The advantages of “cold” telescope optics are apparent; at 300  $\mu\text{m}$  the thermal emission from a 4-K telescope is 5 orders of magnitude lower than for a telescope at 45 K and enables the detection of the CIRB, Galactic ISM, and zodiacal light.

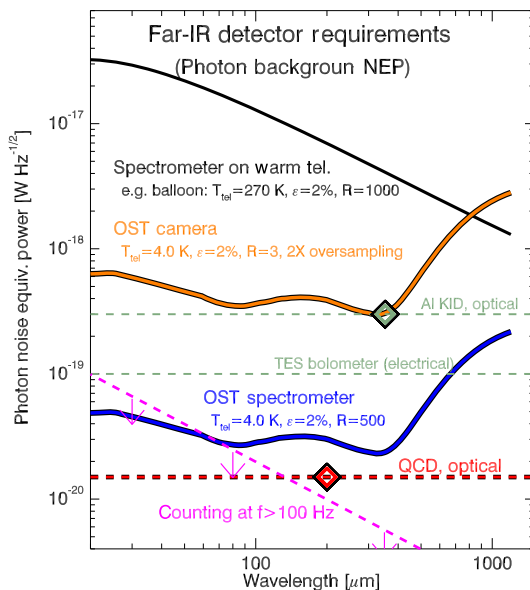


**Fig. 8** Detector sensitivity requirements to meet photon background levels in the far-infrared. With a cryogenic space telescope, the fundamental limits are the zodiacal dust and galactic cirrus emission, and the photon noise-level scales as the square root of the bandwidth. Of particular interest is the requirement for moderate-resolution dispersive spectroscopy (blue). Also shown are detector sensitivity measurements for the TES, KID, and QCD technologies described in Sec. 5.1. The magenta dotted line shows the photon-counting threshold at 100 Hz: a device that can identify individual photons at this rate (photon counting) at high efficiency is limited by the dark count rate rather than classical NEP.

analogous to the comparison between the sky brightness during the day and at night in the optical. Even with Herschel and its  $\sim 85$  K telescope, the telescope emission was the dominant noise term for both its Photodetector Array Camera and Spectrometer (PACS<sup>133</sup>) and Spectral and Photometric Imaging Receiver (SPIRE<sup>134</sup>). Thus, the ultimate scientific promise of the far-infrared is in orbital missions with actively cooled telescopes and instruments. Cooling the telescope to a few kelvins effectively eliminates its emission through most of the far-infrared band. When combined with appropriate optics and instrumentation, this results in orders-of-magnitude improvement in discovery speed over what is achievable from atmospheric-based platforms (Figs. 8 and 9). A “cold” telescope can bring sensitivities at observed frame of 30 to 500  $\mu\text{m}$  into parity with those at shorter (JWST) and longer (ALMA) wavelengths.

A further limiting factor is source confusion—the fluctuation level in image backgrounds below which individual sources can no longer be detected. Unlike instrument noise, confusion noise cannot be reduced by increasing integration time. Source confusion can arise from both smooth diffuse emission and fluctuations on scales smaller than the beam size of the telescope. Outside of the plane of the Milky Way, the primary contributors to source confusion are structures in Milky Way dust emissions, individually undetected extragalactic sources within the telescope beam, and individually detected sources that are blended with the primary source. Source confusion is, thus, a strong function of the location on the sky of the observations, the telescope aperture, and observed wavelength. Source confusion is a concern for all previous and current single-aperture infrared

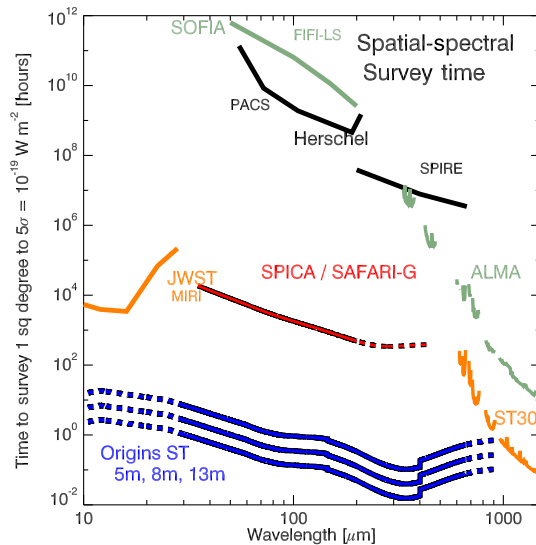


**Fig. 9** A comparison of the times required to perform a blank-field spatial-spectral survey reaching a depth of  $10^{-19} \text{ W m}^{-2}$  over one square degree, as a function of wavelength, for various facilities. This figure uses current estimates for sensitivity, instantaneous bandwidth covered, telescope overheads, and instantaneous spatial coverage on the sky. The OST curves assume  $R = 500$  grating spectrometers with 60 to 200 beams (depending on wavelength), 1:1.5 instantaneous bandwidth. Pixels are assumed to operate with a NEP of  $2 \times 10^{-20} \text{ W Hz}^{-1/2}$ . The SPICA/SAFARI-G curve is for a 2.5-m telescope with  $R = 300$  grating spectrometer modules with four spatial beams, and detector arrays with a NEP of  $2 \times 10^{-19} \text{ W Hz}^{-1/2}$ . ST30 is a ground-based 30-m telescope with 100 spectrometer beams, each with 1:1.5 bandwidth, ALMA band-averaged sensitivity, and survey speed based on 16 GHz bandwidth in the primary beam.

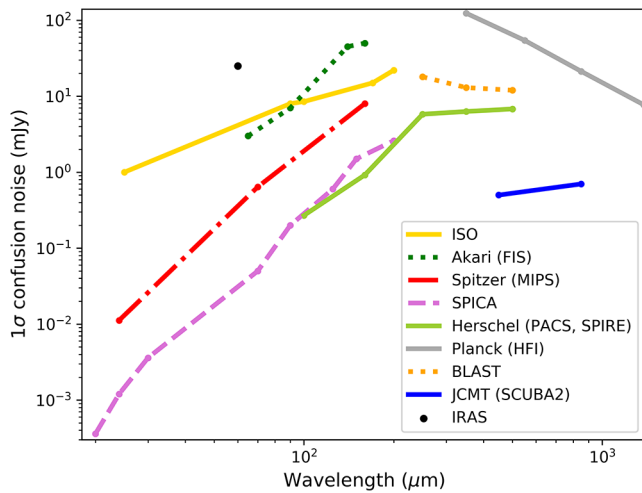


**Fig. 10** A summary of literature estimates of confusion noise levels for selected telescopes. The confusion levels are not calculated with a uniform set of assumptions, but are comparable in that they are applicable to regions of sky away from the galactic plane, and with low galactic cirrus emission. Shown are estimates for IRAS at  $60\ \mu\text{m}$ ,<sup>135</sup> ISO,<sup>136</sup> Spitzer,<sup>137</sup> Herschel,<sup>138</sup> Planck,<sup>139,140</sup> Akari, SPICA,<sup>141</sup> and JCMT. The confusion limits for interferometers such as ALMA or the SMA are all below  $10^{-6}$  mJy.

telescopes, especially space-based facilities whose apertures are modest compared to ground-based facilities. A summary of the confusion limits of some previous infrared telescopes is given in Fig. 10.

A related concept is line confusion, which is caused by the blending and overlapping of individual lines in spectral line surveys. Although this is barely an issue in, e.g., H I surveys as the 21-cm H I line is bright and isolated,<sup>142</sup> it is potentially a pernicious source of uncertainty at far-infrared wavelengths, where there are a large number of bright spectral features. This is true in galactic studies<sup>143</sup> and in extragalactic surveys. Carefully chosen spatial and spectral resolutions are required to minimize line confusion effects.<sup>144</sup>

Several approaches have been adopted to extract information on sources below the standard confusion limit. They include detection methods applied to single-band maps,<sup>145</sup> the use of prior positional information from higher spatial resolution images to deconvolve single far-infrared sources,<sup>146,147</sup> and combination of priors on positions with priors from SED modeling.<sup>148,149</sup> Finally, the spatial-spectral surveys from upcoming facilities such as SAFARI on Space Infrared Telescope for Cosmology and Astrophysics (SPICA) or the OST Survey Spectrometer on the OST should push significantly below the classical confusion limit by including spectral information to break degeneracies in the third spatial dimension.<sup>150</sup>

There are two further challenges that confront space-based far-infrared observatories, which are unfamiliar to suborbital platforms:

**Dynamic range:** Moving to “cold” telescopes, sensitivity is limited only by the far-infrared sky background. We enter a regime where the dominant emission arises from the sources under study, and the sky has genuinely high contrast. This imposes a new requirement on the detector system—to observe the full range of source brightness—that is simple from suborbital platforms but challenging for cooled space-based platforms, as the saturation powers of currently proposed high-resolution detector arrays are within  $\sim 2$  orders of magnitude

of their noise equivalent power (NEP is, briefly, the input signal power that results in a signal-to-noise ratio of unity in a 1-Hz bandwidth—the minimum detectable power per square root of bandwidth. Thus, a lower NEP is better. In-depth discussions of the concept of NEP can be found in Refs. 151–153.). This would limit observations to relatively faint sources. Dynamic range limitations were even apparent for previous-generation instruments such as the multiband imaging photometer onboard Spitzer and PACS onboard Herschel, with saturation limits at  $70\ \mu\text{m}$  of 57 and 220 Jy, respectively. Thus, we must either design detector arrays with higher dynamic range or populate the focal plane with detector arrays, each suited to part of the range of intensities.

**Interference:** The susceptibility of cooled detector arrays to interference from ionizing radiation in space was noted in the development of microcalorimeter arrays for x-ray telescopes.<sup>154–156</sup> Moreover, this susceptibility was clearly demonstrated by the bolometers on Planck. An unexpectedly high rate and magnitude of ionizing radiation events were a major nuisance for this mission, requiring corrections to be applied to nearly all of the data. Had this interference been a factor of  $\sim 2$  worse, it would have caused significant loss of science return from Planck. Techniques are being developed and demonstrated to mitigate this interference for x-ray microcalorimeters by the addition of a few-micron-thick layer of gold on the back of the detector frame. It is likely that a similar approach can mitigate interference in high-resolution far-infrared detector arrays as well. Moreover, work on reducing interference in far-infrared detector arrays is being undertaken in the SPACEKIDS program (Sec. 5.1.2).

NASA, the ESA, and the Japan Aerospace Exploration Agency (JAXA), in collaboration with astronomers and technologists around the world, are studying various options for cryogenic space observatories for the far-infrared. There are also opportunities to broaden the far-infrared astrophysics domain to new observing platforms. We give an overview of these space-based observing platforms in the following sections. We do not address the JWST, as comprehensive overviews of this facility are given elsewhere.<sup>157</sup> We also do not review non-U.S./E.U. projects, such as Millimetron/Spektr-M.<sup>158,159</sup>

### 3.1 Space Infrared Telescope for Cosmology and Astrophysics

First proposed by JAXA scientists in 1998, the SPICA<sup>160–164</sup> garnered worldwide interest due to its sensitivity in the mid- and far-infrared, enabled by the combination of the actively cooled telescope and the sensitive far-infrared detector arrays. Both ESA and JAXA have invested in a concurrent study, and an ESA–JAXA collaboration structure has gelled. ESA will provide the 2.5-m telescope, science instrument assembly, satellite integration and testing, and the spacecraft bus. JAXA will provide the passive and active cooling systems (supporting a telescope cooled to below 8 K), cryogenic payload integration, and launch vehicle. JAXA has indicated commitment to their portion of the collaboration, and the ESA selected SPICA as one of the three candidates for the Cosmic Visions M5 mission. The ESA phase-A study is underway now, and the downselect among the three missions will occur in 2021. Launch is envisioned for 2031. An example concept design of SPICA is shown in Fig. 11.

SPICA will have three instruments. JAXA’s SPICA MIRI will offer imaging and spectroscopy from 12 to  $38\ \mu\text{m}$ . It is designed to complement JWST-MIRI with wide-field mapping (broadband and spectroscopic),  $R \sim 30,000$  spectroscopy with

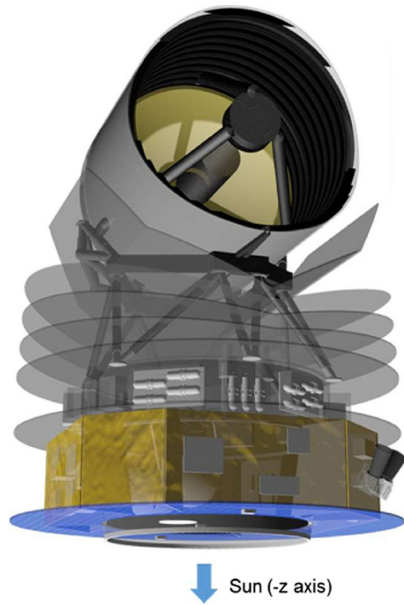


**Fig. 11** A concept image for the proposed SPICA satellite (Sec. 3.1).

an immersion grating, and an extension to  $38\ \mu\text{m}$  with antimony-doped silicon detector arrays. A polarimeter from a French-led consortium will provide dual-polarization imaging in 2 to 3 bands using high-impedance semiconductor bolometers similar to those developed for Herschel-PACS, but modified for the lower background and to provide differential polarization. A sensitive far-infrared spectrometer, SAFARI, is being provided by an SRON-led consortium.<sup>165,166</sup> It will provide full-band instantaneous coverage over 35 to  $230\ \mu\text{m}$ , with a longer wavelength extension under study, using four  $R = 300$  grating modules. A Fourier transform module, which can be engaged in front of the grating modules, will offer a boost to the resolving power, up to  $R = 3000$ . A U.S. team is working in collaboration with the European team and aims to contribute detector arrays and spectrometer modules to SAFARI<sup>167</sup> through NASA's Mission of Opportunity.

### 3.2 Probe-Class Missions

Recognizing the need for astronomical observatories beyond the scope of Explorer-class missions but with a cadence more rapid than flagship observatories, such as the Hubble Space Telescope (HST), JWST, and the Wide-Field Infrared Survey Telescope, NASA announced a call for Astrophysics Probe concept studies in 2017. Ten probe concepts were selected in Spring 2017 for 18-month studies. Probe study reports will be submitted to NASA and to the Astro 2020 Decadal Survey to advocate for the creation of a probe observatory line, with budgets of \$400 million to \$1 billion.

Among the probe concepts under development is the far-infrared Galaxy Evolution Probe (GEP), led by the University of Colorado Boulder and the Jet Propulsion Laboratory. The GEP concept is a two-meter-class, mid/far-infrared observatory with both wide-area imaging and follow-up spectroscopy capabilities. The primary aim of the GEP is to understand the roles of star formation and black hole accretion in regulating the growth of stellar and black hole mass. In the first year of the GEP mission, it will detect  $\geq 10^6$  galaxies, including  $\geq 10^5$  galaxies at  $z > 3$ , beyond the peak in redshift of cosmic star formation, by surveying several hundred square degrees of the sky. A unique

and defining aspect of the GEP is that it will detect galaxies by bands of rest-frame midinfrared emission from polycyclic aromatic hydrocarbons (PAHs), which are indicators of star formation, while also using the PAH emission bands and silicate absorption bands to measure photometric redshifts.

The GEP will achieve these goals with an imager using  $\sim 25$  photometric bands spanning  $10\ \mu\text{m}$  to at least  $230\ \mu\text{m}$ , giving a spectral resolution of  $R \simeq 8$  (Fig. 12). Traditionally, an imager operating at these wavelengths on a 2-m telescope would be significantly confusion-limited, especially at the longer wavelengths (see e.g., the discussion in the introduction to Sec. 3). However, the combination of many infrared photometric bands, and advanced multi-wavelength source extraction techniques, will allow the GEP to push significantly below typical confusion limits. The GEP team is currently simulating the effects of confusion on their surveys, with results expected in early 2019. The imaging surveys from the GEP will, thus, enable new insights into the roles of redshift, environment, luminosity, and stellar mass in driving obscured star formation and black hole accretion over most of the cosmic history of galaxy assembly.

In the second year of the GEP survey, a grating spectrometer will observe a sample of galaxies from the first-year survey to identify embedded active galactic nucleus (AGN). The current concept for the spectrometer includes four or five diffraction gratings with  $R \simeq 250$ , and spectral coverage from  $23\ \mu\text{m}$  to at least  $190\ \mu\text{m}$ . The spectral coverage is chosen to enable detection of the high-excitation [NeV]  $24.2\text{-}\mu\text{m}$  line, which is an AGN indicator, over  $0 < z < 3.3$ , and the [OI]  $63.2\text{-}\mu\text{m}$  line, which is predominantly a star formation indicator, over  $0 < z < 2$ .

Recent advances in the far-infrared detector array technology have made an observatory such as the GEP feasible. It is now possible to fabricate large arrays of sensitive kinetic inductance detectors (KIDs; see Sec. 5.1.2) that have a high-frequency multiplex factor. The GEP concept will likely employ Silicon blocked impurity band arrays (similar to those used on JWST-MIRI) for wavelengths from 10 to  $24\ \mu\text{m}$  and KIDs at wavelengths longer than  $24\ \mu\text{m}$ . Coupled with a cold ( $\sim 4\ \text{K}$ ) telescope such that the GEP's sensitivity would be photon-limited by astrophysical backgrounds (Fig. 7), the GEP will detect the progenitors of Milky Way-type galaxies at  $z = 2 (\geq 10^{12} L_{\odot})$ . Far-infrared KID sensitivities have reached the NEPs required for the GEP imaging to be background-limited ( $3 \times 10^{-19}\ \text{W/Hz}^{-0.5}$ <sup>169,170</sup>), although they would need to be lowered further, by a factor of at least 3, for the spectrometer to be background-limited. The GEP would serve as a pathfinder for the OST (Sec. 3.3), which would have a greater reach in redshift by virtue of its larger telescope. SOFIA and balloons will also serve as technology demonstrators for the GEP and OST.

The technology drivers for the GEP center on detector array size and readout technology. Whereas KID arrays with  $10^4 - 10^5$  pixels are within reach, investment must be made for the development of low-power-consumption readout technology (Sec. 5.1.4). Large KID (or other direct-detection technology) arrays with low-power readouts on SOFIA and balloons would raise their respective TRLs, enabling the GEP and OST.

### 3.3 Origins Space Telescope

As part of the preparations for the 2020 Decadal Survey, NASA is supporting four studies of flagship astrophysics missions. One of these studies is for a far-infrared observatory. A Science and Technology Definition Team (STDT) is pursuing this study with support from NASA Goddard Space Flight Center (GSFC). The

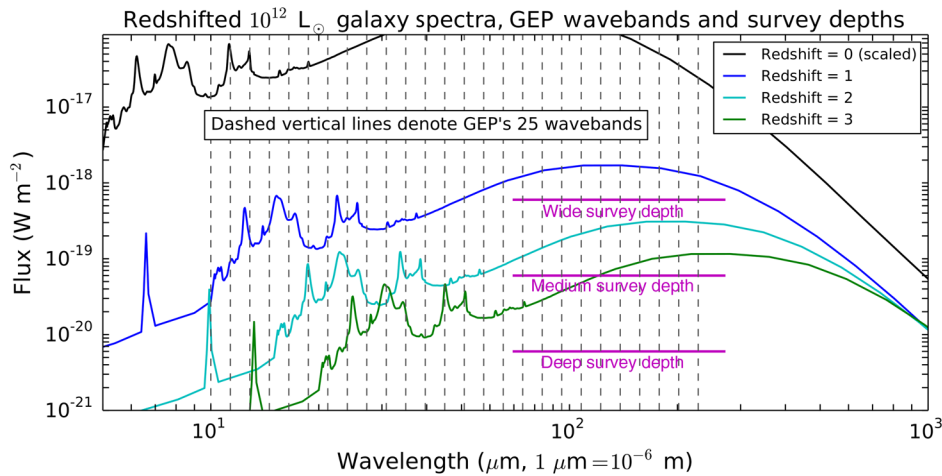


**Fig. 12** A mid/far-infrared galaxy spectrum, the GEP photometric bands, and notional survey depths. The spectrum is a model of a star-forming galaxy<sup>168</sup> exhibiting strong PAH features and far-infrared dust continuum emission. The black spectrum is the galaxy at a redshift of  $z = 0$ , but scaled vertically by a luminosity distance corresponding to  $z = 0.1$  to reduce the plot range. The same spectrum is shown at redshifts  $z = 1, 2$ , and  $3$ . The vertical dashed lines mark the GEP photometric bands. As the galaxy spectrum is redshifted, the PAH features move through the bands, enabling photometric redshift measurements. This figure does not include the effects of confusion noise.

STDT has settled on a single-dish telescope, and coined the name “Origins Space Telescope.” The OST will trace the history of our origins, starting with the earliest epochs of dust and heavy-element production through to the search for extrasolar biomarkers in the local universe. It will answer textbook-altering questions, such as “How did the universe evolve in response to its changing ingredients?” and “How common are planets that support life?”

Two concepts for the OST are being investigated, based on an Earth-Sun L2 orbit, and a telescope and instrument module actively cooled with 4 K-class cryocoolers. Concept 1 (Fig. 13) has an open architecture, similar to that of JWST. It has a deployable segmented 9-m telescope with five instruments covering the mid-infrared through the submillimeter. Concept 2 is smaller and simpler and resembles the Spitzer Space Telescope architecturally. It has a 5.9-m diameter telescope (with the same light collecting area as JWST) with no deployable components. Concept 2 has four instruments, which span the same wavelength range and have comparable spectroscopic and imaging capabilities as the instruments in concept 1.

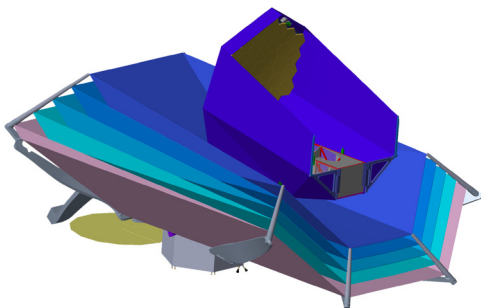


**Fig. 13** A concept image for the proposed OST (Sec. 3.3). This image shows a design for the more ambitious “concept 1.” The design includes nested sunshields and a boom, in which the instrument suite is located. The color coding of the image gives a qualitative indication of telescope temperature.

Because OST would commence in the middle of the next decade, improvements in far-infrared detector arrays are anticipated, both in per-pixel sensitivity and array format, relative to what is currently mature for spaceflight (Sec. 5.1). Laboratory demonstrations, combined with initial OST instrument studies which consider the system-level readout requirements, suggest that total pixel counts of 100,000 to 200,000 will be possible, with each pixel operating at the photon background limit. This is a huge step forward over the 3200 pixels total on Herschel PACS and SPIRE, and the  $\sim 4000$  pixels anticipated for SPICA.

The OST is studying the impact of confusion on both wide- and deep-survey concepts. Their approach is as follows. First, a model of the far-infrared sky is used to generate a three-dimensional (3-D) hyperspectral data cube. Each slice of the cube is then convolved with the telescope beam, and the resulting cube is used to conduct a search for galaxies with no information given on the input catalogs. Confusion noise is then estimated by comparing the input galaxy catalog to the recovered galaxy catalog. The results from this work are not yet available, but this approach is a significant step forward in robustness compared to prior methods.<sup>144</sup>

### 3.4 CubeSats

CubeSats are small satellites built in multiples of 1U (10 cm  $\times$  10 cm  $\times$  10 cm,  $<1.33$  kg). Because they are launched within containers, they are safe secondary payloads, reducing the cost of launch for the payload developer. In addition, a large ecosystem of CubeSat vendors and suppliers is available, which further reduces costs. CubeSats, thus, provide quick, affordable access to space, making them attractive technology pathfinders and risk mitigation missions toward larger observatories. Moreover, according to a 2016 National Academies report,<sup>171</sup> CubeSats have demonstrated their ability to perform high-value science, especially via missions to make a specific measurement, and/or that complement a larger project. To date, well over 700 CubeSats have been launched, most of them 3Us.

Within general astrophysics, CubeSats can produce competitive science, although the specific area needs to be chosen carefully.<sup>172,173</sup> For example, long-duration pointed monitoring is a unique niche. So far, the Astrophysics division within NASA's Science Mission Directorate has funded four CubeSat missions: in  $\gamma$ -rays (BurstCube<sup>174</sup>), in x-rays (HaloSat<sup>175</sup>), and in the ultraviolet (SPARCS;<sup>176</sup> CUTE<sup>177</sup>).

For the far-infrared, the CubeSat technology requirements are daunting. Most far-infrared detectors require cooling to reduce the thermal background to acceptable levels, to 4 K or even 0.1 K, although CubeSats equipped with Schottky-based instruments that do not require active cooling may be sufficiently sensitive for certain astronomical and Solar System applications (see also e.g., Ref. 178). CubeSat platforms are, thus, constrained by the lack of low-power, high-efficiency cryocoolers. Some applications are possible at 40 K, and small Stirling coolers can provide 1 W of heat lift at this temperature (see also Sec. 5.5). However, this would require the majority of the volume and power budget of even a large CubeSat (which typically have total power budgets of a few tens of watts), leaving little for further cooling stages, electronics, detector systems, and telescope optics.

CubeSats are also limited by the large beam size associated with small optics. A diffraction-limited 10-cm aperture operating at 100  $\mu\text{m}$  would have a beam size of about  $3.5'$ . There are concepts for larger, deployable apertures,<sup>179</sup> up to  $\sim 20$  cm, but none has been launched.

For these reasons, it is not currently feasible to perform competitive far-infrared science with CubeSats. However, CubeSats can serve to train the next generation of space astronomers, as platforms for technology demonstrations that may be useful to far-infrared astronomy, and as complements to larger observing systems. For example, the CubeSat Infrared Atmospheric Sounder (CIRAS) is an Earth Observation 6U mission with a 4.78 to 5.09  $\mu\text{m}$  imaging spectrograph payload. The detector array will be cooled to 120 K, using a Lockheed Martin Coaxial MPT Cryocooler, which provides a 1-W heat lift (Fig. 14). At longer wavelengths, the Aerospace Corporation's CUMULOS<sup>181</sup> has demonstrated 8 to 15  $\mu\text{m}$  Earth imaging with an uncooled



**Fig. 14** The Lockheed Martin Coaxial Micro Pulse Tube Cryocooler, which will provide cooling up to 120 K for the CIRAS, scheduled for launch in 2019.<sup>180</sup> This cooler weighs  $<0.4$  kg and has reached TRL of  $\geq 6$ .

bolometer from a CubeSat. CubeSats can also serve as support facilities. In the submillimeter range, CalSat uses a CubeSat as a calibration source for CMB polarization observatories.<sup>182</sup>

### 3.5 International Space Station

The International Space Station (ISS) is a stable platform for both science and technology development. Access to the ISS is currently provided to the U.S. astronomical community through Mission of Opportunity calls, which occur approximately every two years and have  $\sim 60\text{M}$  cost caps. Several payload sites are available for hosting U.S. instruments, with typically 1  $\text{m}^3$  of volume, at least 0.5 and up to 6 kW of power, wired and wireless Ethernet connectivity, and at least 20 kbps serial data bus downlink capability.<sup>183</sup>

In principle, the ISS is an attractive platform for astrophysics, as it offers a long-term platform at a mean altitude of 400 km, with the possibility for regular instrument servicing. Infrared observatories have been proposed for space station deployment at least as far back as 1990.<sup>184</sup> There are, however, formidable challenges in using the ISS for infrared astronomy. The ISS environment is, for infrared science, significantly unstable, with 16 sunrises in every 24-h period, “glints” from equipment near the FoV, and vibrations and electromagnetic fields from equipment in the ISS. Furthermore, the external instrument platforms are not actively controlled and are subject to various thermal instabilities over an orbit, which would require active astrometric monitoring.

Even with these challenges, there are two paths forward for productive infrared astronomy from the ISS:

- For hardware that can tolerate and mitigate the dynamic environment of the ISS, there is ample power and space for the deployment of instruments, potentially with mission lifetimes of a year or more. Example applications that may benefit from this platform include monitoring thermal emission from interplanetary dust or time-domain astronomy.
- The long-term platform, freely available power, and opportunities for direct servicing by astronauts make the ISS an excellent location to raise TRLs of technologies so that they can be deployed on other space-based platforms.

Efforts, thus, exist to enable infrared observing from the ISS. For example, the Terahertz Atmospheric/Astrophysics Radiation Detection in Space is a proposed infrared experiment that will observe both in the upper atmosphere of Earth and in the ISM of the Milky Way.

## 4 New Instruments and Methods

Continuing advances in telescope and detector technology will enable future-generation observatories to have much greater capabilities than their predecessors. Technological advancement also raises the possibility of new observing techniques in the far-infrared, with the potential for transformational science. We discuss two such techniques in this section: interferometry and time-domain astronomy.

### 4.1 Interferometry

Most studies of future far-infrared observatories focus on single-aperture telescopes. There is, however, enormous potential for

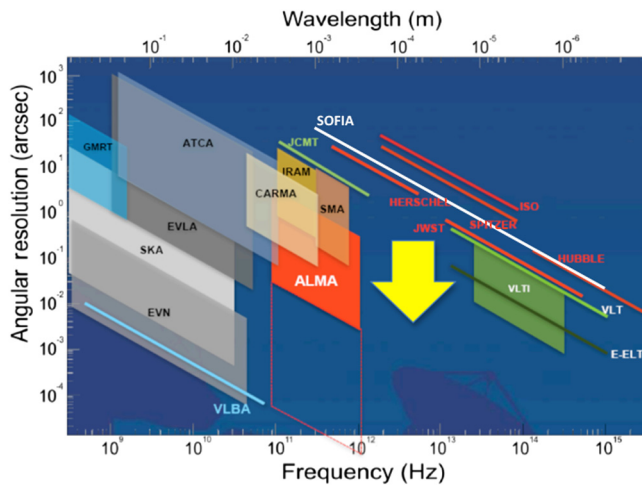


**Fig. 15** The angular resolutions of selected facilities as a function of wavelength. Very high spatial resolutions are achievable at millimeter to radio wavelengths using ground-based interferometers, whereas current and next-generation large-aperture telescopes can achieve high spatial resolutions in the optical and near-infrared. In the mid/far-infrared, however, the best achievable spatial resolutions still lag several orders of magnitude behind those achievable at other wavelengths. Far-infrared interferometry from space will remedy this, providing an increase in spatial resolution shown by the yellow arrow. A version of this figure originally appeared in the FISICA report, courtesy of Thijs de Graauw.

interferometry in the far-infrared (Fig. 15). Far-infrared interferometry is now routine from the ground (as demonstrated by ALMA, NOEMA, and the SMA) but has been barely explored from space- and balloon-based platforms. However, the combination of access to the infrared without atmospheric absorption and angular resolutions that far exceed those of any single-aperture facility and enables entirely new areas of investigation.<sup>185–187</sup>

In our Solar System, far-infrared interferometry can directly measure the emission from icy bodies in the Kuiper belt and Oort cloud. Around other stars, far-infrared interferometry can probe planetary disks to map the spatial distribution of water, water ice, gas, and dust, and search for structure caused by planets. At the other end of the scale, far-infrared interferometry can measure the rest-frame near/midinfrared emission from high-redshift galaxies without the information-compromising effects of spatial confusion. This was recognized within NASA's 2010 long-term roadmap for Astrophysics, *Enduring Quests/Daring Visions*,<sup>188</sup> which stated that, within the next few decades, scientific goals will begin to outstrip the capabilities of single-aperture telescopes. For example, imaging of exo-Earths, determining the distribution of molecular gas in protoplanetary disks, and directly observing the event horizon of a black hole, all require single-aperture telescopes with diameters of hundreds of meters, over an order of magnitude larger than is currently possible. Conversely, interferometry can provide the angular resolution needed for these goals with much less difficulty.

Far-infrared interferometry is also an invaluable technology development platform. Because certain technologies for interferometry, such as ranging accuracy, are more straightforward for longer wavelengths, far-infrared interferometry can help enable interferometers operating in other parts of the electromagnetic spectrum (interferometer technology has, however, been

developed for projects outside the infrared; examples include the Keck Interferometer, CHARA, LISA Pathfinder, the Terrestrial Planet Finder, and several decades of work on radio interferometry). This was also recognized within *Enduring Quests/Daring Visions*: “the technical requirements for interferometry in the far-infrared are not as demanding as for shorter wavelength bands, so far-infrared interferometry may again be a logical starting point that provides a useful training ground while delivering crucial science.” Far-infrared interferometry, thus, has broad appeal, beyond the far-infrared community, as it holds the potential to catalyze development of space-based interferometry across multiple wavelength ranges.

The 2000 Decadal Survey<sup>189</sup> recommended development of a far-infrared interferometer (FIRI), and the endorsed concept [the submillimeter probe of the evolution of cosmic structure (SPECS)] was subsequently studied as a “vision mission.”<sup>190</sup> Recognizing that SPECS was extremely ambitious, a smaller, structurally connected interferometer was studied as a potential origins probe—the Space Infrared Interferometric Telescope (SPIRIT,<sup>191</sup> Fig. 16). At around the same time, several interferometric missions were studied in Europe, including FIRI<sup>192</sup> and the heterodyne interferometer Exploratory Submm Space Radio-Interferometric Telescope.<sup>193</sup> Another proposed mission, TALC,<sup>194,195</sup> is a hybrid between a single-aperture telescope and an interferometer and, thus, demonstrates technologies for a structurally connected interferometer. There are also concepts using nanosats.<sup>196</sup> Recently, the European community carried out the Far-Infrared Space Interferometer Critical Assessment (FP7-FISICA), resulting in a design concept for the Far-Infrared Interferometric Telescope. Finally, the “double Fourier” technique that would enable simultaneous high spatial and spectral observations over a wide FoV is maturing through laboratory experimentation, simulation, and algorithm development.<sup>197–201</sup>

Two balloon payloads have been developed to provide scientific and technical demonstration of interferometry. They are the FITE<sup>99</sup> and the BETTII,<sup>100</sup> first launched in June 2017. The first BETTII launch resulted in a successful engineering flight, demonstrating nearly all of the key systems needed for future science flights. Unfortunately, an anomaly at the end of the flight resulted in complete loss of the payload. A rebuilt BETTII should fly before 2020.

Together, BETTII and FITE will serve as an important development step toward future space-based interferometers, while also providing unique scientific return. Their successors, taking advantage of many of the same technologies as other balloon experiments (e.g., new cryocoolers and lightweight optics), will provide expanded scientific capability while continuing the path toward space-based interferometers.

FIRIs have many of the same technical requirements as their single-aperture cousins. In fact, an interferometer could be used in “single aperture” mode, with instruments similar to those on a single-aperture telescope. However, in interferometric mode, the development requirements for space-based far-infrared interferometry are as follows:

- Detailed simulations, coupled with laboratory validation, of the capabilities of interferometers. For example, imaging with an interferometer is sometimes assumed to require full coverage of the synthetic aperture; however, for many science cases, partial coverage (akin to coverage of ground-based radio interferometers) may be sufficient.

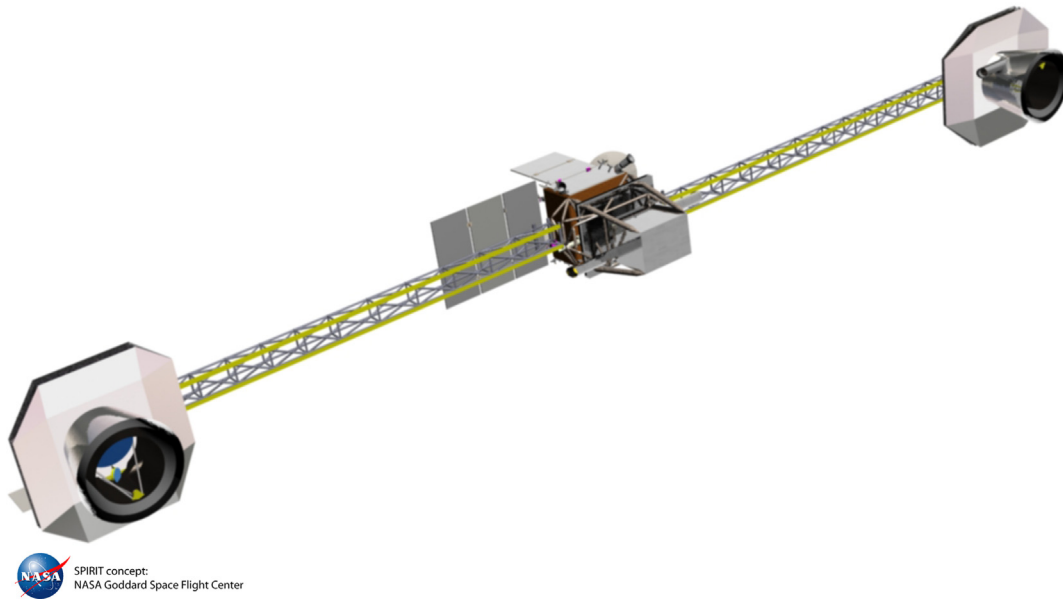


**Fig. 16** The SPIRIT structurally connected interferometer concept.<sup>191</sup> SPIRIT is a spatio-spectral “double Fourier” interferometer that has been developed to Phase A level. SPIRIT has sub-arcsecond resolution at  $100\ \mu\text{m}$ , along with  $R \sim 4000$  spectral resolution. The maximum interferometric baseline is 36 m.

- High-speed detector arrays are desirable for interferometry missions, to take advantage of fast-scanning techniques.
- Free-flying interferometers can benefit from advances in sub-Newton thruster technology, as well as techniques for efficient formation flying.
- Structurally connected interferometers can benefit from studying deployment of connected structures and boom development.
- Demonstration of the system-level integration of interferometers. Balloon-borne pathfinders provide an ideal platform for doing this.

Finally, we comment on the temporal performance requirements. The temporal performance requirements of different parts of an interferometer depend on several factors, including the FoV, sky and telescope backgrounds, rate of baseline change, and desired spectral resolution. We do not discuss these issues in detail here, as they are beyond the scope of a review paper. We do, however, give an illustrative example; a  $1'$  FoV, with a baseline of 10 m, spectral resolution of  $R = 100$ , and 16 points per fringe results in a readout speed requirement of 35 Hz. However, increasing the spectral resolution to  $R = 1000$  (at the same scan speed) raises the readout speed requirement to 270 Hz. These correspond to detector time constants of 17 and 3 ms. A baseline requirement for a relatively modest interferometer (e.g., SHARP-IR<sup>202</sup>) is, thus, a detector time constant of a few milliseconds. The exact value is, however, tied tightly to the overall mission architecture and operation scheme.

#### 4.2 Time-Domain and Rapid-Response Astronomy

Time-domain astronomy is an established field at x-ray through optical wavelengths, with notable observations including Swift’s studies of transient high-energy events and the Kepler mission using optical photometry to detect exoplanets. Time-domain astronomy in the far-infrared holds the potential for

similarly important studies of phenomena on timescales of days to years, namely, (1) searching for infrared signatures of (dust-obscured)  $\gamma$ -ray bursts, (2) monitoring the temporal evolution of waves in debris disks to study the earliest stages of planet formation, and (3) monitoring supernovae light curves to study the first formation stages of interstellar dust. To date, however, such capabilities in the far-infrared have been limited. For example, Spitzer was used to measure secondary transits of exoplanets,<sup>203</sup> but only when the ephemeris of the target was known.

The limitations of far-infrared telescopes for time-domain astronomy are twofold. First, to achieve high photometric precision in the time domain, comparable to that provided by Kepler, the spacecraft must be extremely stable, to requirements beyond those typically needed for cameras and spectrographs. This is not a fundamental technological challenge, but the stability requirements must be taken into consideration from the earliest design phase of the observatory. Second, if the intent is to discover transient events in the far-infrared (rather than monitor known ones), then the FoV of the telescope must be wide, as most transient events cannot be predicted and, thus, must be found via observations of a large number of targets.

## 5 Technology Priorities

The anticipated improvements in existing far-infrared observatories, as well as the realization of next-generation space-based far-infrared telescopes, all require sustained, active development in key technology areas. We, here, review the following areas: direct-detector arrays (Sec. 5.1), medium-resolution spectroscopy (Sec. 5.2), heterodyne spectroscopy (Sec. 5.3), Fabry–Pérot interferometry (Sec. 5.4), cooling systems (Sec. 5.5), and mirrors (Sec. 5.6). We briefly discuss a selection of other topics in Sec. 5.7.

### 5.1 Direct-Detector Arrays

A key technical challenge for essentially any future far-infrared space observatory (whether single aperture or interferometer) is

the development of combined direct-detector + multiplexer readout systems. These systems are not typically developed by the same industrial teams that build near-infrared device and midinfrared device. Instead, they are usually developed by dedicated groups at universities or national laboratories. These systems have two core drivers:

1. **Sensitivity:** The per-pixel sensitivity should meet or exceed the photon background noise set by the unavoidable backgrounds: zodiacal light, galactic cirrus, and the microwave background (Fig. 7). An especially important target is that for moderate-resolution ( $R \sim 1000$ ) spectroscopy, for which the per-pixel NEP is  $3 \times 10^{-20} \text{ W Hz}^{-1/2}$ . For the high-resolution direct-detection spectrometers considered for the OST, the target NEP is  $\sim 10^{-21} \text{ W Hz}^{-1/2}$ . A representative set of direct-detector sensitivities and requirements is given in Table 1.
2. **High pixel counts:** Optimal science return from a mission such as the OST demands total pixel counts (in all instruments) in the range of  $10^{5-6}$ . This is still a small number compared to arrays for the optical and near-infrared, for which millions of pixels can be fielded in a single chip, but  $\sim 100\times$  larger than the total number of pixels on Herschel. Moreover, mapping speed is also influenced by the per-pixel aperture efficiency. Large, high-efficiency feedhorn systems (such as that used on Herschel SPIRE) can offer up to twice the mapping speed per detector, though such systems are slower per-unit focal plane area than more closely packed horns or filled arrays.<sup>204</sup>

There are also the challenges of interference and dynamic range (Sec. 3).

The world leaders in far-infrared detector technology include SRON in the Netherlands, Cambridge and Cardiff in the U.K., and NASA in the USA, with at least three approaches under development. In order of technical readiness they are as follows:

- **Superconducting transition-edge-sensed (TES) bolometers**, which have been used in space-based instruments and in many atmosphere-based platforms.
- **KIDs**, which have progressed rapidly and have been used on several ground- and atmosphere-based instruments. The best KID sensitivities are comparable to TES detectors and have been demonstrated at larger (kilopixel) scales, though the sensitivities needed for spectroscopy with future large space missions remain to be demonstrated. Although KIDs lead in some areas (e.g., pixel count), overall they are a few years behind TES-based systems in technological maturity.
- **Quantum capacitance detectors (QCDs)**, which have demonstrated excellent low-background sensitivity but at present have modest yield and are substantially behind both TES- and KID-based systems in terms of technological maturity.

All are potentially viable for future far-infrared missions. We consider each one in turn, along with a short discussion of multiplexing.

### 5.1.1 Transition edge sensors

A TES (Fig. 17) consists of a superconducting film operated near its superconducting transition temperature. This means that the functional form of the temperature dependence of resistance,  $R(T)$ , is very sharp. The sharpness of the  $R(T)$  function allows for substantially better sensitivity than semiconducting thermistors (though there are other factors to consider, such as readout schemes; see Sec. 5.1.4). Arrays of TES bolometers have been used in CMB experiments<sup>206,207-210</sup> and in calorimeters in the  $\gamma$ -ray,<sup>211</sup> x-ray,<sup>212,213</sup> ultraviolet, and optical. They are also anticipated for future x-ray missions, such as Athena.<sup>214,215</sup>

In the infrared, TES bolometers are widely used. A notable ground-based example is SCUBA2 on the JCMT<sup>216</sup> (Table 1). Other sub-orbital examples include HAWC+ and the upcoming HIRMES instrument, both on SOFIA. TES bolometers are also planned for use in the SAFARI instrument for SPICA.<sup>217-220</sup> In terms of sensitivity, groups at SRON and Jet Propulsion Laboratory (JPL) have demonstrated TES sensitivities of  $1 \times 10^{-19} \text{ W Hz}^{-1/2}$ .<sup>219,221,222</sup>

The advantages of TES arrays over KIDs and QCD arrays are technological maturity and versatility in readout schemes (see Sec. 5.1.4). However, TES detector arrays do face challenges. The signal in TES bolometers is a current through a (sub- $\Omega$ ) resistive film at sub-kelvin temperatures, so conventional amplifiers are not readily impedance matched to conventional low-noise amplifiers (LNAs) with high-input impedance. Instead, superconducting quantum interference devices (SQUIDs) are used as first-stage amplifiers and SQUID-based circuits have been fashioned into a switching time-domain multiplexers (the TDMs, from NIST and UBC<sup>223</sup>), which has led to array formats of up to  $\sim 10^4$  pixels. Although this time-domain multiplexing system is mature and field-tested in demanding scientific settings, it is not an approach that can readily scale above  $\sim 10^4$  pixels, due primarily to wire count considerations. Other issues with TES arrays include (1) challenging array fabrication, (2) relatively complex SQUID-based readout systems, and (3) no on-chip multiplexing (yet).

### 5.1.2 Kinetic inductance detectors

The simplest approach to high-multiplex-factor frequency-domain multiplexing (FDM; see also Sec. 5.1.4) thus far is the KID<sup>224,225</sup> (Fig. 18). In a KID, photons incident on a superconducting film break Cooper pairs, which results in an increase in the inductance of the material. When embedded in a resonant circuit, the inductance shift creates a measureable frequency shift, which is encoded as a phase shift of the probe tone. KIDs originated as far-infrared detector arrays, with on-telescope examples, including MAKO<sup>226</sup> and MUSIC<sup>227</sup> at the CSO, A-MKID<sup>228</sup> at APEX, NIKA/NIKA2<sup>229-231</sup> at IRAM, the extremely compact  $\mu$ -Spec,<sup>232,233</sup> SuperSpec,<sup>234</sup> and the sub-millimeter wave imaging spectrograph DESHIMA.<sup>235</sup> KIDs were later adapted for the optical/near-infrared,<sup>236</sup> where they provide advances in time resolution and energy sensitivity. Examples include ARCONS,<sup>237</sup> DARKNESS and MEC,<sup>238,239</sup> the KRAKENS IFU,<sup>240</sup> and PICTURE-C.<sup>241</sup> KIDs are also usable for millimeter-wave/CMB studies,<sup>242-246</sup> although there are challenges in finding materials with suitably low  $T_c$ 's when operating below 100 GHz. KIDs are now being built in large arrays for several ground-based and sub-orbital infrared observatories, including the BLAST-Pol2 balloon experiment.

There exist three primary challenges in using KIDs in space-based infrared observatories:

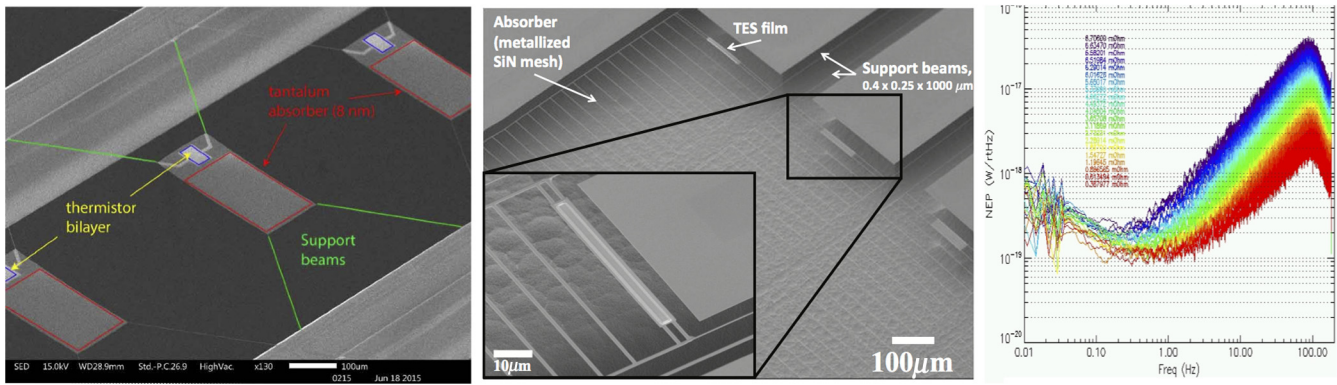


**Fig. 17** TES bolometers developed at (a) SRON and (b) JPL, targeting high sensitivity for far-infrared spectroscopy from cold telescopes. These are silicon-nitride suspensions, similar to the Herschel and Planck bolometers, but they feature long ( $\sim 1$  mm), narrow ( $\sim 0.4 \mu\text{m}$ ) suspension legs and are cooled to below 100 mK. Both programs have demonstrated NEPs of  $1\text{--}3 \times 10^{-19} \text{ W Hz}^{-1/2}$ .<sup>205</sup> (c) An example NEP measurement of the JPL system.

**Sensitivity:** Sub-orbital far-infrared observatories have relatively high backgrounds and thus have sensitivities that are 2 to 3 orders of magnitude above those needed for background-limited observations from space. For space-based KID instruments, better sensitivities are needed. The state of the art is from SPACEKIDS, for which NEPs of  $3 \times 10^{-19} \text{ W Hz}^{-1/2}$  have been demonstrated in aluminum devices coupled via an antenna.<sup>169,247,248</sup> This program has also demonstrated 83% yield in a 961-pixel array cooled to 120 mK. A further important outcome of the SPACEKIDS program was the demonstration that the effects of cosmic ray impacts can be effectively minimized.<sup>169,249</sup> In the U.S., the Caltech/JPL group and the SuperSpec collaboration have demonstrated sensitivities below  $1 \times 10^{-18} \text{ W Hz}^{-1/2}$  in a small-volume titanium nitride devices at 100 mK, also with radiation coupled via an antenna.

**Structural considerations:** KIDs must have both small active volume (to increase response to optical power) and

a method of absorbing photons directly without using superconducting transmission lines. Options under development include:

- devices with small-volume meandered absorbers/inductors, potentially formed via electron-beam lithography for small feature widths; and
- thinned substrate devices, in which the KID is patterned on a very thin (micron or submicron) membrane which may help increase the effective lifetime of the photo-produced quasiparticles, thereby increasing the response of the device.

**Antenna coupling at high frequencies:** Although straightforward for the submillimeter band, the antenna coupling becomes nontrivial for frequencies above the superconducting cutoff of the antenna material (e.g.,  $\sim 714$  GHz for Nb and 1.2 THz for NbTiN). To mitigate this, one possible strategy

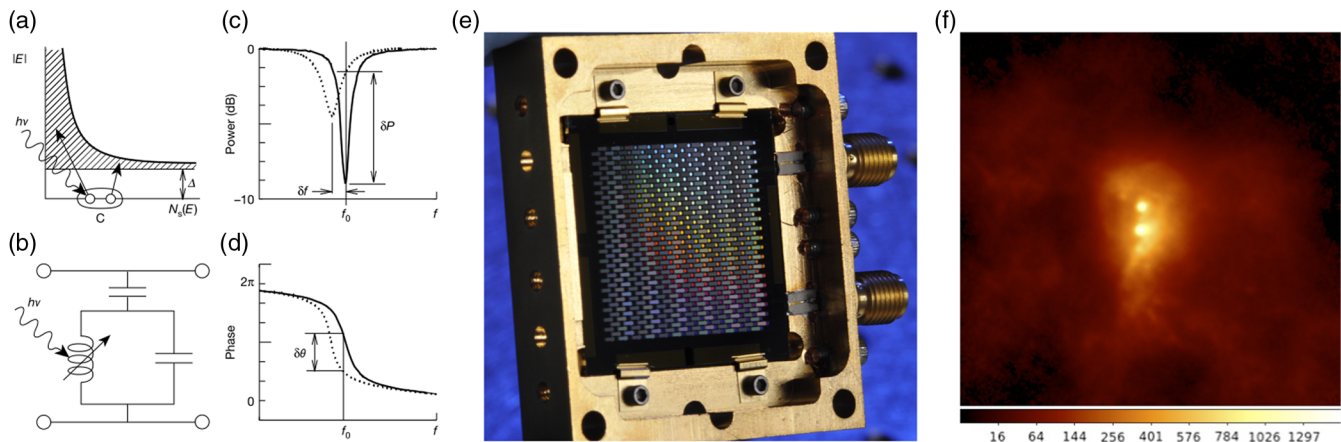


**Fig. 18** Kinetic inductance detectors. The schematic representation in the left is reprinted from Ref. 224. (a) Photons are absorbed in a superconducting film operated below its transition temperature, breaking Cooper pairs to create free electrons; (b) the increase in free electron density increases the inductance (via the kinetic inductance effect) of an RF or microwave resonator, depicted schematically here as a parallel LC circuit which is capacitively coupled to a through line. (c) On resonance, the LC circuit loads the through line, producing a dip in its transmission. The increase in inductance moves the resonance to lower frequency ( $f \sim 1/\sqrt{L}$ ), which produces a phase shift (d) of a RF or microwave probe signal transmitted through the circuit. Because the resonators can have high quality factor, many hundreds to thousands can be accessed on a single transmission line. (e) The 432-pixel KID array in the Caltech/JPL MAKO camera, and (f) shows an image of SGR B2 obtained with MAKO at the CSO.

is to integrate the antenna directly into the KID, using only aluminum for the parts of the detector that interact with the THz signal. This approach has been demonstrated at 1.55 THz, using a thick aluminum ground plane and a thin aluminum central line to limit ground plane losses to 10%.<sup>169,170</sup> This approach does not rely on superconducting stripline technology and could be extended to frequencies up to  $\sim 10$  THz.

A final area of research for KIDs, primarily for CMB experiments, is the KID-sensed bolometer, in which the thermal response of the KID is used to sense the temperature of a bolometer island. These devices will be limited by the fundamental phonon transport sensitivity of the bolometer and so are likely to have sensitivity limits comparable to TES bolometers, but may offer advantages, including simplified readout, on-array multiplexing, lower sensitivity to magnetic fields, and larger dynamic range.

### 5.1.3 Quantum capacitance detectors

The QCD<sup>250–254</sup> is based on the single Cooper-pair box (SCB), a superconducting device initially developed as a qubit for quantum computing applications. The SCB consists of a small island of superconducting material connected to a ground electrode via a small (100 nm  $\times$  100 nm) tunnel junction. The island is biased with respect to ground through a gate capacitor, and because it is sufficiently small to exhibit quantum behavior, its capacitance becomes a strong function of the presence or absence of a single free electron. By embedding this system capacitively in a resonator (similar to that used for a KID), a single electron entering or exiting the island (via tunneling through the junction) produces a detectable frequency shift.

To make use of this single-electron sensitivity, the QCD is formed by replacing the ground electrode with a superconducting photon absorber. As with the KIDs, photons with energy larger than the superconducting gap breaks Cooper pairs, thereby establishing a density of free electrons in the absorber that then tunnel onto (and rapidly back out of) the island through the tunnel junction. The rate of tunneling into the island, and thus the average electron occupation in the island, is determined by the free-electron density in the absorber, set by the photon flux. Because each photo-produced electron tunnels back and forth many times before it recombines, and because these tunneling events can be detected individually, the system has the potential to be limited by the photon statistics with no additional noise.

This has indeed been demonstrated. QCDs have been developed to the point where a 25-pixel array yields a few devices which are photon-noise-limited for 200- $\mu$ m radiation under a load of  $10^{-19}$  W, corresponding to a NEP of  $2 \times 10^{-20}$  WHz<sup>-1/2</sup>. The system seems to have good efficiency as well, with inferred detection of 86% of the expected photon flux for the test setup. As an additional demonstration, a fast-readout mode has been developed which can identify individual photon arrival events based on the subsequent increase in tunneling activity for a timescale on order of the electron recombination time (Fig. 19).

With its demonstrated sensitivity and natural FDM, the QCD is promising for future far-infrared space systems. Optical NEPs of below  $10^{-20}$  WHz<sup>-1/2</sup> at 200  $\mu$ m have been demonstrated, with the potential for photon counting at far-infrared wavelengths.<sup>255</sup> However, QCDs are some way behind both TES and KID arrays in terms of technological maturity. To be viable for infrared instruments, challenges in (1) yield and

array-level uniformity, (2) dark currents, and (3) dynamic range must all be overcome. The small tunnel junctions are challenging, but it is hoped that advances in lithography and processing will result in improvements.

### 5.1.4 System considerations for direct-detector readouts

There exist three commonly used multiplexing (muxing) schemes<sup>256</sup> for readout of arrays: FDM, TDM, and Code Division Muxing (CDM). In this section, we briefly review their applicability and advantages.

FDM is a promising path for reading out the large arrays anticipated in future infrared observatories. In FDM, a single readout circuit services up to  $\sim 1000$  pixels, each coupled through a microresonator tuned to a distinct frequency. Each pixel is then probed individually with a radio frequency (RF) or microwave tone at its particular frequency. The warm electronics must create the suite of tones, which is transmitted to the array for each circuit, then digitize, Fourier transform, and channel the output data stream to measure the phase and amplitude shifts of each tone independently. The number of resonators (and thus pixels) that can be arrayed onto a single readout circuit depends on the quality factor (Q) of the resonators and the bandwidth available in the circuit. For micro-resonators patterned in superconducting films, resonator Qs exceeding  $10^7$  are possible but more typical values are around  $10^5$ , which permits  $\sim 10^3$  pixels per octave of readout bandwidth to be operated with sufficiently low cross talk.

In these systems, all of the challenging electronics are on the warm side, and the detector array is accessed via low-loss RF/microwave lines (one from the warm side down through the cryostat stages and another for the return signal). Moreover, FDM readout schemes can be applied to both TES and KID arrays, whereas other multiplexing schemes are TES-only. An example of recent progress is the development of a FDM scheme that can read out 132 TES pixels simultaneously, using a single SQUID, without loss of sensitivity.<sup>220</sup> This is very close to the 160 detectors per SQUID targeted for SPICA/SAFARI.

There are, however, the following limitations to FDM schemes:

1. **Thermal constraints:** Whereas the detector arrays themselves are essentially passive, the conductors, whether coaxial or twisted pair, will have thermal conduction from the warm stages, impacting the overall thermal design. In addition, these systems require a single LNA on each circuit, likely deployed somewhere between 4 and 20 K, and the LNAs will have some dissipation.
2. **Signal processing:** FDM schemes pose significant challenges for backend electronics-processing capability: they must digitize the returning waveforms, then Fourier transform in real time at the science sampling rate, and extract the full array of tone phases that encode the pixel signal levels. These hurdles become nontrivial for the large arrays envisaged for future missions.

A further challenge, which applies to readout schemes for any far-infrared resonant detector array (including TES, KID, and QCD systems), is the power required to read out  $10^{4-5}$  detector arrays, due in part to the signal-processing requirements.

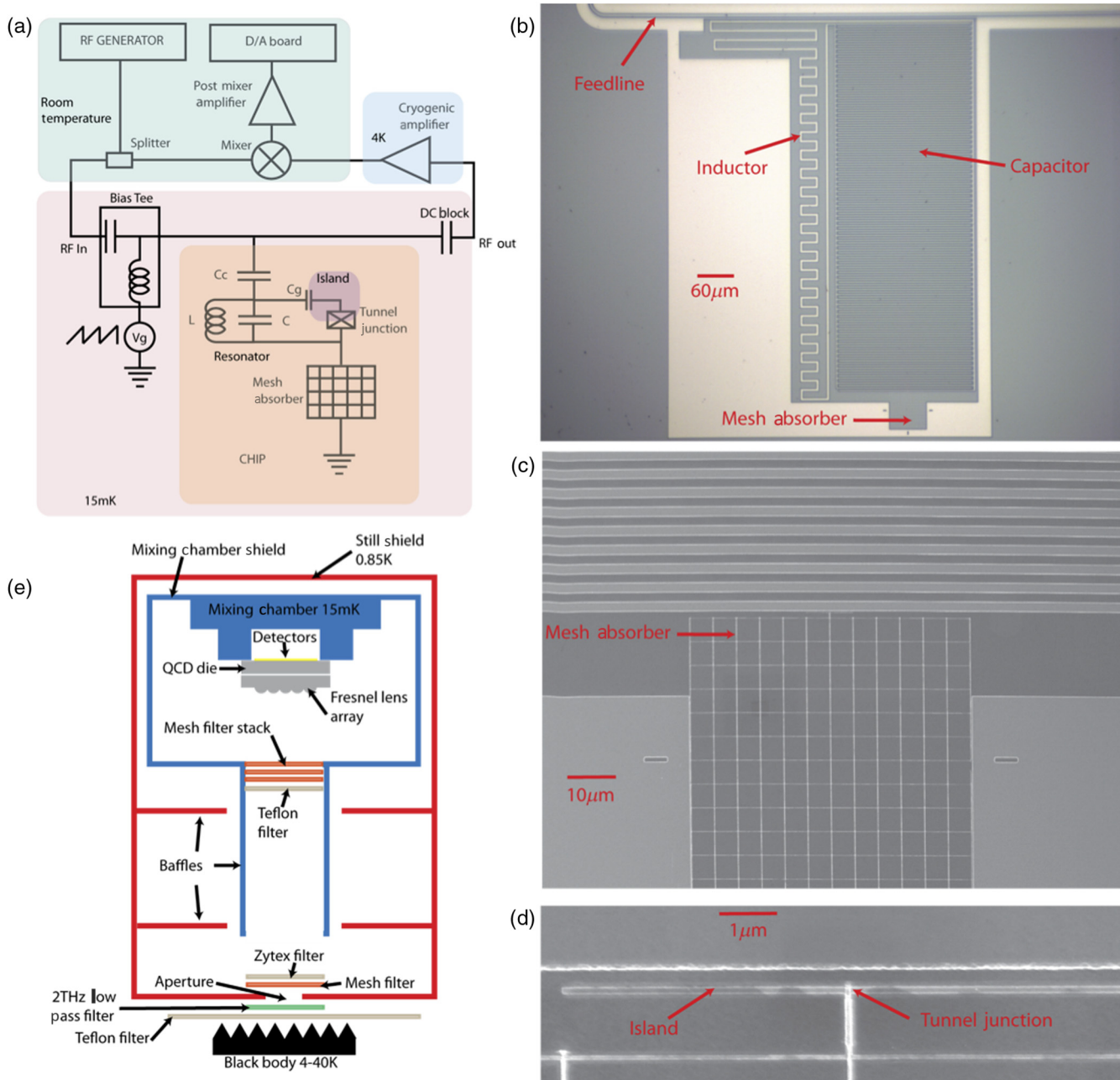


**Fig. 19** The quantum capacitance detector. (a) Schematic representation showing the mesh absorber QCD with its LC resonator coupling it to the readout circuit. The SCB island is formed between the tunnel junction and the gate capacitor. The tunnel junction is connected to the mesh absorber which in turn is connected to the ground plane. The SCB presents a variable capacitance in parallel with an LC resonator. (b) Optical microscope picture of a device, showing the feedline, the inductor, the interdigitated capacitor, all fabricated in Nb and the Al mesh absorber. (c) SEM picture of mesh absorber consisting of 50-nm wide aluminum lines on a 5 μm wide grid. (d) Detail of the SCB showing the aluminum island (horizontal line) in close proximity to the lowest finger of the interdigitated capacitor and the tunnel junction (overlap between the island and vertical line connecting to the mesh absorber below). (e) Optical setup schematic representation showing temperature-tunable blackbody, aperture, and filters that define the spectral band. This device has demonstrated an optical NEP of  $2 \times 10^{-20} \text{ W Hz}^{-1/2}$  at 200 μm, as well as the ability to count individual photons.<sup>254,255</sup>

The power requirements are such that they may pose a significant obstacle to reading out  $\sim 10^5$  detector arrays on *any* balloon- or space-based platform.

For the OST, power dissipation in the warm electronics will be a particular challenge. An example is the medium-resolution survey spectrometer (MRSS), which targets 200,000 pixels

among all six spectrometer bands. The concept assumes resonator frequencies between 75 MHz and 1 GHz, and 1500 pixels can be arrayed in this bandwidth (a relatively comfortable multiplexing density assuming 400 per readout octave). This requires 130 readout circuits, each with two coaxial lines all the way to the cold stage, and a cold amplifier on the output. The conducted

loads through the coaxial lines, as well as reasonable assumptions about the LNA dissipation (1 mW at 4 K plus 3 mW at 20 K for each circuit), do not stress the observatory thermal design. However, the electronics for each circuit requires a 2 giga-sample-per-second analog-to-digital converter working at  $\sim 12$ -bits depth, followed by FFTs of this digital signal stream in real time—1024 point FFTs every  $0.5 \mu\text{s}$ . Systems such as these implemented in field programmable gate array used in the laboratory dissipate  $\sim 100$  W for each readout circuit, which is not compatible with having 130 such systems on a space mission.

For these reasons, development of muxing schemes is a high priority for large-format arrays, irrespective of the detector technology used. A promising path for such development is to employ a dedicated application-specific integrated circuit (ASIC), designed to combine the digitization, FFT, and tone extraction in a single chip. Power dissipation estimates obtained for the MRSS study based on custom spectrometer chips developed for flight systems, and extrapolating to small-gate CMOS technology, suggest that such a custom chip could have a power dissipation of  $\sim 14$  W per circuit, including all aspects. At this level, the total scales to  $\sim 1.8$  kW. This power dissipation is well within the range of that of other subsystems on future missions—for example, such missions will require several kilowatts to operate the cryocoolers—and thus does not pose a unique problem.

Finally, we make four observations:

- (1) Although the power-scaling calculations are straightforward, the development of this silicon ASIC is a substantial design effort, in large part because of the 12-bit depth; most fast digital spectrometers implemented in CMOS operate at 3- or 4-bits depth.
- (2) The power dissipation scales as the total bandwidth, so the per-pixel electronics power dissipation could be reduced if lower resonant frequencies were used. The downside of this though is that the physical size of the resonators scale approximately as  $1/\sqrt{f}$ , and (with current designs) becomes several square millimeters per resonator for frequencies below  $\sim 50$  MHz.
- (3) Hybrid schemes, such as combining CDM with frequency-domain readout, are attractive for their power efficiency, both at 4 K due to lower number of high-electron-mobility transistors or parametric amps and for the warm electronics due to lower bandwidths and lower wire counts. These schemes, however, are only applicable to TES-based systems.
- (4) With  $Q = 10^5$  and 1000 resonators per octave, the FDM scheme utilizes only a few percentage of the readout bandwidth. Factors of 10 or more improvement in multiplexing density and reduction in readout power are possible if the resonator frequency placement could be improved to avoid collisions, e.g., through postfabrication trimming (PFT) is a family of techniques that permanently alters the refractive index of a material to change the optical path length.<sup>257–259</sup> The advantage of PFT is that it does not require complex control electronics, but concerns have been raised over the long-term stability of some of the trimming mechanisms.

## 5.2 Medium-Resolution Spectroscopy

A variety of spectrometer architectures can be used to disperse light at far-infrared wavelengths. Architectures that have been successfully used on air-borne and space instruments include grating dispersion such as FIFI-LS on SOFIA<sup>260</sup> and PACS on Herschel,<sup>133</sup> Fourier transform spectrometers such as the Herschel/SPIRE-FTS,<sup>134</sup> and Fabry–Pérot etalons such as FIFI on the KAO telescope.<sup>261</sup> These technologies are well understood and can achieve spectral resolutions of  $R = 10^2 - 10^4$ . However, future spectrometers will need to couple large FoVs to many thousands of imaging detectors, a task for which all three of these technologies have drawbacks. Grating spectrometers are mechanically simple devices that can achieve  $R \sim 1000$  but are challenging to couple to wide FoVs as the spectrum is dispersed along one spatial direction on the detector array. FTS systems require moving parts and suffer from noise penalties associated with the need for spectral scanning. They are also not well suited for studying faint objects because of systematics associated with long-term stability of the interferometer and detectors.<sup>262</sup> Fabry–Pérot systems are also mechanically demanding, requiring tight parallelism tolerances of mirror surfaces, and typically have restricted free spectral range due to the difficulty of manufacturing sufficiently precise actuation mechanisms.<sup>263</sup> A new technology that can couple the large FoVs anticipated in next-generation far-infrared telescopes to kilo-pixel or larger detector arrays would be transformative for far-infrared spectroscopy.

A promising approach to this problem is the far-infrared filter bank technology.<sup>264,265</sup> This technology has been developed as a compact solution to the spectral dispersion problem and has potential for use in space. These devices require the radiation to be dispersed to propagate down a transmission line or waveguide. The radiation encounters a series of tuned resonant filters, each of which consists of a section of transmission line of length  $\lambda_i/2$ , where  $\lambda_i$  is the resonant wavelength of channel  $i$ . These half-wave resonators are evanescently coupled to the feedline with designable coupling strengths described by the quality factors  $Q_{\text{feed}}$  and  $Q_{\text{det}}$  for the feedline and detector, respectively. The filter bank is formed by arranging a series of channels monotonically increasing in frequency, with a spacing between channels equal to an odd multiple of  $\lambda_i/4$ . The ultimate spectral resolution  $R = \lambda/\Delta\lambda$  is given as

$$\frac{1}{R} = \frac{1}{Q_{\text{filt}}} = \frac{1}{Q_{\text{feed}}} + \frac{1}{Q_{\text{det}}} + \frac{1}{Q_{\text{loss}}}, \quad (1)$$

where  $Q_{\text{loss}}$  accounts for any additional sources of dissipation in the circuit and  $Q_{\text{filt}}$  is the net quality factor. This arrangement has several advantages in low- and medium-resolution spectroscopy from space, including (1) compactness (fitting on a single chip with area of tens of square centimeters), (2) integrated on-chip dispersion and detection, (3) high end-to-end efficiency equal to or exceeding existing technologies, and (4) a mechanically stable architecture. A further advantage of this architecture is the low intrinsic background in each spectrometer, which only couples to wavelengths near its resonance. This means that very low backgrounds can be achieved, requiring detector NEPs below  $10^{-20}$  W Hz<sup>-1/2</sup>. Filter banks do, however, have drawbacks.<sup>264</sup> For example, although filter banks are used in instruments operating from millimeter to radio wavelengths, they are currently difficult to manufacture for use at wavelengths shortward of about  $500 \mu\text{m}$ .

Two ground-based instruments are being developed that make use of filter banks. A prototype transmission-line system has been fabricated for use in SuperSpec<sup>266,267</sup> for the LMT. SuperSpec will have  $R \sim 300$  near 250 GHz and will allow photon-background-limited performance. A similar system is WSPEC, a 90-GHz filter bank spectrometer that uses machined waveguide to propagate the radiation.<sup>268</sup> This prototype instrument has five channels covering the 130- to 250-GHz band. Though neither instrument is optimized for space applications, this technology can be adapted to space, and efforts are underway to deploy it on suborbital rockets.

### 5.3 High-Resolution Spectroscopy

Several areas of investigation in mid/far-infrared astronomy call for spectral resolution of  $R \geq 10^5$ , higher than can be achieved with direct-detection approaches. At this very high spectral resolution, heterodyne spectroscopy is routinely used,<sup>269,270</sup> with achievable spectral resolution of up to  $R \simeq 10^7$ . In heterodyne spectroscopy, the signal from the “sky” source is mixed with a spectrally pure, large-amplitude, locally generated signal, called the “local oscillator (LO),” in a nonlinear device. The nonlinearity generates the sum and difference of the sky and LO frequencies. The latter, the “intermediate frequency (IF),” is typically in the 1- to 10-GHz range and can be amplified by LNAs and subsequently sent to a spectrometer, which now is generally implemented as a digital signal processor. A heterodyne receiver is a coherent system, preserving the phase and amplitude of the input signal. Although the phase information is not used for spectroscopy, it is available and can be used in, e.g., interferometry.

The general requirements for LOs are as follows: narrow linewidth, high stability, low noise, tunability over the required frequency range, and sufficient output power to couple effectively to the mixer. For far-infrared applications, LO technologies are usually one of the two following types: multiplier chain and quantum cascade laser (QCL). Multiplier chains offer relatively broad tuning, high spectral purity, and known output frequency. The main limitation is reaching higher frequencies ( $>3$  THz). QCLs are attractive at higher frequencies, as their operating frequency range extends to 5 THz and above, opening up the entire far-infrared range for high-resolution spectroscopy.

For mixers, most astronomical applications use one or more of the following three technologies: Schottky diodes, SIS mixers, and hot electron bolometer (HEB) mixers.<sup>271</sup> Schottky diodes function at temperatures of  $>70$  K, can operate at frequencies as high as  $\sim 3$  THz (100  $\mu\text{m}$ ), and provide large IF bandwidths of  $>8$  GHz, but offer sensitivities that can be an order of magnitude or more poorer than either SIS or HEB mixers. They also require relatively high LO power, in the order of 1 mW. SIS and HEB mixers, in contrast, have operating temperatures of  $\sim 4$  K and require LO powers of only  $\sim 1$   $\mu\text{W}$ . SIS mixers are most commonly used at frequencies up to about 1 THz, whereas HEB mixers are used over the 1 to 6 THz range. At present, the SIS mixers offer IF bandwidths and sensitivities both a factor of 2 to 3 better than the HEB mixers. All three mixer types have been used on space-flown hardware: SIS and HEB mixers in the Herschel HIFI instrument,<sup>272,273</sup> and Schottky diodes on instruments in SWAS and Odin.

Heterodyne spectroscopy can currently achieve spectral resolutions of  $R \simeq 10^7$ , and in principle the achievable spectral resolution is limited only by the purity of the signal from the LO.

Moreover, heterodyne spectroscopy preserves the phase of the sky signal as well as its frequency, lending itself naturally to interferometric applications. Heterodyne arrays are used on SOFIA, as well as many ground-based platforms. They are also planned for use in several upcoming observatories, including GUSTO. A further example is FIRSPEX, a concept study for a small-aperture telescope with heterodyne instruments to perform several large-area surveys targeting bright far-infrared fine-structure lines, using a scanning strategy similar to that used by Planck.<sup>274</sup>

There are, however, challenges for the heterodyne approach. We highlight five here:

- **The antenna theorem:** Coherent systems are subject to the antenna theorem that allows them to couple to only a single spatial mode of the electromagnetic field. The result is that the product of the solid angle subtended by the beam of a heterodyne receiver system ( $\Omega$ ) and its collecting area for a normally incident plane wave ( $A_e$ ) is determined,  $A_e \Omega = \lambda^2$ .<sup>275</sup>
- **The quantum noise limit:** A heterodyne receiver, being a coherent system, is subject to the quantum noise limit on its input noise temperature,  $T \geq hf/k$  (e.g., Ref. 262). Whereas SIS mixers have noise temperatures only a few times greater than the quantum noise limit, HEB mixer receivers typically have noise temperatures  $\sim 10$  times the quantum noise limit, e.g.,  $10 \times 91$  K at  $f = 1900$  GHz. Improved sensitivity for HEB and SIS mixers operating at higher frequencies will offer significant gains in astronomical productivity.
- **Limited bandwidth:** There is a pressing need to increase the IF bandwidth of HEB mixers, with a minimum of 8-GHz bandwidth required at frequencies of  $\sim 3$  THz. This will allow for complete coverage of galactic spectral lines with a single LO setting, as well as the lines of nearby galaxies. Simultaneous observation of multiple lines also becomes possible, improving both the efficiency and the relative calibration accuracy.
- **Array size:** The largest arrays currently deployed (such as in upGREAT on SOFIA) contain fewer than 20 pixels although a 64-pixel ground-based array operating at 850  $\mu\text{m}$  has been constructed.<sup>276</sup> Increasing array sizes to hundreds or even thousands of pixels will require SIS and HEB mixers that can be reliably integrated into these new large-format arrays, low-power IF amplifiers, and for efficient distribution of LO power.
- **Power requirements:** Existing technology typically demands significantly more power per pixel than is available for large-format arrays on satellite-based platforms.

On a final note, for the higher frequency ( $>3$  THz) arrays, high-power (5 to 10 mW) QCL LOs are a priority for development, along with power division schemes (e.g., Fourier phase gratings) to utilize QCLs effectively.<sup>277–279</sup> At  $<3$  THz, frequency-multiplied sources remain the system of choice and have been successfully used in missions including SWAS, Herschel-HIFI, STO2, and in GREAT and upGREAT on SOFIA. However, to support large-format heterodyne arrays, and to allow operation with reduced total power consumption for space missions, further development of this technology is

necessary. Further valuable developments include SIS and HEB mixers that can operate at temperatures of  $>20$  K and integrated focal planes of mixers and low-noise IF amplifiers.

#### 5.4 Fabry–Pérot Interferometry

Fabry–Pérot Interferometers (FPIs) have been used for astronomical spectroscopy for decades, with examples, such as FIFI,<sup>280</sup> KWIC,<sup>281</sup> ISO-SWS/LWS,<sup>282,283</sup> and SPIFI.<sup>284</sup> FPIs similar to the one used in ISO have also been developed for balloon-borne telescopes.<sup>285</sup>

FPIs consist of two parallel, highly reflective (typically with reflectivities of  $\sim 96\%$ ), very flat mirror surfaces. These two mirrors create a resonator cavity. Any radiation whose wavelength is an integral multiple of twice the mirror separation meets the condition for constructive interference and passes the FPI with high transmission. As the radiation bounces many times between the mirrors before passing, FPIs can be fabricated very compactly, even for high spectral resolution, making them attractive for many applications. In addition, FPIs allow for large FoVs, making them an excellent choice as devices for spectroscopic survey instruments.

Observations with FPI are most suitable for extended objects and surveys of large fields, where moderate-to-high spectral resolution ( $R \sim 10^2 - 10^5$ ) is required. For example:

- It is suited for mapping nearby galaxies in multiple molecular transitions and atomic or ionic fine-structure lines in the far-infrared. This traces the properties of the ISM and relates small-scale effects such as the star-forming regions to the larger-scale environment of their host galaxies.
- For high-redshift observations, FPI is suited to survey large fields and obtain a 3-D data cube by stepping an emission line over a sequence of redshift bins. This results in line detections from objects located at the corresponding redshift bins and allows, e.g., probing ionization conditions or metallicities for large samples simultaneously.

FPIs do, however, face challenges. We highlight four examples here:

- (1) To cover a certain bandwidth, the FPI mirror separation has to be continuously or discretely changed, i.e., the FPI has to be scanned, which requires time, and may result in poor channel-to-channel calibration in the spectral direction if the detector system is not sufficiently stable.
- (2) Unwanted wavelengths that fulfill the resonance criteria also pass through the FPI and need to be filtered out. Usually, additional FPIs operated in lower order combined with bandpass or blocking/edge filters are used for order sorting. However, as most other spectrometers need additional filters to remove undesired bands, the filtration of unwanted orders in FPIs is not a profound disadvantage.
- (3) In current far-infrared FPIs, the reflective components used for the mirrors are free-standing metal meshes. The finesse (the spectral range divided by the FWHMs of individual resonances; see, e.g., Ref. 286) of the meshes changes with wavelength

and therefore a FPI is only suitable over a limited wavelength range. Also, the meshes can vibrate, which requires special attention especially for high spectral resolution, where the diameters can be large. Replacing the free-standing metal meshes with a different technology is therefore enabling for broader applications of FPI. For example, flat silicon wafers with an antireflection structure etched on one side and coated with a specific thin metal pattern on the other side, optimized for a broader wavelength range, can substitute for a mirror. This silicon wafer mirror is also less susceptible to vibrations and could be fabricated with large enough diameters.

- (4) Currently, FPIs usually use piezoelectric elements (PZTs) for scanning. However, PZTs have limited travel range, especially at 4 K. Moreover, mechanical devices or PZT-driven motors are still not reliable enough at cryogenic temperatures or are too large to be used in the spaces available inside the instruments. It is thus important to develop either smaller PZT-driven devices, which can travel millimeters with resolutions of nanometers at a temperature of 4 K, or an alternative scanning technology that overcomes the limitations of PZT devices and satisfies the requirements of FPIs.

#### 5.5 Small and Low-Power Coolers

For any spaceborne observatory operating at mid/far-infrared wavelengths, achieving high sensitivity requires that the telescope, instrument, and detectors be cooled, with the level of cooling dependent on the detector technology, the observation wavelength, and the goals of the observations. Cooling technology is thus fundamentally enabling for all aspects of mid/far-infrared astronomy.

The cooling required for the telescope depends on the wavelengths being observed (Fig. 7). For some situations, cooling the telescope to 30 to 40 K is sufficient. At these temperatures, it is feasible to use radiative (passive) cooling solutions if the telescope is space-based *and* if the spacecraft orbit and attitude allow for a continuous view of deep space.<sup>287</sup> Radiative coolers typically resemble a set of thermal/solar shields in front of a black radiator to deep space (Fig. 6). This is a mature technology, having been used on Spitzer, Planck, and JWST (for an earlier proposed example, see Ref. 288).

For many applications, however, cooling the telescope to a few tens of kelvins is suboptimal. Instead, cooling to an order of 4 K is required, e.g., zodiacal background limited observations (see also Sec. 3). Moreover, detector arrays require cooling at least to this level. For example, SIS and HEB mixers need cooling up to 4 K, whereas TES, KID, and QCD arrays need cooling to 0.1 K or below. Achieving cooling at these temperatures requires a cooling chain—a staged series of cooling technologies selected to maximize the cooling per-mass and per-input power.

To achieve temperatures below  $\sim 40$  K, or where a continuous view of deep space is not available, cryocoolers are necessary. In this context, the Advanced Cryocooler Technology Development Program (ACTDP<sup>289</sup>), initiated in 2001, has made excellent progress in developing cryogen-free multiyear

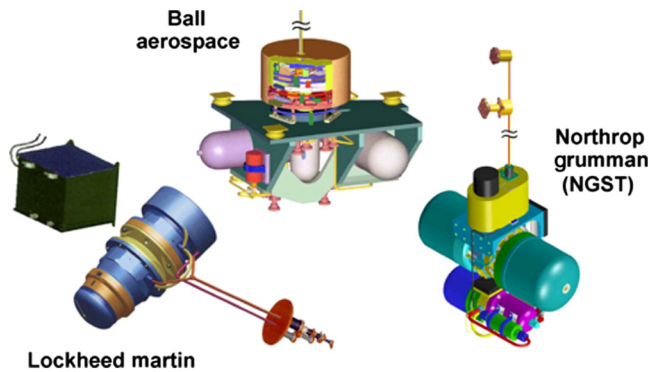


**Fig. 20** Three cryocoolers for 6 K cooling developed through the ACTDP.

cooling for low-noise detector arrays at temperatures of 6 K and below (Fig. 20). The state of the art for these coolers include those onboard Planck, JWST, and Hitomi.<sup>290</sup> Similar coolers that could achieve 4 K are at TRL 4-5, having been demonstrated as a system in a laboratory environment<sup>291</sup> or as a variant of a cooler that has a high TRL (JWST/MIRI). Mechanical cryocoolers for higher temperatures have already demonstrated impressive on-orbit reliability (Table 2). The moving components of a 4 K cooler are similar (expanders) or the same (compressors) as those that have flown. Further development of these coolers to maximize cooling per input power for small cooling loads (<100 mW at 4 K) and lower mass is however needed. There is also a need to minimize the vibration from the cooler system. The miniature reverse-Brayton cryocoolers under development by Creare are examples of reliable coolers with negligible exported vibration. These coolers are at TRL 6 for 80 K and TRL 4 for 10 K operation.

For cooling to below 0.1 K, adiabatic demagnetization refrigerators (ADRs) are currently the only proven technology, although work has been funded by ESA to develop a continuously recirculating dilution refrigerator [continuous adiabatic demagnetization refrigerator (CADR)]. A single-shot DR was flown on Planck producing 0.1  $\mu$ W of cooling at 100 mK for about 1.5 years, whereas a three-stage ADR was used on Hitomi producing 0.4  $\mu$ W of cooling at 50 mK with an indefinite lifetime. In contrast, a TRL 4 CADR has demonstrated 6  $\mu$ W of cooling at 50 mK with no life-limiting parts<sup>292</sup> (Fig. 21). This technology is being advanced toward TRL 6 by 2020 via funding from the NASA SAT/TPCOS program.<sup>293</sup> Demonstration of a 10-K upper stage for this machine, as is planned, would enable coupling to a higher temperature cryocooler, such as that of Creare, that has near-zero vibration. The flight control electronics for this ADR are based on the flight-proven Hitomi ADR control and has already achieved TRL 6. ADR coolers are the current reference design for the Athena x-ray observatory. For the OST, all three of the above technologies are required to maintain the telescope at near 4 K and the detector arrays at near 50 mK.

Continuous development of 0.1 and 4 k coolers with cooling powers of tens of milliwatt, high reliability, and lifetimes of 10+ years is of great importance for future far-infrared observatories. Moreover, the development of smaller, lighter, vibration-resistant, power-efficient cryocoolers enables expansion of infrared astronomy to new observing platforms. An extremely challenging goal would be the development of a 0.1 K cooler with power, space, and vibration envelopes that enable its use inside a 6U

CubeSat, while leaving adequate resources for detector arrays, optics, and downlink systems (see also Sec. 3.4). More generally, the ubiquity of cooling in infrared astronomy means that the development of low-mass, low-power, and low-cost coolers will reduce mission costs and development time across all observational domains.

## 5.6 High Surface Accuracy Lightweight Mirrors

As far-infrared observing platforms mature and develop, there emerge new opportunities to use large aperture mirrors for which the only limitations are (1) mirror mass and (2) approaches to active control and correction of the mirror surface. This raises the possibility of a high-altitude, long-duration far-infrared-observing platform with a mirror factors of 2 to 5 larger than on facilities such as SOFIA or Herschel.

The key enabling technology for such an observing platform is the manufacturing of lightweight, high surface accuracy mirrors, and their integration into observing platforms. This is especially relevant for ULDBs, which are well suited for this activity. Lightweight mirrors with apertures of 3 m to several tens of meters are ideal for observations from balloon-borne platforms. Carbon-fiber mirrors are an attractive option; they have low mass and can offer high sensitivity in the far-infrared, at low cost of manufacture. Apertures of 2.5 m are used on projects, such as BLAST-TNG.<sup>95</sup> Apertures of up to ~10-m are undergoing ground-based tests, including the phase 2 NIAC study for the large balloon reflector.<sup>294–296</sup>

A conceptually related topic is the physical size and mass of optical components. The physical scale of high-resolution spectrometers in the far-infrared is determined by the optical path difference required for the resolution. For resolutions of  $R \gtrsim 10^5$ , this implies scales of several meters for a grating spectrometer. This scale can be reduced by folding, but mass remains a potentially limiting problem. Moreover, larger physical sizes are needed for optical components to accommodate future large format arrays, posing challenges for uniformity, thermal control, and antireflection coatings. The development of low-mass optical elements suitable for diffraction-limited operation at  $\lambda \geq 25 \mu\text{m}$  would open the range of technical solutions available for the highest performance instruments.

## 5.7 Other Needs

There exist several further areas for which technology development would be beneficial. We briefly summarize them below:

**Lower-loss THz optics:** Lenses, polarizers, filters, and duplexers.

**Digital backends:** Low-power (of order a few watts or less) digital backends with >1000 channels covering up to several tens of gigahertz of bandwidth.

**Wide-field imaging Fourier transform spectrometers:** Expanding on the capabilities of, e.g., SPIRE on Herschel, balloon- or space-based imaging Fourier transform spectrometer with FoVs of tens of square arcminutes.<sup>297</sup> Examples include the concept H2EX.<sup>298</sup>

**Deployable optics:** Development of deployable optic schemes across a range of aperture sizes would be enabling for a range of platforms. Examples range from 20- to 50-cm systems for CubeSats to 5- to 10-m systems for JWST.

**Data downlinking and archiving:** The advent of infrared observatories with large-format detector arrays presents challenges in downlinking and archiving. Infrared observatories

**Table 2** Long-life space cryocooler operating experiences as of May 2016.

Cooler, mission, and manufacturer	T (K)	Hours/unit	Notes
<b>Turbo Brayton</b>			
ISS—MELFI (Air Liquide)	190	85,600	Turn-on 7/06, ongoing, no degradation
HST—NICMOS (Creare)	77	57,000	3/02 through 10/09, off, coupling to load failed
<b>Stirling</b>			
HIRDLS: 1-stage (Ball Aerospace)	60	83,800	8/04 through 3/14, instrument failed 03/08, data turned off 3/14
TIRS: 2-stage (Ball Aerospace)	35	27,900	Turn-on 6/13, ongoing, no degradation
ASTER-TIR (Fujitsu)	80	141,7000	Turn-on 3/00, ongoing, no degradation
ATSR-1 on ERS-1 (RAL)	80	75,300	7/91 through 3/00, satellite failed
ATSR-2 on ERS-2 (RAL)	80	112,000	4/95 through 2/08, instrument failed
Suzaku: one stage (Sumitomo)	100	59,300	7/05 through 4/12, mission ended, no degradation
SELENE/Kaguya GRS: one stage (Sumitomo)	70	14,600	10/07 through 6/09, mission ended, no degradation
<b>Akari: two stage (Sumitomo)</b>	<b>20</b>	<b>39,000</b>	<b>2/06 through 11/11, mission ended</b>
RHESSI (Sunpower)	80	124,600	Turn-on 2/02, ongoing, modest degradation
CHIRP (Sunpower)	80	19,700	9/11 through 12/13, mission ended, no degradation
ASTER-SWIR (Mitsubishi)	77	137,500	Turn-on 3/00, ongoing, load off at 71,000 h
ISAMS (Oxford/RAL)	80	15,800	10/91 through 7/92, instrument failed
HTSSE-2 (Northrop Grumman)	80	24,000	3/99 through 3/02, mission ended, no degradation
HTSSE-2 (BAe)	80	24,000	3/99 through 3/02, mission ended, no degradation
MOPITT (BAe)	50-80	138,600	Turn on 3/00, lost one disp. at 10.300 h
<b>Odin (Astrium)</b>	<b>50-80</b>	<b>132,600</b>	<b>Turn-on 3/01, ongoing, no degradation</b>
ERS-1: AATSR and MIPAS (Astrium)	50-80	88,200	3/02 through 4/12, no degradation, satellite failed
INTEGRAL (Astrium)	50-80	118,700	Turn-on 10/02, ongoing, no degradation
Helios 2A (Astrium)	50-80	96,600	Turn-on 4/05, ongoing, no degradation
Helios 2B (Astrium)	50-80	58,800	Turn-on 4/10, ongoing, no degradation
SLSTR (Airbus)	50-80	1,4000	Turn-on 3/16, ongoing, no degradation
<b>Pulse-Tube</b>			
CX (Northrop Grumman)	150	161,600	Turn-on 2/98, ongoing, no degradation
MTI (Northrop Grumman)	60	141,600	Turn-on 3/00, ongoing, no degradation
Hyperion (Northrop Grumman)	110	133,600	Turn-on 12/00, ongoing, no degradation
SABER on TIMED (Northrop Grumman)	75	129,600	Turn-on 1/02, ongoing, no degradation
AIRS (Northrop Grumman)	55	121,600	Turn-on 6/02, ongoing, no degradation
TES (Northrop Grumman)	60	102,600	Turn-on 8/04, ongoing, no degradation
JAMI (Northrop Grumman)	65	91,000	4/05 through 12/15, mission ended, no degradation
IBUKI/GOSAT (Northrop Grumman)	65	63,300	Turn-on 2/09, ongoing, no degradation

**Table 2 (Continued).**

Cooler, mission, and manufacturer	T (K)	Hours/unit	Notes
OCO-2 (Northrop Grumman)	110	14,900	Turn-on 8/14, ongoing, no degradation
Himawari-8 (Northrop Grumman)	65	12,800	Turn-on 12/14, ongoing, no degradation
Joule-Thompson			
ISS—SMILES (Sumitomo)	4.5	4500	10/09 through 04/10, instrument failed
<b>Planck (RAL/ESA)</b>	<b>4</b>	<b>38,500</b>	<b>5/09 through 10/13, mission ended, no degradation</b>
<b>Planck (JPL)</b>	<b>18</b>	<b>27,500</b>	<b>FM1: 8/10-10/13 (EOM), FM2: failed at 10,500 h</b>

Note: Almost all cryocoolers have continued to operate normally until turned off at the end of the instrument life. Mid/far-infrared and CMB astrophysics observatories are highlighted in bold. The data in this table are courtesy of Ron Ross, Jr.

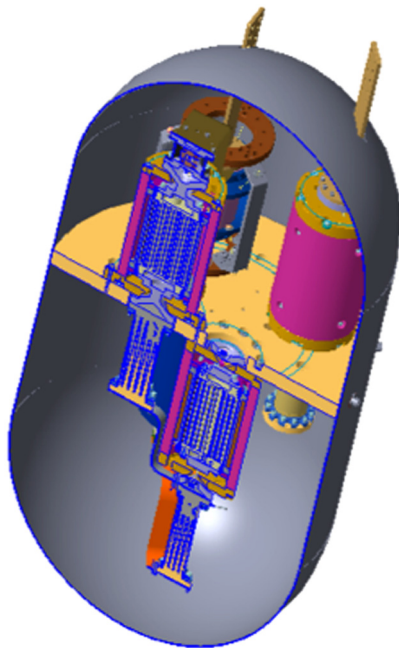


**Fig. 21** The CADR under development at NASA GSFC. This will provide  $6 \mu\text{W}$  of cooling at 50 mK. It also has a precooling stage that can be operated from 0.3 to 1.5 K. The picture also shows a notional enclosing magnetic shield for a  $<1 \mu\text{T}$  fringing field.

have, to date, not unduly stressed downlinking systems, but this could change in the future with multiple instruments each with  $10^4$  to  $10^5$  pixels on a single observatory. Moreover, the increasing number and diversity of PI and facility-class infrared observatories poses challenges to data archiving, in particular for enabling investigators to efficiently use data from multiple observatories in a single study. One way to mitigate this challenge is by increasing the use of onboard data processing and compression, as is already done for missions operating at shorter wavelengths.

#### **Commonality and community in instrument software:**

Many tasks are similar across a single platform, and even between platforms (e.g., pointing algorithms, focus, and data download). Continuous adherence to software development best practices, code sharing via repositories via GitHub, and fully open-sourcing software, will continue to drive down

associated operating costs, speed up development, and facilitate ease of access.

## **6 Conclusions: The Instrument Development Landscape for Infrared Astronomy**

The picture that coalesces from this review is that far-infrared astronomy is still an emerging field, even after over 40 years of development. Optical and near-infrared astronomy has a mature and well-understood landscape in terms of technology development for different platforms. In contrast, far-infrared astronomy has more of the “wild west” about it; there are several observing platforms that range widely in maturity, all with overlapping but complementary domains of excellence. Moreover, considering the state of technology, all areas have development paths where huge leaps forward in infrared observing capability can be obtained. In some cases, entirely new platforms can be made possible.

To conclude this review, we bring together and synthesize this information in order to lay out how the capabilities of each platform can be advanced. To do so, we use the following definitions:

- **Enabling:** Enabling technologies satisfy a capability need for a platform, allowing that platform to perform science observations in a domain that was previously impossible with that platform.
- **Enhancing:** Enhancing technologies provide significant benefits to a platform over the current state of the art, in terms of, e.g., observing efficiency or cost effectiveness, but do not allow that platform to undertake observations in new science domains.

These definitions correspond closely to the definitions of enabling (a pull technology) and enhancing (a push technology) as used in the 2015 NASA Technology Roadmap.

As different technology fields vary in relevance for different platforms, technologies can be enabling for some platforms and enhancing for others. In Fig. 22, we assess the status of selected technology areas as enabling or enhancing, as a function of observing platform. This table is solely the view of the authors and not obtained via a community consultation.

With this caveat in mind, based on Fig. 22, we present a non-exhaustive list of important technology development areas for far-infrared astronomy:



since the saturation powers of currently proposed high-resolution detector arrays are within  $\sim 2$  orders of magnitude of their NEPs. It would be advantageous to increase the dynamic range of detector arrays to 5 or more orders of magnitude of their NEPs, as this would mitigate the need to populate the focal plane with multiple detector arrays, each with different NEPs.

**LOs for heterodyne spectroscopy:** The extremely high spectral resolutions achievable by heterodyne spectroscopy at mid/far-infrared wavelengths are of great value, both for scientific investigations in their own right and for complementarity with the moderate spectral resolutions of facilities, such as JWST. This motivates continued development of high-quality LO sources to increase the sensitivity and bandwidth of heterodyne receivers. An important development area is high spectral purity, narrow-line, phase-locked, high-power (5 to 10 mW) QCL LOs, as the QCL LOs operate effectively for the higher frequency ( $>3$  THz) arrays. A complementary development area is power division schemes (e.g., Fourier phase gratings) to utilize QCLs effectively.

**High bandwidth heterodyne mixers:** The current bandwidth of heterodyne receivers means that only very small spectral ranges can be observed at any one time, meaning that some classes of observation, such as multiple line scans of single objects, are often prohibitively inefficient. There is, thus, a need to increase the IF bandwidth of 1- to 5-THz heterodyne mixers. A reference goal is a minimum of 8-GHz bandwidth required at frequencies of  $\sim 3$  THz. This will allow for simultaneous observation of multiple lines, improving both efficiency and calibration accuracy. A related development priority is low-noise 1- to 5-THz mixers that can operate at temperatures of  $>20$  K. At present, the most promising paths toward such mixers align with the HEB and SIS technologies.

**Interferometry:** Ground-based observations have conclusively demonstrated the extraordinary power of interferometry in the centimeter to submillimeter, with facilities such as the VLA and ALMA providing orders of magnitude increases in spatial resolution and sensitivity over any existing single-dish telescope. As Fig. 22 illustrates, the technology needs for space-based far-infrared interferometry are relatively modest and center on direct-detector developments. For interferometry, high-speed readout is more important than a large pixel count or extremely low NEP. For example, SPIRIT requires  $14 \times 14$  pixel arrays of detectors with a NEP of  $\sim 10^{-19}$  W/ $\sqrt{\text{Hz}}$  and a detector time constant of  $\sim 185 \mu\text{s}$ .<sup>76</sup> Detailed simulations, coupled with rigorous laboratory experimentation and algorithm development, are the greatest priorities for interferometry.

**Cryocoolers:** As cooling to 4- and 0.1-K temperatures is required for all far-infrared observations, improvements in the efficiency, power requirements, size, and vibration of cryocoolers are valuable for all far-infrared space- and suborbital-based platforms. For  $<0.1$  K coolers, there is a need for further development of both CADR and DRs that enable cooling of up to tens of  $\mu\text{W}$  at  $<0.1$  K, to enable cooling of larger arrays. For 4 K coolers, further development to maximize cooling power per input power for small cooling loads ( $<100$  mW at 4 K) and lower mass is desirable, along with minimizing the exported vibration from the cooler system. For  $\sim 30$  K coolers, development of a cooling solution with power, space, and vibration envelopes that enable its use inside a 6U CubeSat, while leaving adequate resources for detector arrays, optics, and downlink systems, would enable far-infrared observations from CubeSat platforms, as well as enhancing larger observatories.

**Deployable and/or lightweight telescope mirrors:** The advent of long-duration, high-altitude observing platforms, and the expanded capabilities of future launch vehicles, enable the consideration of mirrors for far-infrared observatories with diameters 2 to 5 times larger than on facilities such as SOFIA and Herschel. The most important limitations on mirror size are then the (1) mass and (2) approaches to active control of the mirror surface. The development of large-aperture, lightweight, high-surface-accuracy mirrors is thus an important consideration, including those in a deployable configuration. A related area is the development of optical components that accommodate large-format arrays or very high-resolution spectroscopy.

**Technology maturation platforms:** Suborbital far-infrared platforms, including ground-based facilities, SOFIA, and balloon-borne observatories, continue to make profound advances in all areas of astrophysics. However, they also serve as a tiered set of platforms for technology maturation and raising TRLs. The continuous use of all these platforms for technology development is essential to realize the long-term ambitions of the far-infrared community for large, actively cooled, space-based infrared telescopes. A potentially valuable addition to this technology maturation tier is the ISS, which offers a long-term, stable orbital platform with abundant power.

**Software and data archiving:** In the post-Herschel era, SOFIA and other sub-orbital platforms will play a critical role in mining the information-rich far-infrared spectral range, and in keeping the community moving forward. For example, the instruments flying on SOFIA and currently under development did not exist when Herschel instrumentation was defined. During this time, and henceforth, there is an urgent need to ensure community best practices in software design, code sharing, and open sourcing via community-wide mechanisms. It is also important to maintain and enhance data-archiving schemes that effectively bridge multiple complex platforms in a transparent way and which enable access to the broadest possible spectrum of the community.

## Acknowledgments

We thank George Nelson and Kenol Jules for their help on the capabilities of the ISS, and Jochem Baselmans for insights into KIDs. We also thank all speakers who took part in the FIR SIG Webinar series. This report is developed in part from the presentations and discussions at the Far-Infrared Next Generation Instrumentation Community Workshop, held in Pasadena, California, in March 2017. It is written as part of the activities of the Far-Infrared Science Interest Group. This work is supported by CNES. A portion of the research was carried out at the Jet Propulsion Laboratory, California Institute of Technology, under a contract with the National Aeronautics and Space Administration.

## References

1. D. E. Backman, A. Dasgupta, and R. E. Stencel, "Model of a Kuiper belt small grain population and resulting far-infrared emission," *Astrophys. J.* **450**, L35 (1995).
2. P. Santos-Sanz et al., "'TNOs are Cool': a survey of the trans-Neptunian region. IV. Size/albedo characterization of 15 scattered disk and detached objects observed with Herschel-PACS," *Astron. Astrophys.* **541**, A92 (2012).
3. J. Lebreton et al., "An icy Kuiper belt around the young solar-type star HD 181327," *Astron. Astrophys.* **539**, A17 (2012).
4. C. Eiroa et al., "DUst around NEArby stars. The survey observational results," *Astron. Astrophys.* **555**, A11 (2013).

5. D. Nesvorný et al., “Cometary origin of the zodiacal cloud and carbonaceous micrometeorites. implications for hot debris disks,” *Astrophys. J.* **713**, 816–836 (2010).
6. A. Morbidelli et al., “Source regions and time scales for the delivery of water to Earth,” *Meteorit. Planet. Sci.* **35**, 1309–1320 (2000).
7. M. J. Mumma and S. B. Charnley, “The chemical composition of comets—emerging taxonomies and natal heritage,” *Annu. Rev. Astron. Astrophys.* **49**, 471–524 (2011).
8. P. Hartogh et al., “Ocean-like water in the Jupiter-family comet 103P/Hartley 2,” *Nature* **478**, 218–220 (2011).
9. W. S. Holland et al., “Submillimetre images of dusty debris around nearby stars,” *Nature* **392**, 788–791 (1998).
10. S. M. Andrews and J. P. Williams, “Circumstellar dust disks in Taurus–Auriga: the submillimeter perspective,” *Astrophys. J.* **631**, 1134–1160 (2005).
11. G. Bryden et al., “Frequency of debris disks around solar-type stars: first results from a Spitzer MIPS survey,” *Astrophys. J.* **636**, 1098–1113 (2006).
12. M. C. Wyatt, “Evolution of debris disks,” *Annu. Rev. Astron. Astrophys.* **46**, 339–383 (2008).
13. M. R. Hogerheijde et al., “Detection of the water reservoir in a forming planetary system,” *Science* **334**, 338–340 (2011).
14. L. Kaltenegger, W. A. Traub, and K. W. Jucks, “Spectral evolution of an Earth-like planet,” *Astrophys. J.* **658**, 598–616 (2007).
15. P. Hedelt et al., “Spectral features of Earth-like planets and their detectability at different orbital distances around F, G, and K-type stars,” *Astron. Astrophys.* **553**, A9 (2013).
16. P. André et al., “From filamentary clouds to prestellar cores to the stellar IMF: initial highlights from the Herschel Gould Belt Survey,” *Astron. Astrophys.* **518**, L102 (2010).
17. ALMA Partnership et al., “The 2014 ALMA long baseline campaign: first results from high angular resolution observations toward the HL Tau Region,” *Astrophys. J.* **808**, L3 (2015).
18. F. Motte, P. André, and R. Neri, “The initial conditions of star formation in the rho Ophiuchi main cloud: wide-field millimeter continuum mapping,” *Astron. Astrophys.* **336**, 150–172 (1998).
19. N. J. Evans, II et al., “The Spitzer c2d legacy results: star-formation rates and efficiencies; evolution and lifetimes,” *Astrophys. J. Suppl. Ser.* **181**, 321–350 (2009).
20. F. Schuller et al., “ATLASGAL—the APEX telescope large area survey of the galaxy at 870  $\mu\text{m}$ ,” *Astron. Astrophys.* **504**, 415–427 (2009).
21. L. E. Kristensen et al., “Water in star-forming regions with Herschel (WISH). II. Evolution of 557 GHz  $1_{10}\text{-}1_{01}$  emission in low-mass protostars,” *Astron. Astrophys.* **542**, A8 (2012).
22. P. Manoj et al., “Herschel/PACS spectroscopic survey of protostars in orion: the origin of far-infrared CO emission,” *Astrophys. J.* **763**, 83 (2013).
23. E. F. van Dishoeck et al., “Water in star-forming regions with the Herschel Space Observatory (WISH). I. Overview of key program and first results,” *Publ. Astron. Soc. Pac.* **123**, 138–170 (2011).
24. D. M. Watson et al., “Evolution of mass outflow in protostars,” *Astrophys. J.* **828**, 52 (2016).
25. M. M. Dunham et al., “Identifying the low-luminosity population of embedded protostars in the c2d observations of clouds and cores,” *Astrophys. J. Suppl. Ser.* **179**, 249–282 (2008).
26. E. Furlan et al., “The Herschel orion protostar survey: spectral energy distributions and fits using a Grid of protostellar models,” *Astrophys. J. Suppl. Ser.* **224**, 5 (2016).
27. W. J. Fischer et al., “The Herschel orion protostar survey: luminosity and envelope evolution,” *Astrophys. J.* **840**, 69 (2017).
28. B. A. Whitney et al., “Two-dimensional radiative transfer in protostellar envelopes. II. An evolutionary sequence,” *Astrophys. J.* **598**, 1079–1099 (2003).
29. R. Launhardt et al., “The Earliest Phases of Star Formation (EPoS): a Herschel key project. The thermal structure of low-mass molecular cloud cores,” *Astron. Astrophys.* **551**, A98 (2013).
30. A. M. Stutz et al., “A Herschel and APEX census of the reddest sources in Orion: searching for the youngest protostars,” *Astrophys. J.* **767**, 36 (2013).
31. C. D. Howard et al., “Herschel/PACS survey of protoplanetary disks in Taurus/Auriga – observations of [O I] and [C II], and far-infrared continuum,” *Astrophys. J.* **776**, 21 (2013).
32. B. Acke et al., “Herschel images of Fomalhaut. An extrasolar Kuiper belt at the height of its dynamical activity,” *Astron. Astrophys.* **540**, A125 (2012).
33. N. Billot et al., “Herschel far-infrared photometric monitoring of protostars in the Orion Nebula Cluster,” *Astrophys. J.* **753**, L35 (2012).
34. S. J. Kenyon et al., “An IRAS survey of the Taurus–Auriga molecular cloud,” *Astron. J.* **99**, 869–887 (1990).
35. D. Calzetti et al., “The dust content and opacity of actively star-forming galaxies,” *Astrophys. J.* **533**, 682–695 (2000).
36. A. Li and B. T. Draine, “Infrared emission from interstellar dust. II. The diffuse interstellar medium,” *Astrophys. J.* **554**, 778–802 (2001).
37. D. A. Dale et al., “The infrared spectral energy distribution of normal star-forming galaxies,” *Astrophys. J.* **549**, 215–227 (2001).
38. S. Molinari et al., “Hi-GAL: the Herschel infrared galactic plane survey,” *Publ. Astron. Soc. Pac.* **122**, 314–325 (2010).
39. M. K. Crawford et al., “Far-infrared spectroscopy of galaxies—the 158 micron C(+) line and the energy balance of molecular clouds,” *Astrophys. J.* **291**, 755–771 (1985).
40. P. Panuzzo et al., “Probing the molecular interstellar medium of M82 with Herschel-SPIRE spectroscopy,” *Astron. Astrophys.* **518**, L37 (2010).
41. J. Fischer et al., “Herschel-PACS spectroscopic diagnostics of local ULIRGs: conditions and kinematics in Markarian 231,” *Astron. Astrophys.* **518**, L41 (2010).
42. T. Daz-Santos et al., “Explaining the [C II] 157.7  $\mu\text{m}$  deficit in luminous infrared galaxies—first results from a Herschel/PACS study of the GOALS sample,” *Astrophys. J.* **774**, 68 (2013).
43. D. Farrah et al., “Far-infrared fine-structure line diagnostics of ultraluminous infrared galaxies,” *Astrophys. J.* **776**, 38 (2013).
44. G. Lagache, J.-L. Puget, and H. Dole, “Dusty infrared galaxies: sources of the cosmic infrared background,” *Annu. Rev. Astron. Astrophys.* **43**, 727–768 (2005).
45. P. Madau and M. Dickinson, “Cosmic star-formation history,” *Annu. Rev. Astron. Astrophys.* **52**, 415–486 (2014).
46. C. J. Lonsdale, D. Farrah, and H. E. Smith, “Ultraluminous Infrared Galaxies,” *Astrophysics Update 2*, J. W. Mason, Ed., p. 285 (2006).
47. G. Rodighiero et al., “The lesser role of starbursts in star formation at  $z = 2$ ,” *Astrophys. J.* **739**, L40 (2011).
48. D. Lutz et al., “PACS evolutionary probe (PEP)—a Herschel key program,” *Astron. Astrophys.* **532**, A90 (2011).
49. S. J. Oliver et al., “The Herschel multi-tiered extragalactic survey: HerMES,” *MNRAS* **424**, 1614–1635 (2012).
50. C. M. Casey, D. Narayanan, and A. Cooray, “Dusty star-forming galaxies at high redshift,” *Phys. Rep.* **541**, 45–161 (2014).
51. R. Genzel et al., “A study of the gas-star formation relation over cosmic time,” *MNRAS* **407**, 2091–2108 (2010).
52. A. C. Fabian, “Observational evidence of active galactic nuclei feedback,” *Annu. Rev. Astron. Astrophys.* **50**, 455–489 (2012).
53. D. Farrah et al., “Direct evidence for termination of obscured star formation by radiatively driven outflows in reddened QSOs,” *Astrophys. J.* **745**, 178 (2012).
54. L. Page et al., “Three-year Wilkinson microwave anisotropy probe (WMAP) observations: polarization analysis,” *Astrophys. J. Suppl. Ser.* **170**, 335–376 (2007).
55. Planck Collaboration et al., “Planck 2015 results. XV. Gravitational lensing,” *Astron. Astrophys.* **594**, A15 (2016).
56. B. T. Soifer and J. L. Pipher, “Instrumentation for infrared astronomy,” *Annu. Rev. Astron. Astrophys.* **16**, 335–369 (1978).
57. F. J. Low, G. H. Rieke, and R. D. Gehrz, “The beginning of modern infrared astronomy,” *Annu. Rev. Astron. Astrophys.* **45**, 43–75 (2007).
58. G. H. Rieke, “Infrared detector arrays for astronomy,” *Annu. Rev. Astron. Astrophys.* **45**, 77–115 (2007).
59. P. H. Siegel, “THz instruments for space,” *IEEE Trans. Antennas Propag.* **55**, 2957–2965 (2007).
60. S. Price, “History of space-based infrared astronomy and the air force infrared celestial backgrounds program,” Tech. Rep., Air Force Research Lab Hanscom AFB MA Space Vehicles Directorate (2008).
61. S. D. Price, “Infrared sky surveys,” *Space Sci. Rev.* **142**, 233–321 (2009).
62. G. H. Rieke, “History of infrared telescopes and astronomy,” *Exp. Astron.* **25**, 125–141 (2009).
63. J. Lequeux, “Early infrared astronomy,” *J. Astron. Hist. Heritage* **12**(2), 125–140 (2009).

64. M. Rowan-Robinson, *Night Vision: Exploring the Infrared Universe*, Cambridge University Press, Cambridge (2013).
65. D. L. Clements, *Infrared Astronomy—Seeing the Heat: from William Herschel to the Herschel Space Observatory*, CRC Press, Florida (2014).
66. D. Rigopoulou et al., “The European far-infrared space roadmap,” arXiv e-prints (2017).
67. T. Webb et al., “A roadmap for canadian submillimetre astronomy,” arXiv:1312.5013 (2013).
68. C. Walker, *Terahertz Astronomy*, CRC Press, Florida (2015).
69. Y. Lee, *Principles of Terahertz Science and Technology*, Lecture Notes in Physics, Springer US, New York (2009).
70. S. S. Dhillon et al., “The 2017 terahertz science and technology roadmap,” *J. Phys. D: Appl. Phys.* **50**(4), 043001 (2017).
71. S. D. Lord, “A new software tool for computing Earth’s atmospheric transmission of near- and far-infrared radiation,” Tech. Rep. (1992).
72. B. Koopman et al., “The CCAT-prime extreme field-of-view submillimeter telescope on Cerro Chajnantor,” *Am. Astron. Soc. Meeting Abstr.* **229**, 437.01 (2017).
73. M. D. Niemack, “Designs for a large-aperture telescope to map the CMB 10x faster,” *Appl. Opt.* **55**, 1688 (2016).
74. S. J. E. Radford and J. B. Peterson, “Submillimeter atmospheric transparency at Maunakea, at the south pole, and at Chajnantor,” *Publ. Astron. Soc. Pac.* **128**, 075001 (2016).
75. B. Jackson et al., “The spica-safari detector system: Tes detector arrays with frequency-division multiplexed squid readout,” *IEEE Trans. Terahertz Sci. Technol.* **2**(1), 12–21 (2012).
76. D. J. Benford et al., “Cryogenic far-infrared detectors for the Space Infrared Interferometric Telescope (SPIRIT),” *Proc. SPIE* **6687**, 66870E (2007).
77. P. Temi et al., “The SOFIA observatory at the start of routine science operations: mission capabilities and performance,” *Astrophys. J. Suppl. Ser.* **212**, 24 (2014).
78. E. T. Young et al., “Early science with SOFIA, the stratospheric observatory for infrared astronomy,” *Astrophys. J.* **749**, L17 (2012).
79. S. M. Feeney et al., “Cosmic microwave background science at commercial airline altitudes,” *MNRAS* **469**, L6–L10 (2017).
80. J. D. Adams et al., “FORCAST: a first light facility instrument for SOFIA,” *Proc. SPIE* **7735**, 77351U (2010).
81. T. L. Herter et al., “First science observations with SOFIA/FORCAST: the FORCAST mid-infrared camera,” *Astrophys. J.* **749**, L18 (2012).
82. M. J. Richter et al., “High-resolution mid-infrared spectroscopy from SOFIA using EXES,” *Proc. SPIE* **4857**, 37–46 (2003).
83. S. Colditz et al., “The SOFIA far-infrared spectrometer FIFI-LS: spear-heading a post Herschel era,” *Proc. SPIE* **8446**, 844617 (2012).
84. D. A. Harper et al., “Development of the HAWC far-infrared camera for SOFIA,” *Proc. SPIE* **5492**, 1064–1073 (2004).
85. S. Heyminck et al., “GREAT: the SOFIA high-frequency heterodyne instrument,” *Astron. Astrophys.* **542**, L1 (2012).
86. B. Klein et al., “High-resolution wide-band fast Fourier transform spectrometers,” *Astron. Astrophys.* **542**, L3 (2012).
87. E. W. Dunham et al., “HIPO: a high-speed imaging photometer for occultations,” *Proc. SPIE* **5492**, 592–603 (2004).
88. I. S. McLean et al., “FLITECAM: a 1–5 micron camera and spectrometer for SOFIA,” *Proc. SPIE* **6269**, 62695B (2006).
89. C. D. Dowell et al., “HAWC+: a detector, polarimetry, and narrow-band imaging upgrade to SOFIA’s far-infrared facility camera,” *Am. Astron. Soc. Meeting Abstr.* **221**, 345.14 (2013).
90. C. Risacher et al., “The upGREAT 1.9 THz multi-pixel high resolution spectrometer for the SOFIA Observatory,” *Astron. Astrophys.* **595**, A34 (2016).
91. J. C. Mankins, “Technology readiness levels,” *White Paper*, April 6 (1995).
92. J. C. Mankins, “Technology readiness assessments: a retrospective,” *Acta Astronaut.* **65**(9), 1216–1223 (2009).
93. G. S. Tucker et al., “The balloon-borne large aperture sub-millimeter telescope,” *Adv. Space Res.* **33**, 1793–1796 (2004).
94. L. M. Fissel et al., “The balloon-borne large-aperture submillimeter telescope for polarimetry: BLAST-Pol,” *Proc. SPIE* **7741**, 77410E (2010).
95. N. Galitzki et al., “The next generation BLAST experiment,” *J. Astron. Instrum.* **3**, 1440001 (2014).
96. J.-P. Bernard et al., “PILOT: a balloon-borne experiment to measure the polarized FIR emission of dust grains in the interstellar medium,” *Exp. Astron.* **42**, 199–227 (2016).
97. C. Walker et al., “The stratospheric THz observatory (STO),” *Proc. SPIE* **7733**, 77330N (2010).
98. <https://www.csbf.nasa.gov/antarctica/payloads.htm> (March 2019).
99. H. Shibai et al., “Far-infrared interferometric experiment (FITE): toward the first flight,” in *Pathways Towards Habitable Planets*, Astronomical Society of the Pacific Conference Series, V. Coudé du Foresto, D. M. Gelino, and I. Ribas, Eds., Vol. **430**, p. 541 (2010).
100. S. A. Rinehart et al., “The balloon experimental twin telescope for infrared interferometry (BETTII): an experiment for high angular resolution in the far-infrared,” *Publ. Astron. Soc. Pac.* **126**, 660 (2014).
101. BICEP2 Collaboration, “Detection of B-mode polarization at degree angular scales by BICEP2,” *Phys. Rev. Lett.* **112**, 241101 (2014).
102. R. Flauger, J. C. Hill, and D. N. Spergel, “Toward an understanding of foreground emission in the BICEP2 region,” *J. Cosmol. Astropart. Phys.* **2014**, 039–039 (2014).
103. BICEP2/Keck Collaboration et al., “Joint analysis of BICEP2/Keck array and Planck data,” *Phys. Rev. Lett.* **114**, 101301 (2015).
104. A. Kogut et al., “The primordial inflation polarization explorer (PIPER),” *Proc. SPIE* **8452**, 84521J (2012).
105. N. N. Gandilo et al., “The primordial inflation polarization explorer (PIPER),” *Proc. SPIE* **9914**, 99141J (2016).
106. EBEX Collaboration, “The EBEX balloon borne experiment—optics, receiver, and polarimetry,” arXiv e-prints (2017).
107. K. Shivanandan, J. R. Houck, and M. O. Harwit, “Preliminary observations of the far-infrared night-sky background radiation,” *Phys. Rev. Lett.* **21**, 1460–1462 (1968).
108. J. R. Houck and M. Harwit, “Far-infrared observations of the night sky,” *Science* **164**, 1271–1273 (1969).
109. S. D. Price and R. G. Walker, *The AFGL Four Color Infrared Sky Survey: Catalog of Observations at 4.2, 11.0, 19.8, and 27.4 Micrometer* (1976).
110. G. Seibert, “The history of sounding rockets and their contribution to European Space Research,” Tech. Rep. (2006).
111. M. Zemcov et al., “The Cosmic Infrared Background Experiment (CIBER): a sounding rocket payload to study the near infrared extragalactic background light,” *Astrophys. J. Suppl. Ser.* **207**, 31 (2013).
112. N. R. Council, *Revitalizing NASA’s Suborbital Program: Advancing Science, Driving Innovation, and Developing Workforce*, The National Academies Press, Washington, DC (2010).
113. G. Neugebauer et al., “The Infrared Astronomical Satellite (IRAS) mission,” *Astrophys. J.* **278**, L1–L6 (1984).
114. J. D. Mill et al., “Midcourse space experiment: introduction to the spacecraft, instruments, and scientific objectives,” *J. Spacecr. Rockets* **31**, 900–907 (1994).
115. H. Murakami et al., “The IRTS (Infrared Telescope in Space) mission,” *Publ. Astron. Soc. Jpn.* **48**, L41–L46 (1996).
116. M. F. Kessler et al., “The Infrared Space Observatory (ISO) mission,” *Astron. Astrophys.* **315**(2), L27–L31 (1996).
117. G. J. Melnick et al., “The submillimeter wave astronomy satellite: science objectives and instrument description,” *Astrophys. J.* **539**, L77–L85 (2000).
118. H. L. Nordh et al., “The Odin orbital observatory,” *Astron. Astrophys.* **402**, L21–L25 (2003).
119. H. Murakami et al., “The infrared astronomical mission AKARI\*,” *Publ. Astron. Soc. Jpn.* **59**, S369–S376 (2007).
120. G. L. Pilbratt et al., “Herschel space observatory: an ESA facility for far-infrared and submillimetre astronomy,” *Astron. Astrophys.* **518**, L1 (2010).
121. E. L. Wright et al., “The Wide-Field Infrared Survey Explorer (WISE): mission description and initial on-orbit performance,” *Astron. J.* **140**, 1868–1881 (2010).
122. M. W. Werner et al., “The Spitzer space telescope mission,” *Astrophys. J. Suppl. Ser.* **154**, 1–9 (2004).
123. Planck Collaboration, “Planck early results. I. The Planck mission,” *Astron. Astrophys.* **536**, A1 (2011).
124. C. L. Bennett et al., “The microwave anisotropy probe mission,” *Astrophys. J.* **583**, 1–23 (2003).
125. N. W. Boggess et al., “The COBE mission—its design and performance two years after launch,” *Astrophys. J.* **397**, 420–429 (1992).
126. D. J. Fixsen et al., “The spectrum of the extragalactic far-infrared background from the COBE FIRAS observations,” *Astrophys. J.* **508**, 123–128 (1998).

127. A. Kogut et al., “The primordial inflation explorer (PIXIE),” *Proc. SPIE* **9904**, 99040W (2016).
128. T. Matsumura et al., “Mission design of LiteBIRD,” *J. Low Temp. Phys.* **176**, 733–740 (2014).
129. J. Delabrouille et al., “Exploring cosmic origins with CORE: survey requirements and mission design,” *J. Cosmol. Astropart. Phys.* **2018** (2018).
130. D. J. Fixsen, “The temperature of the cosmic microwave background,” *Astrophys. J.* **707**, 916–920 (2009).
131. D. Paradis et al., “Far-infrared to millimeter astrophysical dust emission. II. Comparison of the two-level systems (TLS) model with astronomical data,” *Astron. Astrophys.* **534**, A118 (2011).
132. C. Leinert et al., “The 1997 reference of diffuse night sky brightness,” *Astron. Astrophys. Suppl. Ser.* **127**, 1–99 (1998).
133. A. Poglitsch et al., “The photodetector array camera and spectrometer (PACS) on the Herschel space observatory,” *Astron. Astrophys.* **518**, L2 (2010).
134. M. J. Griffin et al., “The Herschel-SPIRE instrument and its in-flight performance,” *Astron. Astrophys.* **518**, L3 (2010).
135. P. Hacking and J. R. Houck, “A very deep IRAS survey at  $L = 97$  deg,  $B = 30$  deg,” *Astrophys. J. Suppl. Ser.* **63**, 311–333 (1987).
136. C. Kiss, U. Klaas, and D. Lemke, “Determination of confusion noise for far-infrared measurements,” *Astron. Astrophys.* **430**, 343–353 (2005).
137. H. Dole et al., “Confusion of extragalactic sources in the mid- and far-infrared: spitzer and beyond,” *Astrophys. J. Suppl. Ser.* **154**, 93–96 (2004).
138. H. T. Nguyen et al., “HerMES: the SPIRE confusion limit,” *Astron. Astrophys.* **518**, L5 (2010).
139. M. Negrello et al., “Confusion noise at far-infrared to millimetre wavelengths,” *MNRAS* **352**, 493–500 (2004).
140. N. Fernandez-Conde et al., “Simulations of the cosmic infrared and submillimeter background for future large surveys. I. Presentation and first application to Herschel/SPIRE and Planck/HFI,” *Astron. Astrophys.* **481**, 885–895 (2008).
141. T. T. Takeuchi et al., “Estimation of the confusion limit for spica,” in *JAXA Spec. Publ.: Proc. SPICA Sci. Conf. from Exoplanets to Distant Galaxies: SPICA’s New Window on the Cool Univ.*, p. 157 (2018).
142. M. G. Jones et al., “When is stacking confusing? The impact of confusion on stacking in deep H I galaxy surveys,” *MNRAS* **455**, 1574–1583 (2016).
143. B. Tercero et al., “A line confusion limited millimeter survey of Orion KL. I. Sulfur carbon chains,” *Astron. Astrophys.* **517**, A96 (2010).
144. A. Kogut, E. Dwek, and S. H. Moseley, “Spectral confusion for cosmological surveys of Redshifted C II emission,” *Astrophys. J.* **806**, 234 (2015).
145. K. K. Knudsen et al., “An ultra-deep submillimetre map: beneath the SCUBA confusion limit with lensing and robust source extraction,” *MNRAS* **368**, 487–496 (2006).
146. I. G. Roseboom et al., “The Herschel Multi-Tiered Extragalactic Survey: source extraction and cross-identifications in confusion-dominated SPIRE images,” *MNRAS* **409**, 48–65 (2010).
147. M. Safarzadeh et al., “A novel technique to improve photometry in confused images using graphs and Bayesian priors,” *Astrophys. J.* **798**, 91 (2015).
148. T. P. MacKenzie, D. Scott, and M. Swinbank, “SEDBLEND: a new method for deblending spectral energy distributions in confused imaging,” *MNRAS* **463**, 10–23 (2016).
149. P. D. Hurley et al., “HELP: XID+, the probabilistic de-blender for Herschel SPIRE maps,” *MNRAS* **464**, 885–896 (2017).
150. G. Raymond et al., “The effectiveness of mid IR / far IR blind, wide area, spectral surveys in breaking the confusion limit,” *Publ. Astron. Soc. Jpn.* **62**, 697–708 (2010).
151. J. M. Lamarre, “Photon noise in photometric instruments at far-infrared and submillimeter wavelengths,” *Appl. Opt.* **25**, 870–876 (1986).
152. P. L. Richards, “Bolometers for infrared and millimeter waves,” *J. Appl. Phys.* **76**(1), 1–24 (1994).
153. D. J. Benford, T. R. Hunter, and T. G. Phillips, “Noise equivalent powers of background limited thermal detectors at submillimeter wavelengths,” *Int. J. Infrared Millimeter Waves* **19**, 931–938 (1998).
154. C. K. Stahle et al., “Design and performance of the ASTRO-E/XRS microcalorimeter array and anticoincidence detector,” *Proc. SPIE* **3765**, 128–136 (1999).
155. C. K. Stahle et al., “Cosmic ray effects in microcalorimeter arrays,” *Nucl. Instrum. Methods Phys. Res. A* **520**, 472–474 (2004).
156. T. Saab et al., “GEANT modeling of the low-Earth-orbit cosmic-ray background for the Astro-E2 XRS instrument,” *Proc. SPIE* **5501**, 320–327 (2004).
157. J. P. Gardner et al., “The James Webb space telescope,” *Space Sci. Rev.* **123**, 485–606 (2006).
158. A. V. Smirnov et al., “Space mission Millimetron for terahertz astronomy,” *Proc. SPIE* **8442**, 84424C (2012).
159. N. S. Kardashev et al., “Review of scientific topics for the Millimetron space observatory,” *Phys. Usp.* **57**, 1199–1228 (2014).
160. T. Nakagawa et al., “HII/L2 mission: future Japanese infrared astronomical mission,” *Proc. SPIE* **3356**, 462–470 (1998).
161. T. NakagawaSpica Working Group, “SPICA: space infrared telescope for cosmology and astrophysics,” *Adv. Space Res.* **34**, 645–650 (2004).
162. B. Swinyard et al., “The space infrared telescope for cosmology and astrophysics: SPICA A joint mission between JAXA and ESA,” *Exp. Astron.* **23**, 193–219 (2009).
163. T. Nakagawa et al., “The next-generation infrared space mission Spica: project updates,” *Publ. Korean Astron. Soc.* **32**, 331–335 (2017).
164. B. Sibthorpe et al., “The SPICA mission,” *EAS Publ. Ser.* **75**, 411–417 (2015).
165. P. Roelfsema et al., “SAFARI new and improved: extending the capabilities of SPICA’s imaging spectrometer,” *Proc. SPIE* **9143**, 91431K (2014).
166. C. Pastor et al., “SAFARI optical system architecture and design concept,” *Proc. SPIE* **9904**, 99043U (2016).
167. C. BradfordSPICA Consortium, and SAFARI Consortium, “The space infrared telescope for cosmology and astrophysics and pending US contribution,” *Am. Astron. Soc. Meeting Abstr.* **229**, 238.25 (2017).
168. D. A. Dale and G. Helou, “The infrared spectral energy distribution of normal star-forming galaxies: calibration at far-infrared and submillimeter wavelengths,” *Astrophys. J.* **576**, 159–168 (2002).
169. J. J. A. Baselmans et al., “A kilo-pixel imaging system for future space based far-infrared observatories using microwave kinetic inductance detectors,” *Astron. Astrophys.* **601**, A89 (2017).
170. J. Bueno et al., “Full characterisation of a background limited antenna coupled KID over an octave of bandwidth for THz radiation,” *Appl. Phys. Lett.* **110**, 233503 (2017).
171. T. H. Zurbuchen, “Achieving Science with CubeSats: Thinking Inside the Box,” *Proc. SPIE* **9978** (2016).
172. D. R. Ardila, E. Shkolnik, and V. Gorjian, “Cubesats for astrophysics: the current perspective,” *Am. Astron. Soc. Meeting Abstr.* **229**, 206.05 (2017).
173. E. L. Shkolnik, “On the verge of an astronomy CubeSat revolution,” *Nat. Astron.* **2**, 374–378 (2018).
174. J. S. Perkins et al., “BurstCube: a CubeSat for gravitational wave counterparts,” *Am. Astron. Soc. Meeting Abstr.* **231**, 361.14 (2018).
175. P. Kaaret, “HaloSat—a CubeSat to study the hot galactic halo,” *Am. Astron. Soc. Meeting Abstr.* **229**, 328.03 (2017).
176. E. L. Shkolnik et al., “Monitoring the high-energy radiation environment of exoplanets around low-mass stars with SPARCS (Star-Planet Activity Research CubeSat),” *Am. Astron. Soc. Meeting Abstr.* **231** (2018).
177. B. T. Fleming et al., “Colorado ultraviolet transit experiment: a dedicated CubeSat mission to study exoplanetary mass loss and magnetic fields,” *J. Astron. Telesc. Instrum. Syst.* **4**, 014004 (2018).
178. A. Joseph, E. Barrentine, and A. Brown, “A thermal imaging instrument with uncooled detectors,” in *EGU Gen. Assembly Conf. Abstr.* **20**, 18357 (2018).
179. E. Agasid, K. Ennico-Smith, and A. Rademacher, “Collapsible space telescope (CST) for nanosatellite imaging and observation” (2013).
180. T. S. Pagano, “Cubesat infrared atmospheric sounder (CIRAS) NASA invest technology demonstration,” *Proc. SPIE* **10177**, 101770K (2017).
181. D. Ardila and D. Pack, “The cubesat multispectral observation system (cumulos)” (2016).
182. B. R. Johnson et al., “A CubeSat for calibrating ground-based and sub-orbital millimeter-wave polarimeters (CalSat),” *J. Astron. Instrum.* **4**, 1550007 (2015).

183. L. Primm, K. Jules, and L. Bullock, *External Payloads Proposer's Guide to the International Space Station*, Goddard Space Flight Center (2016).
184. R. L. Brown et al., "High-resolution imaging spectroscopy at terahertz frequencies," in *IAU Colloq. 123: Observatories in Earth Orbit and Beyond*, Astrophysics and Space Science Library, Y. Kondo, Ed., Vol. **166**, pp. 509–515 (1990).
185. M. Sauvage et al., "Sub-arcsecond far-infrared space observatory: a science imperative," *Submission to ESA Science Programme M-class Mission Call* (2013).
186. D. Leisawitz et al., "Advancing toward far-infrared interferometry in space through coordinated international efforts," *Proc. SPIE* **8860**, 88600A (2013).
187. R. Juanola-Parramon, "A far-infrared spectro-spatial space interferometer: instrument simulator and testbed implementation," Springer Theses, Springer International Publishing (2016).
188. C. Kouveliotou et al., "Enduring quests-daring visions (NASA astrophysics in the next three decades)," arXiv e-prints (2014).
189. N. R. Council, *Astronomy and Astrophysics in the New Millennium*, The National Academies Press, Washington, DC (2001).
190. M. Harwit, D. Leisawitz, and S. Rinehart, "A far-infrared/submillimeter kilometer-baseline interferometer in space," *New Astron. Rev.* **50**, 228–234 (2006).
191. D. Leisawitz et al., "The space infrared interferometric telescope (SPIRIT): high-resolution imaging and spectroscopy in the far-infrared," *Adv. Space Res.* **40**, 689–703 (2007).
192. F. P. Helmich and R. J. Ivison, "FIRI—a far-infrared interferometer," *Exp. Astron.* **23**, 245–276 (2009).
193. W. Wild et al., "ESPRIT: a study concept for a far-infrared interferometer in space," *Proc. SPIE* **7013**, 70132R (2008).
194. G. Durand et al., "TALC: a new deployable concept for a 20 m far-infrared space telescope," *Proc. SPIE* **9143**, 91431A (2014).
195. M. Sauvage et al., "A development roadmap for critical technologies needed for TALC: a deployable 20 m annular space telescope," *Proc. SPIE* **9904**, 99041L (2016).
196. K. Dohlen et al., "Design of a nano-satellite demonstrator of an infrared imaging space interferometer: the HyperCube," *Proc. SPIE* **9146**, 914603 (2014).
197. N. M. Elias, II et al., "The mathematics of double-Fourier interferometers," *Astrophys. J.* **657**, 1178–1200 (2007).
198. D. Leisawitz et al., "Developing wide-field spatio-spectral interferometry for far-infrared space applications," *Proc. SPIE* **8445**, 84450A (2012).
199. W. F. Grainger et al., "Demonstration of spectral and spatial interferometry at thz frequencies," *Appl. Opt.* **51**(12), 2202–2211 (2012).
200. P. Ade et al., "Progress in spectral-spatial interferometry at multi-thz frequencies: potential applications," in *2015 8th UK, Eur., China Millimeter Waves and THz Technol. Workshop (UCMMT)*, pp. 1–4 (2015).
201. C. Bracken et al., "Quasi-optical analysis of a far-infrared spatio-spectral space interferometer concept," *Infrared Phys. Technol.* **77**, 171–178 (2016).
202. S. A. Rinehart et al., "The space high angular resolution probe for the infrared (SHARP-IR)," *Proc. SPIE* **9904**, 99042L (2016).
203. D. Deming et al., "Spitzer transit and secondary eclipse photometry of GJ 436b," *Astrophys. J.* **667**, L199–L202 (2007).
204. M. J. Griffin, J. J. Bock, and W. K. Gear, "Relative performance of filled and feedhorn-coupled focal-plane architectures," *Appl. Opt.* **41**, 6543–6554 (2002).
205. T. Suzuki et al., "Development of ultra-low-noise TES bolometer arrays," *J. Low Temp. Phys.* **184**, 52–59 (2016).
206. BICEP2 Collaboration, Keck Array Collaboration, and SPIDER Collaboration, "Antenna-coupled TES bolometers used in BICEP2, Keck array, and spider," *Astrophys. J.* **812**, 176 (2015).
207. S. W. Henderson et al., "Readout of two-kilopixel transition-edge sensor arrays for Advanced ACTPol," *Proc. SPIE* **9914**, 99141G (2016).
208. J. Hubmayr et al., "Design of 280 GHz feedhorn-coupled TES arrays for the balloon-borne polarimeter SPIDER," *Proc. SPIE* **9914**, 99140V (2016).
209. R. J. Thornton et al., "The Atacama cosmology telescope: the polarization-sensitive ACTPol instrument," *Astrophys. J. Suppl. Ser.* **227**, 21 (2016).
210. K. L. Denis et al., "Fabrication of feedhorn-coupled transition edge sensor arrays for measurement of the cosmic microwave background polarization," *J. Low Temp. Phys.* **184**, 668–673 (2016).
211. O. Noroozian et al., "High-resolution gamma-ray spectroscopy with a microwave-multiplexed transition-edge sensor array," *Appl. Phys. Lett.* **103**, 202602 (2013).
212. K. D. Irwin et al., "X-ray detection using a superconducting transition-edge sensor microcalorimeter with electrothermal feedback," *Appl. Phys. Lett.* **69**, 1945–1947 (1996).
213. D. A. Wollman et al., "Superconducting transition-edge-microcalorimeter X-ray spectrometer with 2 eV energy resolution at 1.5 keV," *Nucl. Instrum. Methods Phys. Res. A* **444**, 145–150 (2000).
214. S. J. Smith et al., "Transition-edge sensor pixel parameter design of the microcalorimeter array for the x-ray integral field unit on Athena," *Proc. SPIE* **9905**, 99052H (2016).
215. L. Gottardi et al., "Development of the superconducting detectors and read-out for the X-IFU instrument on board of the X-ray observatory Athena," *Nucl. Instrum. Methods Phys. Res. A* **824**, 622–625 (2016).
216. W. S. Holland et al., "SCUBA-2: the 10 000 pixel bolometer camera on the James Clerk Maxwell Telescope," *MNRAS* **430**, 2513–2533 (2013).
217. D. J. Goldie et al., "Ultra-low-noise transition edge sensors for the SAFARI L-band on SPICA," *Proc. SPIE* **8452**, 84520A (2012).
218. D. J. Goldie et al., "Performance of horn-coupled transition edge sensors for L- and S-band optical detection on the SAFARI instrument," *Proc. SPIE* **9914**, 99140A (2016).
219. P. Khosropanah et al., "Ultra-low noise TES bolometer arrays for SAFARI instrument on SPICA," *Proc. SPIE* **9914**, 99140B (2016).
220. R. A. Hijmering et al., "Readout of a 176 pixel FDM system for SAFARI TES arrays," *Proc. SPIE* **9914**, 99141C (2016).
221. A. D. Beyer et al., "Development of fast, background-limited transition-edge sensors for the background-limited infrared/sub-mm spectrograph (BLISS) for SPICA," *Proc. SPIE* **8452**, 84520G (2012).
222. B. S. Karasik et al., "Normal metal hot-electron nanobolometer with Johnson noise thermometry readout," *IEEE Trans. Terahertz Sci. Technol.* **5**(1), 16–21 (2014).
223. K. D. Irwin and G. C. Hilton, *Transition-Edge Sensors*, p. 63 (2005).
224. P. K. Day et al., "A broadband superconducting detector suitable for use in large arrays," *Nature* **425**, 817–821 (2003).
225. J. Zmuidzinas, "Superconducting microresonators: physics and applications," *Ann. Rev. Condens. Matter Phys.* **3**(1), 169–214 (2012).
226. L. J. Swenson et al., "MAKO: a pathfinder instrument for on-sky demonstration of low-cost 350 micron imaging arrays," *Proc. SPIE* **8452**, 84520P (2012).
227. P. R. Maloney et al., "MUSIC for sub/millimeter astrophysics," *Proc. SPIE* **7741**, 77410F (2010).
228. S. Heyminck et al., "Development of a MKID Camera for APEX," in *Twenty-First Int. Symp. Space Terahertz Technol.*, p. 262 (2010).
229. A. Monfardini et al., "NIKA: a millimeter-wave kinetic inductance camera," *Astron. Astrophys.* **521**, A29 (2010).
230. A. Monfardini et al., "A dual-band millimeter-wave kinetic inductance camera for the IRAM 30 m telescope," *Astrophys. J. Suppl. Ser.* **194**, 24 (2011).
231. R. Adam et al., "The NIKA2 large-field-of-view millimetre continuum camera for the 30 m IRAM telescope," *Astron. Astrophys.* **609**, A115 (2018).
232. G. Cataldo et al., "Micro-spec: an ultracompact, high-sensitivity spectrometer for far-infrared and submillimeter astronomy," *Appl. Opt.* **53**(6), 1094–1102 (2014).
233. E. M. Barrentine et al., "Design and performance of a high resolution  $\mu$  spec: an integrated sub-millimeter spectrometer," *Proc. SPIE* **9914**, 99143O (2016).
234. E. Shirokoff et al., "Design and performance of superspec: an on-chip, kid-based, mm-wavelength spectrometer," *J. Low Temp. Phys.* **176**(5–6), 657–662 (2014).
235. A. Endo et al., "Development of DESHIMA: a redshift machine based on a superconducting on-chip filterbank," *Proc. SPIE* **8452**, 84520X (2012).
236. B. A. Mazin et al., "A superconducting focal plane array for ultraviolet, optical, and near-infrared astrophysics," *Opt. Express* **20**, 1503 (2012).
237. B. A. Mazin et al., "ARCONS: a 2024 pixel optical through near-IR cryogenic imaging spectrophotometer," *Publ. Astron. Soc. Pac.* **125**, 1348–1361 (2013).

238. S. Meeker et al., "Design and development status of mkid integral field spectrographs for high contrast imaging," in *Adapt. Opt. Extrem. Large Telesc. 4—Conf. Proc.*, Vol. 1, No 1 (2015).
239. B. A. Mazin et al., "MKIDs for direct imaging of exoplanets," *AAS/Div. Extreme Solar Syst. Abstr.* **3**, 104.07 (2015).
240. B. A. Mazin et al., "Science with KRAKENS," arXiv e-prints (2015).
241. T. Cook et al., "Planetary imaging concept testbed using a recoverable experiment-coronagraph (picture c)," *J. Astron. Telesc. Instrum. Syst.* **1**(4), 044001 (2015).
242. M. Calvo et al., "Development of Kinetic Inductance Detectors for Cosmic Microwave Background experiments," *Exp. Astron.* **28**, 185–194 (2010).
243. K. Karatsu et al., "Development of 1000 arrays MKID camera for the CMB observation," *Proc. SPIE* **8452**, 84520Q (2012).
244. H. McCarrick et al., "Horn-coupled, commercially-fabricated aluminum lumped-element kinetic inductance detectors for millimeter wavelengths," *Rev. Sci. Instrum.* **85**(12), 123117 (2014).
245. A. E. Lowitz et al., "Design, fabrication, and testing of lumped element kinetic inductance detectors for 3 mm CMB Observations," *Proc. SPIE* **9153**, 91532R (2014).
246. S. Oguri et al., "Groundbird: observing cosmic microwave polarization at large angular scale with kinetic inductance detectors and high-speed rotating telescope," *J. Low Temp. Phys.* **184**(3–4), 786–792 (2016).
247. P. J. de Visser et al., "Fluctuations in the electron system of a superconductor exposed to a photon flux," *Nat. Commun.* **5**, 3130 (2014).
248. M. Griffin et al., "SPACEKIDS: kinetic inductance detectors for space applications," *Proc. SPIE* **9914**, 991407 (2016).
249. A. Monfardini et al., "Lumped element kinetic inductance detectors for space applications," *Proc. SPIE* **9914**, 99140N (2016).
250. M. D. Shaw et al., "Quantum capacitance detector: a pair-breaking radiation detector based on the single Cooper-pair box," *Phys. Rev. B* **79**, 144511 (2009).
251. J. Bueno et al., "Proof of concept of the quantum capacitance detector," *Appl. Phys. Lett.* **96**, 103503 (2010).
252. J. Bueno et al., "Optical characterization of the quantum capacitance detector at 200  $\mu\text{m}$ ," *Appl. Phys. Lett.* **99**, 173503 (2011).
253. K. Stone et al., "Real time quasiparticle tunneling measurements on an illuminated quantum capacitance detector," *Appl. Phys. Lett.* **100**(26), 263509 (2012).
254. P. M. Echternach et al., "Photon shot noise limited detection of terahertz radiation using a quantum capacitance detector," *Appl. Phys. Lett.* **103**, 053510 (2013).
255. P. M. Echternach et al., "Single photon detection of 1.5 THz radiation with the quantum capacitance detector," *Nat. Astron.* **2**, 90–97 (2018).
256. R. Ramaswami, K. Sivarajan, and G. Sasaki, *Optical Networks: A Practical Perspective*, 3rd ed., Morgan Kaufmann Publishers Inc., San Francisco, California (2009).
257. D. K. Sparacin et al., "Trimming of microring resonators by photo-oxidation of a plasma-polymerized organosilane cladding material," *Opt. Lett.* **30**, 2251–2253 (2005).
258. J. Schrauwen, D. van Thourhout, and R. Baets, "Trimming of silicon ring resonator by electron beam induced compaction and strain," *Opt. Express* **16**, 3738 (2008).
259. A. H. Atabaki et al., "Accurate post-fabrication trimming of ultracompact resonators on silicon," *Opt. Express* **21**, 14139 (2013).
260. R. Klein et al., "FIFILS: the far-infrared integral field spectrometer for SOFIA," *Proc. SPIE* **6269**, 62691F (2006).
261. A. Poglitsch et al., "The MPE/UCB far-infrared imaging Fabry-Perot Interferometer (FIFI)," *Int. J. Infrared Millimeter Waves* **12**(8), 859–884 (1991).
262. J. Zmuidzinas, "Thermal noise and correlations in photon detection," *Appl. Opt.* **42**, 4989–5008 (2003).
263. S. C. Parshley et al., "A miniature cryogenic scanning Fabry-Perot interferometer for mid-IR to submm astronomical observations," *Proc. SPIE* **9147**, 914745 (2014).
264. A. Kovács et al., "SuperSpec: design concept and circuit simulations," *Proc. SPIE* **8452**, 84522G (2012).
265. J. Wheeler et al., "SuperSpec: development towards a full-scale filter bank," *Proc. SPIE* **9914**, 99143K (2016).
266. E. Shirokoff et al., "MKID development for SuperSpec: an on-chip, mm-wave, filter-bank spectrometer," *Proc. SPIE* **8452**, 84520R (2012).
267. S. Hailey-Dunsheath et al., "Status of SuperSpec: a broadband, on-chip millimeter-wave spectrometer," *Proc. SPIE* **9153**, 91530M (2014).
268. S. Bryan et al., "WSPEC: a waveguide filter-bank focal plane array spectrometer for millimeter wave astronomy and cosmology," *J. Low Temp. Phys.* **184**, 114–122 (2016).
269. R. Schieder et al., "The potential of IR-heterodyne spectroscopy," in *The Power of Optical/IR Interferometry: Recent Scientific Results and 2nd Generation*, A. Richichi et al., Eds., pp. 465–471 (2008).
270. P. F. Goldsmith, "Sub-millimeter heterodyne focal-plane arrays for high-resolution astronomical spectroscopy," *URSI Radio Sci. Bull.* **362**, 53–73 (2017).
271. T. M. Klapwijk and A. V. Semenov, "Engineering physics of superconducting hot-electron bolometer mixers," *IEEE Trans. Terahertz Sci. Technol.* **7**, 627–648 (2017).
272. T. de Graauw et al., "The Herschel-heterodyne instrument for the far-infrared (HIFI)," *Astron. Astrophys.* **518**, L6 (2010).
273. P. R. Roelfsema et al., "In-orbit performance of Herschel-HIFI," *Astron. Astrophys.* **537**, A17 (2012).
274. D. Rigopoulou et al., "The far infrared spectroscopic explorer (FIRSPEX): probing the lifecycle of the ISM in the universe," *Proc. SPIE* **9904**, 99042K (2016).
275. P. F. Goldsmith, "Radio telescopes and measurements at radio wavelengths," in *Single-Dish Radio Astronomy: Techniques and Applications*, Astronomical Society of the Pacific Conference Series, S. Stanimirovic et al., Eds., Vol. **278**, pp. 45–79 (2002).
276. C. Groppi et al., "Test and integration results from SuperCam: a 64-pixel array receiver for the 350 GHz atmospheric window," *Proc. SPIE* **7741**, 77410X (2010).
277. D. J. Hayton et al., "A 4.7 THz heterodyne receiver for a balloon borne telescope," *Proc. SPIE* **9153**, 91531R (2014).
278. H. Richter et al., "4.7-thz local oscillator for the great heterodyne spectrometer on sofia," *IEEE Trans. Terahertz Sci. Technol.* **5**(4), 539–545 (2015).
279. H. Richter et al., "Performance of the 4.7thz local oscillator with quantum cascade laser on board sofia," in *40th Int. Conf. Infrared, Millimeter, and Terahertz Waves (IRMMW-THz)*, IEEE, p. 1 (2015).
280. A. Poglitsch et al., "The MPE/UCB far-infrared imaging Fabry-Perot interferometer (FIFI)," *Int. J. Infrared Millimeter Waves* **12**, 859–884 (1991).
281. G. J. Stacey et al., "KWIC: a widefield mid-infrared array camera/spectrometer for the KAO," *Proc. SPIE* **1946**, 238–248 (1993).
282. T. de Graauw et al., "Observing with the ISO Short-Wavelength Spectrometer," *Astron. Astrophys.* **315**, L49–L54 (1996).
283. P. E. Clegg et al., "The ISO long-wavelength spectrometer," *Astron. Astrophys.* **315**, L38–L42 (1996).
284. C. M. Bradford et al., "SPIFI: a direct-detection imaging spectrometer for submillimeter wavelengths," *Appl. Opt.* **41**, 2561–2574 (2002).
285. F. A. Pepe et al., "Liquid-helium cooled scanning far-infrared Fabry-Perot interferometer for astronomical observations with a balloon-borne telescope," *Infrared Phys. Technol.* **35**, 863–871 (1994).
286. N. Ismail et al., "Fabry-perot resonator: spectral line shapes, generic and related airy distributions, linewidths, finesse, and performance at low or frequency-dependent reflectivity," *Opt. Express* **24**, 16366–16389 (2016).
287. T. G. Hawarden et al., "Optimised radiative cooling of infrared space telescopes and applications to possible missions," *Space Sci. Rev.* **61**, 113–144 (1992).
288. H. A. Thronson, Jr. et al., "The Edison infrared space observatory," *Space Sci. Rev.* **74**, 139–144 (1995).
289. R. G. Ross and D. L. Johnson, "NASA's advanced cryocooler technology development program (ACTDP)," in *Advances in Cryogenic Engineering: Transactions of the Cryogenic Engineering Conference*, American Institute of Physics Conference Series, J. G. Weisend, II et al., Eds., Vol. **823**, pp. 607–614 (2006).
290. P. J. Shirron et al., "Design and on-orbit operation of the adiabatic demagnetization refrigerator on the Hitomi Soft X-ray Spectrometer instrument," *Proc. SPIE* **9905**, 99053O (2016).
291. R. G. Ross, R. F. Boyle, and P. Kittel, "NASA space cryocooler programs—a 2003 overview," *Am. Inst. Phys. Conf. Ser.* **710**, 1197–1204 (2004).
292. P. Shirron et al., "A compact, high-performance continuous magnetic refrigerator for space missions," *Cryogenics* **41**(11), 789–795 (2001).

293. J. Tuttle et al., "Development of a space-flight ADR providing continuous cooling at 50 mK with heat rejection at 10 K," in *Mater. Sci. Eng. Conf. Ser.* **278**, 012009 (2017).
294. C. K. Walker et al., "10 meter sub-orbital large balloon reflector (LBR)," in *IEEE Aerosp. Conf.*, pp. 1–7 (2014).
295. D. Lesser et al., "10 meter sub-orbital large balloon reflector (LBR)," in *40th Int. Conf. Infrared, Millimeter, and Terahertz Waves (IRMMW-THz)*, pp. 1–2 (2015).
296. G. Cortes-Medellin et al., "Optical design for the large balloon reflector," *Proc. SPIE* **9906**, 99061Y (2016).
297. J. P. Maillard et al., "Integral wide-field spectroscopy in astronomy: the Imaging FTS solution," *Exp. Astron.* **35**, 527–559 (2013).
298. F. Boulanger et al., "The molecular hydrogen explorer H2EX," *Exp. Astron.* **23**, 277–302 (2009).

Biographies of the authors are not available.